GROUNDWATER POLLUTION FROM ONSITE DISPOSAL SYSTEMS AND OTHER LAND USES ON THE ‘EWA PLAIN, O’AHU

THESIS SUBMITTED TO THE DEPARTMENT OF EARTH SCIENCES AT THE UNIVERSITY OF HAWAII MĀNOA IN PARTIAL FULFILLMENT OF THE REQUIREMENTS FOR THE DEGREE OF

MASTER OF SCIENCE

IN

EARTH SCIENCES

AUGUST 2022

By

Jonathan Cameron

Thesis Committee:

Craig Glenn, Chairperson

Aly El-Kadi

Christopher Shuler

ACKNOWLEDGMENTS

I would like to thank my advisor Dr. Craig Glenn for his knowledge and advice during this project. Without his guidance and support this project would not have been possible. Additionally, I would like to thank my committee members, Dr. Aly El-Kadi and Dr. Christopher Shuler, for their guidance during this project. Also, a thank you to Dr. Henrietta Dulai for her help with electrical resistivity tomography.

I would like to extend a special thank you to my project field partner and fellow graduate student Matthew Duff. Without Matt, this project would not have been completed. I would also like to thank Professor Marek Kirs, Natalie Walsgrove, Danielle Hull, and Catherine Rong for their support in the lab and for analyzing all our water samples. We also extend a thank you to superintendents and land supervisors, Willy, Alex, Bill, Scott, and Vaughn for working with us and helping us to sample the groundwater wells on their properties. Additional thanks are extended to Jeremy Kimura and Bob Chenet of the CWRM. A special thank you is also extended to Lucas Ellison for his help on the project.

This research was supported by grants to Craig Glenn from the Hawaii State Department of Health, and a grant/cooperative agreement from the National Oceanic and Atmospheric Administration project R/IR-50, which is sponsored by the University of Hawaii-Manoa Sea Grant Program under Institutional Grant No. NA18OAR4170076 from NOAA Office Sea Grant, Department of Commerce and Hawaii State Department of Health Grant No. SDWB-20-002-ASD. The views expressed herein are those of the author and do not necessarily reflect the views of NOAA or any of its subagencies.

Abstract

Due to historical and current agricultural practices, the use of recycled wastewater, and high-density on-site disposal systems (OSDS), the ‘Ewa Plain is at risk for harmful impacts related to excess nutrients entering its groundwater and coastal environments. Groundwater pollution on the flat, low gradient ‘Ewa Plain can transport nutrient pollution from source to ocean on short timescales. Identifying the type and concentrations of nutrients present in groundwater is important in understanding the overall impact that these nutrient fluxes have on groundwaters and coastal ecosystem health. Being comprised of thick layers of limestone covering most of the region’s surficial and subsurface geology, the ‘Ewa Plain is a unique geologic setting in Hawaii, and shallow groundwater flow within its flat, low gradient limestone wedge can transport nutrient pollution from source to the ocean on short timescales. This study combines several different approaches to locate and identify relative contributions of groundwater pollution within these sedimentary rocks, including electrical resistivity tomography (ERT), coastal salinity surveys, and geochemical tracers to identify sources of excess nutrients. A numerical groundwater model was created within the MT3DMS modeling environment to incorporate these results and simulates the relative impacts of total dissolved nitrogen (TDN) and dissolved inorganic nitrogen (DIN) pollution within this region. Results from near shore in situ ERT transects and lab tests of sediments indicate a layer of unconsolidated and consolidated beach sediments sitting atop a deeper limestone unit completely saturated with water, but failed to locate karstic conduits at either of the locations. Two along shore salinity surveys conducted located several zones of salinity below 35, and all but 19 measured salinity points were below 31. Submarine groundwater discharge along the shore appears to be mainly saline and diffuse, and may be emanating further offshore. Measured beachface pore water samples and groundwater well samples showed elevated nutrient values compared to standard ocean water. The numerical groundwater model environment MT3DMS was used to simulate the relative impact of total dissolved nitrogen and dissolved inorganic nitrogen from five different sources: background soil processes, OSDS, agriculture, golf courses, and recycled wastewater irrigation (R-1 water). The estimated impact from the MT3DMS model of total dissolved nitrogen and dissolved inorganic nitrogen into the ‘Ewa Plain indicate that the sources of highest relative anthropogenic nitrogen loading to groundwaters are widespread R-1 irrigation and more localized high-density OSDS related effluent.

TABLE OF CONTENTS

LIST OF FIGURES AND TABLES

1. INTRODUCTION

Improper wastewater treatment resulting in groundwater pollution from excess nutrients is a global problem (Tuholske et al., 2021). In the United States alone it is estimated that on-site disposal systems (OSDS), mainly in the form of septic tanks and cesspools, contribute nearly 800 billion gallons of wastewater to subsurface groundwaters (Yates, 1985). OSDS are largely used in areas where there is poor sewage treatment infrastructure or in rural localities where such infrastructure does not exist. The state of Hawai'i was the last state in the United States to allow new cesspool construction, banning new construction as recently as 2016 (HDOH, 2018). There are 88,000 known cesspools across the state of Hawaii that can release upwards of 53 million gallons per day of mostly untreated sewage into the groundwater system (HDOH, 2018). In its most basic construction, a cesspool is nothing more than a pit in the ground that allows for gravitational separation of solid waste from liquid waste. A well maintained, functioning cesspool uses naturally occurring anaerobic bacteria to break down untreated liquid and solid wastes. Liquid waste then flows through the perforated walls of the cesspool into local soil and groundwater systems, solid waste sludge is then periodically pumped out and treated at a wastewater treatment plant. However, due to one or a combination of both, improper upkeep, and age, it is estimated that around 32% of Hawaiian cesspools are failing or in danger of failing and that 80% of surveyed Hawaiian homeowners were not having their cesspool serviced in any way (Babcock et al., 2014).

The Hawaii State Department of Health (Whittier and El-Kadi, 2009) identified several particularly high-density OSDS zones on the island of O'ahu. Highest ranked high-priority OSDS zones are locations of (1) high density of OSDS and (2) are the most at risk for noticeable human and environmental health impacts stemming from sewage effluent leaking from OSDS. The 'Ewa Plain remains one of these highest-ranked high-priority zones as it contains an estimated OSDS density exceeding 18 OSDS units/mi^2, and is estimated to release 181.5 kg/d of nitrogen (Whitter and El-Kadi, 2009). This area ranks second out of all OSDS zones on O'ahu in terms of total number of units. The 'Ewa Plain is unique both because of its subsurface caprock limestone geology, as well as its historic and current land-use practices. A large plain of interbedded terrestrial alluvium and marine limestone deposits, reaching a depth of greater than 300 m (1,000 ft) near the ocean (Oki et al., 1996), comprise the surface geology and subsurface hydrogeology of the plain, rock types that are not common on other Hawaiian Islands (Bauer, 1996). From ca. 1890-1980, land use in 'Ewa was principally devoted to large-scale sugarcane cultivation. As sugarcane farming and production fell, residential housing was built and, ‘Ewa Beach and the surrounding communities experienced a population growth boom that continues today, with an estimated population growth of 71% by 2035 (HSPA, 1994). This is important because past and present agriculturally based land use and present-day OSDS density both introduce excess nitrogen into ‘Ewa’s groundwater system. Due to its proximity to the coast, the fate of this nitrate-laden groundwater is likely largely transported in the subsurface to the surrounding ocean as submarine groundwater discharge (SGD), discharging to the ocean either as diffuse discharge or as small point source discharge locations, or a combination of both. SGD is a known source of excess nutrients being introduced to nearshore coastal environments (Li et al., 1999; Taniguchi et al., 2002; Burnett et al., 2003; Moore, 2010). SGD flux can be hard to accurately quantify as tidal mixing, sea level rise and local and regional geology can all affect SGD flux at any given location (Burnett et al., 2006). The less dense freshwater “floats” on top of the denser seawater that underlies the coastal regime. In island settings, this type of coastal aquifer is referred to as a basal or basal lens aquifer as the freshwater forms a subterranean lens-shaped aquifer system buoyantly floating on top of the more saline seawater below. Between the freshwater lens and the seawater is the transition zone, a zone of recirculated seawater mixing with fresh groundwater producing a brackish mixture of both fresh and salt water.

Although large-scale limestone deposits are not rare globally (Montiel et al., 2018), such deposits are rare in Hawai’i, with the ‘Ewa Caprock being the most notable example of such deposits (Oki et al., 1996; Halliday, 1998). Groundwater movement through limestone can form dissolution tunnels, caves, and subsurface channels referred to as karst, and across the ‘Ewa Plain, there are sinkholes and ponds indicative of this dissolution. These karstic features may have a noticeable impact on groundwater transport and SGD flux as subsurface channels can move large volumes of groundwater much faster than normal groundwater movement through rock pores. Limestone hydrology is unique and different from volcanic hydrology and is marked by the presence of primary and secondary dissolution structures and variable conductivity (Stringfield and LeGrand, 1969). Understanding the dynamics of groundwater beneath the ‘Ewa Plain is therefore integral in understanding how pollution entering this system travels and behaves. In addition, the impact from OSDS effluent and agriculture on reef and coastal community health is well documented (Smith et al., 1999; Kroon et al., 2014; Lyons et al., 2014), yet the impact that limestone geology has on ‘Ewa Plain hydrology is unknown.

Quantifying the flux and type of nutrients present in groundwater in ‘Ewa is thus an important step towards understanding the true scope and scale of OSDS and nutrient problems in Hawai’i.

Given the above, the goal of this project is to locate potential sources of nutrient pollution and estimate the areas where these impacts are expected to be greatest. To achieve this goal, we used a multifaceted approach to best locate, quantify, and understand the sources of nutrients present in groundwater and SGD. This approach consists of ocean surface salinity surveys to locate potential groundwater discharge locations, evaluation of land-use practices that contribute background vs. anthropogenic nutrients, geochemical analysis of nutrient concentrations in groundwater and beachface pore water samples, electrical resistivity tomography in an attempt to locate karstic features that may act as conduits for pollution, and creating a numerical groundwater model to locate potential sources of nutrient pollution and where these impacts are expected to be greatest.

2. REGIONAL SETTING AND BACKGROUND

The Hawaiian Islands are comprised of a chain of hot spot volcanoes in the Pacific Ocean inhabited by over 1.4 million people. O’ahu is the most populated of the Hawaiian Islands with just over 1 million residents (U.S. Census Bureau, 2021). O’ahu has been deeply eroded and is marked by two mountain ranges that are the remnants of two shield volcanoes, the Wai’anae Mountains on the west and the Ko’olau Mountains on the east (**Figure 1**). The oldest dated lavas of these two volcanic ranges date to 3.7 Ma and 2.6 Ma, respectively (Clague and Dalrymple, 1989). The ‘Ewa Plain study area is situated along the southwest shore of O’ahu, west of Pearl Harbor, wherein the ‘Ewa Caprock occurs (Stearns and Chamberlin, 1967; Bauer, 1996). While limestone is known in many coastal environments across the Hawaiian island chain (Oki et al., 1996; Montiel et al., 2017; Izuka et al, 2018), the ‘Ewa Caprock is by far the largest and most extensive limestone deposit present today (Bauer, 1996).

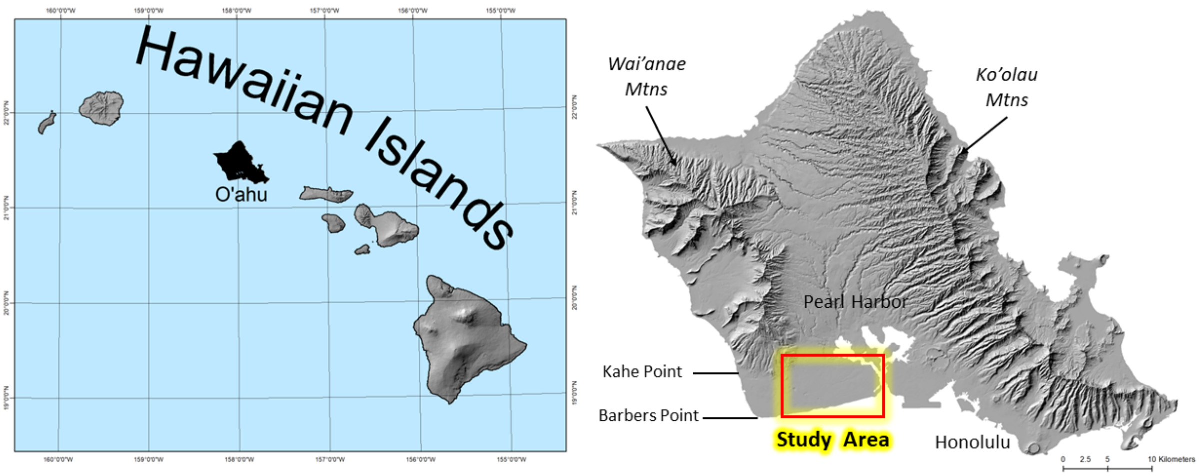

Figure 1*: Left: Image of O'ahu within the Hawaiian Island chain. Right: Map of O'ahu showing the ‘Ewa Plain study area (Data from Hawaii Statewide GIS Program).*

2.1 ‘Ewa Caprock Geology

The ‘Ewa Plain is an extensive broad and flat coastal plain of limestone and alluvial sediments that stretches from Kahe Point and Barbers Points on the west to Pearl Harbor on the east, and which overlies the deeper volcanic rock aquifer derived from the Ko’olau and Wai’anae volcanic events (Bauer, 1996; Oki et al., 1996). **Figure 2** shows the regional surficial geology of the ‘Ewa Plain, displaying volcanic units and ‘Ewa Caprock. The southern terminus of the Wai’anae Mountains lies several miles north of the ‘Ewa coast and does not create significant topographic features within the confines of the study area. This ‘Ewa Plain is dominated by the surface expression of the very thick ‘Ewa Caprock Hydrogeologic Unit (CWRM, 2018) which is more than 300 m (1000 ft) thick beneath the present coastline and thickens to more than 485 m (1600 ft) offshore (Izuka et al., 2018). The boundary between the deeper volcanic rocks and the ‘Ewa Caprock is defined as a low-permeability layer of weathered volcanics that limits water flow between the two units (Bauer, 1996; Oki et al., 1996). **Figure 3** shows two attempts at cross-sections of the ‘Ewa Caprock illustrating its wedge shape and generalized depiction of interbedded marine and terrestrial alluvium deposits as extrapolated from cores (cf. Resig, 1969; Oki et al., 1996) and seismic data (Furumoto et al., 1970). In cross-section, the caprock forms a roughly wedge-shaped deposit, thickening seaward from its abutment along the Waianae Mountains to the north, to over 360 meters thick along the coast (Mink, 1989; Bauer, 1996; Oki et al., 1996). In addition, the caprock limestones are split into two units, the upper limestone and lower limestone (Oki et al., 1996), separated by a medial low permeability mud layer (Bauer, 1996), presumably comprised of terrestrial clays. The ‘Ewa Caprock was built up during repeated rise and fall of sea level during the Pleistocene (Sherman et al., 1993; Bauer, 1996).

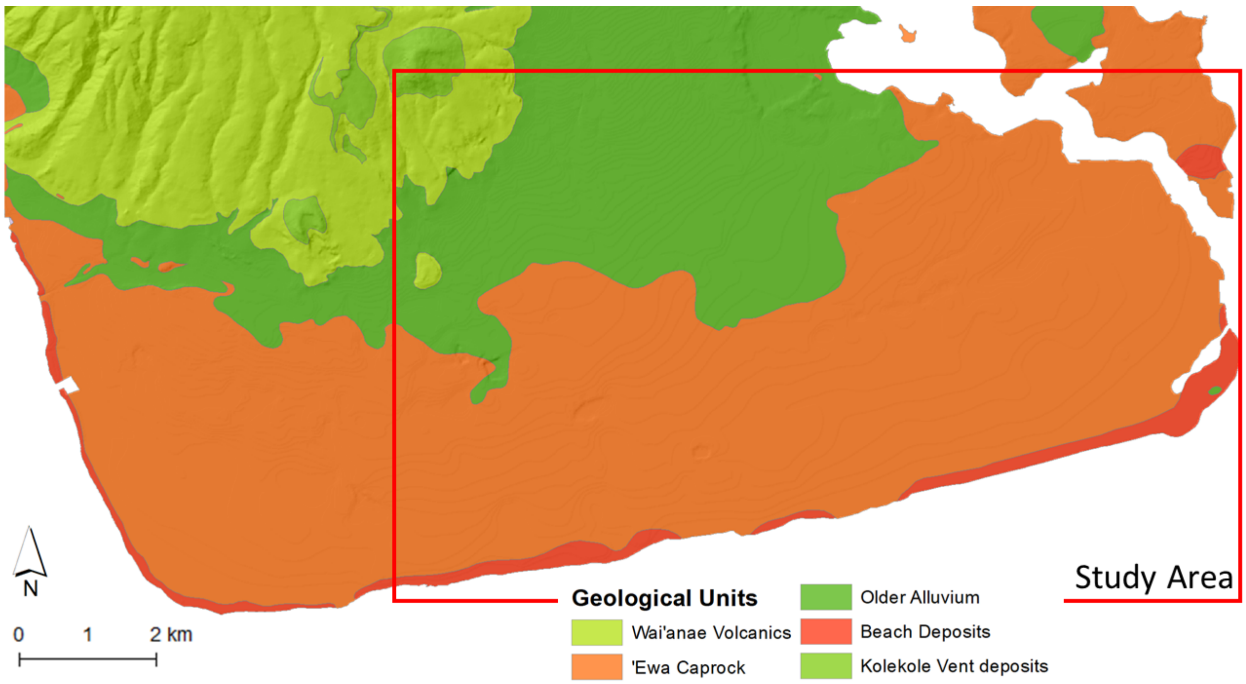

***Figure 2**: Surficial geology of the ‘Ewa Plain (Hawaii Statewide GIS Program)*

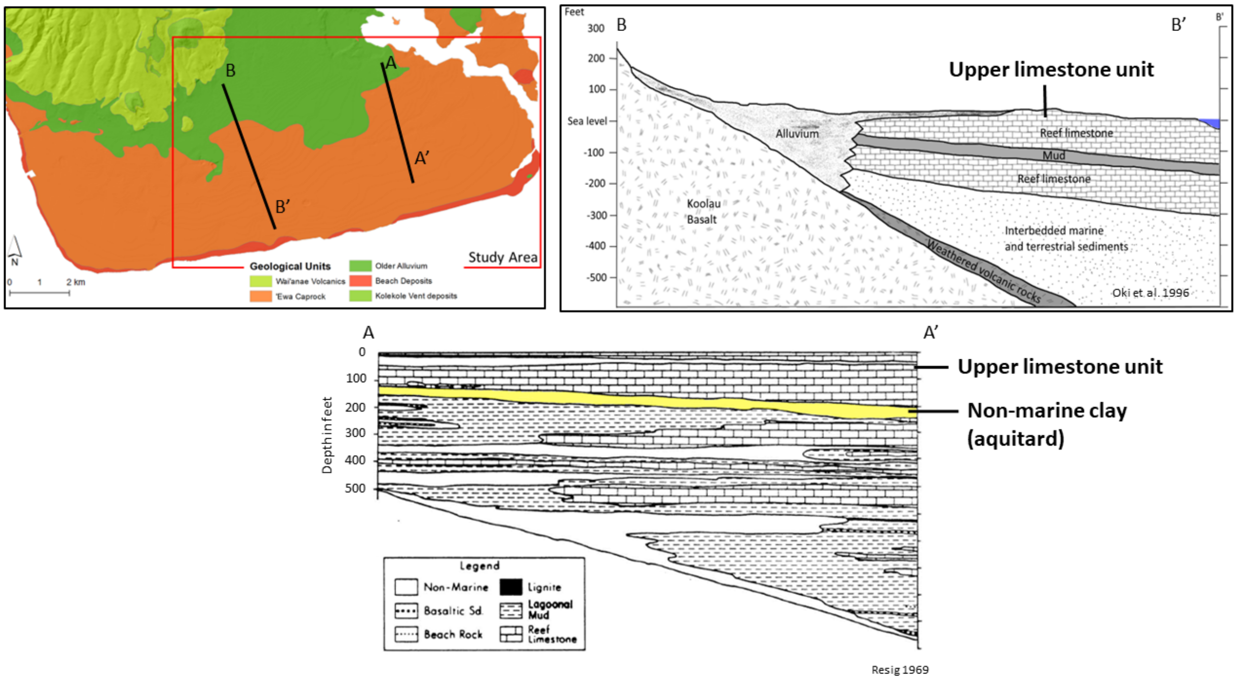

*Figure 3: Interpretative geologic cross-sections through the wedge of 'Ewa Caprock overlying basalts on the 'Ewa Plain of southwest O'ahu, after Oki et al. (1996). Cross-section A-A' (Resig 1969) crosses through the high-density OSDS zone that is detailed in **Figure 8**.*

2.2 Climate and Surface Water Hydrology

The 'Ewa Plain is generally hot and dry, receiving relatively small amounts of rainfall. **Figure 4** shows total recharge in inches per year across the region. The data used to create **Figure 4** is from Engott et al., 2017 and includes recharge data from total irrigation, OSDS effluent, and rainfall. On average, the 'Ewa Plain receives around 20 inches of rain annually, and much of this comes during large-scale winter storm systems (Oki et al., 1996; Hartley and Chen, 2010; Giambelluca et al., 2020). Recharge can also enter the 'Ewa Caprock via seaward-directed flow from the Wai'anae Volcanics to the north and from upwards-directed flow from the volcanic aquifer below, as illustrated in **Figure 5.** The three main watersheds that cover 'Ewa Plain are the Makaiwa, Kaloi, and Honouliuli Watersheds (CWRM, 2018) (**Figure 6**). Terrestrial water features that do exist include 14 small groundwater-fed anchialine ponds of the Kalaeloa units the Pearl Harbor National Wildlife Refuge to the west of the study area proper, and the large artificial Wai Kai Lagoon that remains under construction.

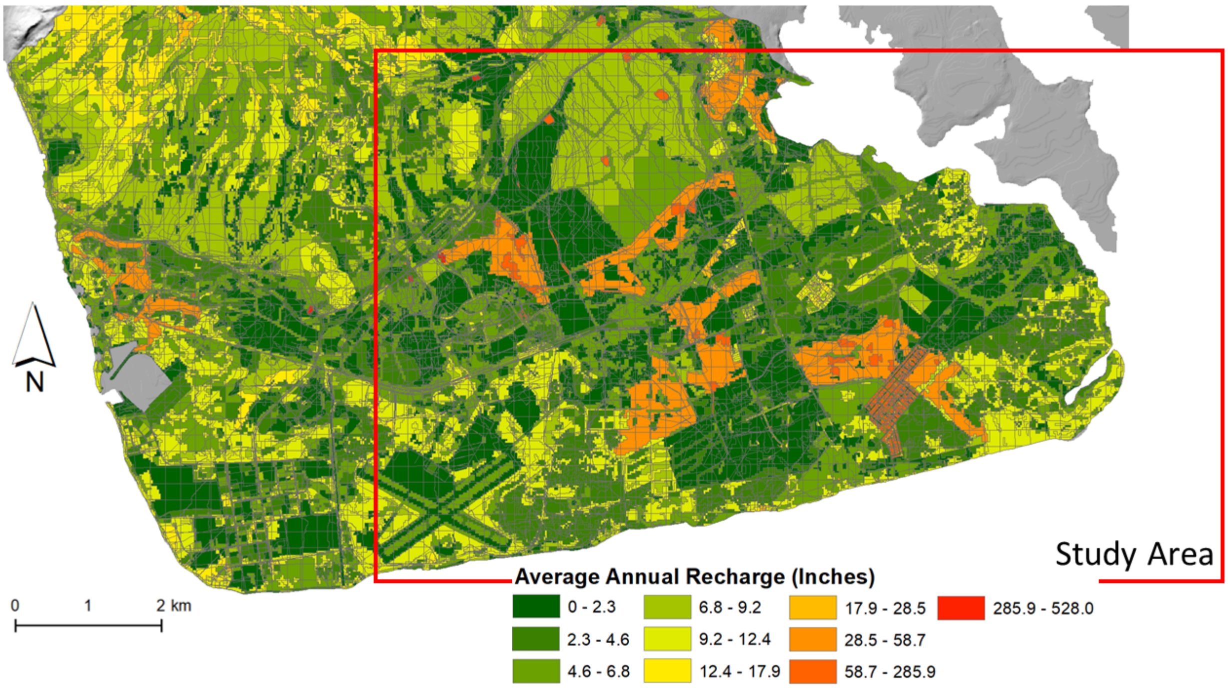

***Figure 4**: Average annual recharge for the ‘Ewa Plain study area (recharge map from Engott et al., 2017)*

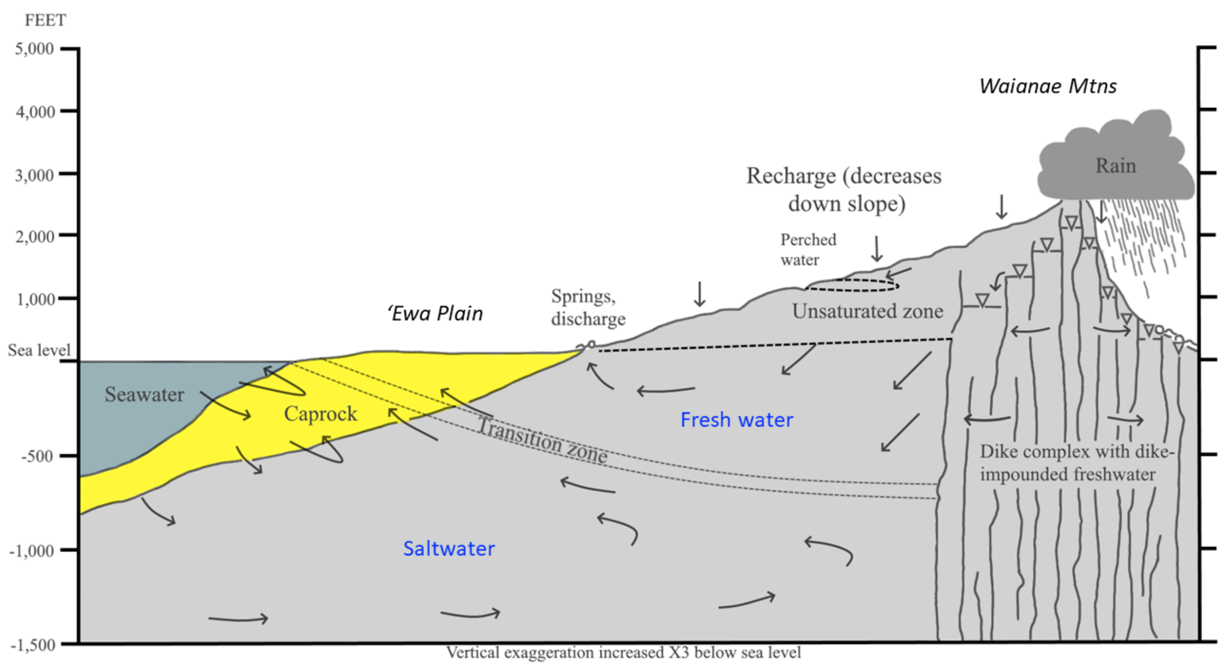

***Figure 5**: General cross-section of Oahu showing groundwater flow through the subsurface, down gradient towards the caprock and sea (Hunt, 1996).*

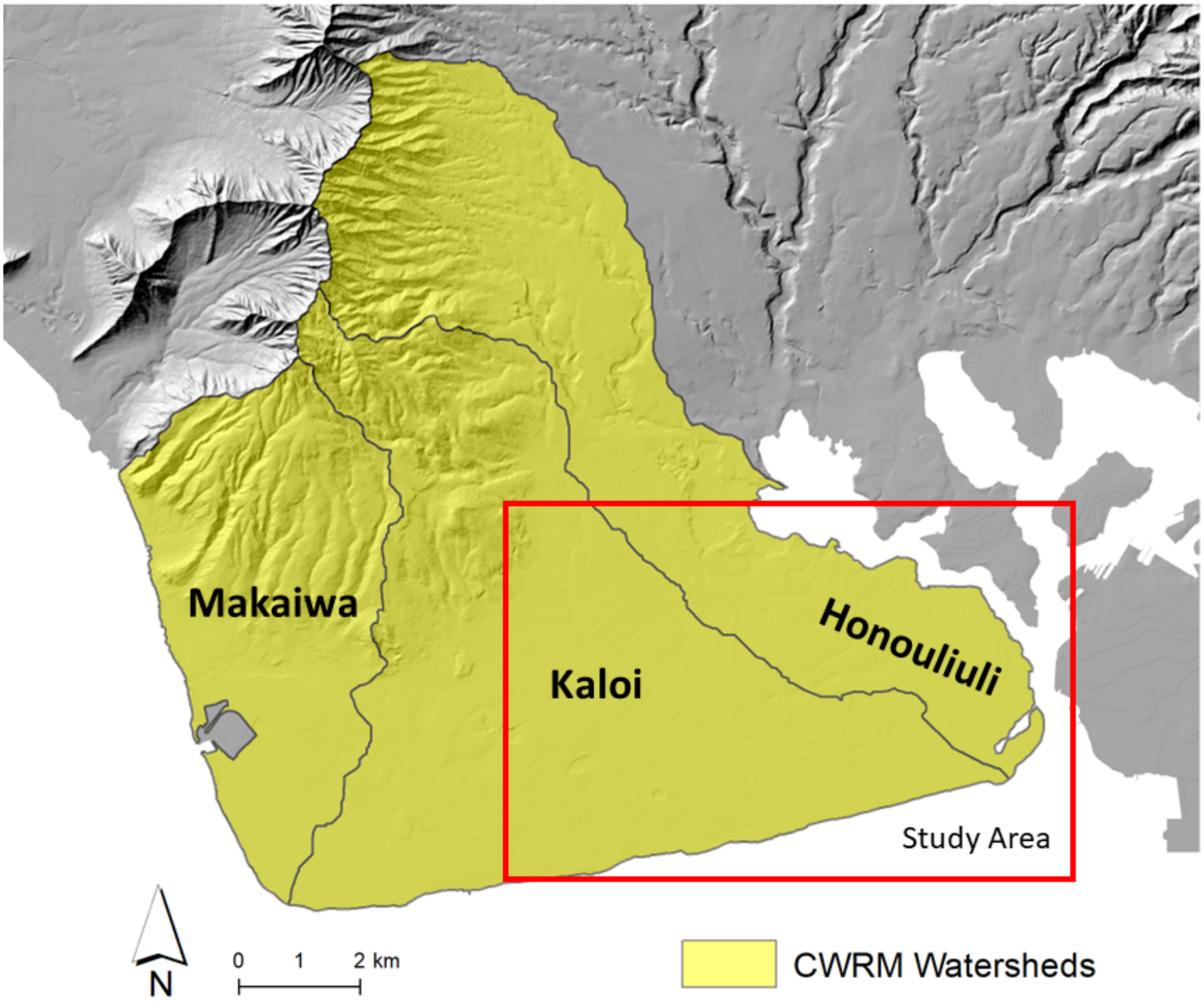

Figure 6: *Watersheds that cover the 'Ewa Plain as defined by the state of Hawaii Department of Land and Natural Resources Commission on Water Resource Management (CWRM). Data from Hawaii Statewide GIS program.*

2.3 Groundwater Hydrogeology

Two main aquifer systems dominate the 'Ewa Plain subsurface, the Pearl Harbor and 'Ewa Caprock Systems (CWRM, 2018: **Figure 7**). The Pearl Harbor aquifer is the deeper aquifer and consists of weathered and unweathered volcanic deposits. The 'Ewa Caprock aquifer was deposited on and lies above the deeper Pearl Harbor aquifer and pinches out landward to the north. Most groundwater wells across the 'Ewa Plain (Figure 7) were drilled into the upper limestone unit of the caprock (Bauer, 1996) and largely used for general irrigation including agricultural fields and golf courses. The 'Ewa Caprock aquifer is a brackish (>1 salinity; >1000 mg/l chloride) limestone aquifer. In general, limestone hydrology which is likely present under the ‘Ewa Plain may likely vary dramatically, as primary and secondary features such as dissolution conduits and caves make hydraulic conductivity values highly variable (Stringfield and LaGrand, 1969). While it is hard to determine exact dissolution rates of a given area, it can be estimated that rate of dissolution of conduit walls in a limestone environment is 0.01-0.1 cm per year (Palmer, 1991). In systems where there are considerable karstic features, groundwater flow can be much quicker through preferential flow conduits than normally found in other aquifers (Wilson and Gardner, 2006; Ghasemizadeh et al., 2012). Additionally, due to recrystallization and cementation, the porosity of the ‘Ewa Caprock limestone may be reduced across the plain.

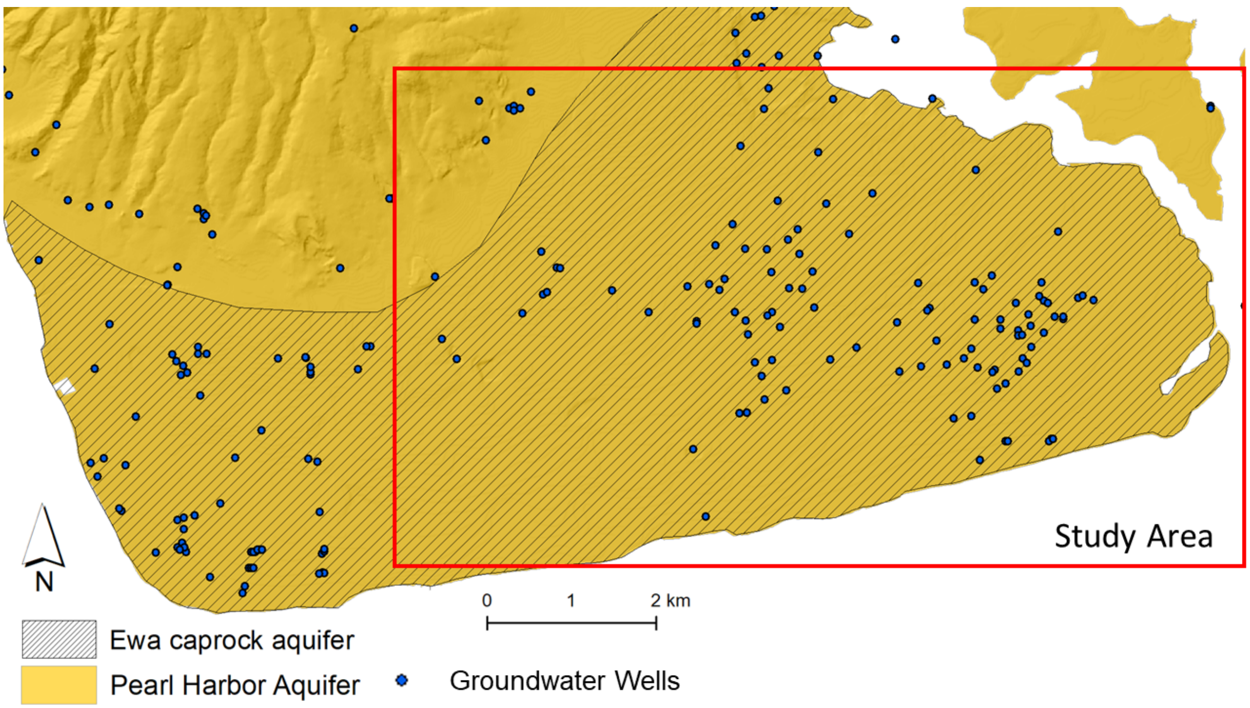

***Figure** 7: Groundwater wells and the two aquifer systems on the ‘Ewa Plain. The sedimentary Ewa Caprock aquifer thins landward and lies above the deeper volcanic Pearl Harbor aquifer (CWRM, 2018).*

2.4 Land Use Practices

Current land use practices on the ‘Ewa Caprock are shown in **Figure 8.** Due to OSDS density (**Figure 9**) and agricultural land use it is speculated here that the main source of excess nutrients on the eastern three quarters of the ‘Ewa Plain come from these two sources. Additionally, the western corner of the ‘Ewa Plain is occupied by a high-density of industry plants centered at the Campbell Industrial Park (Figure 8) which may introduce other spilled contaminants to the groundwater including petroleum refining and storage of hydrocarbons and industrial solvents (Iturbe et al., 2003; Lin, 2021). Due to its complexity, contaminant pollution at the Campbell Industrial Park has not been included within the context of the present study.

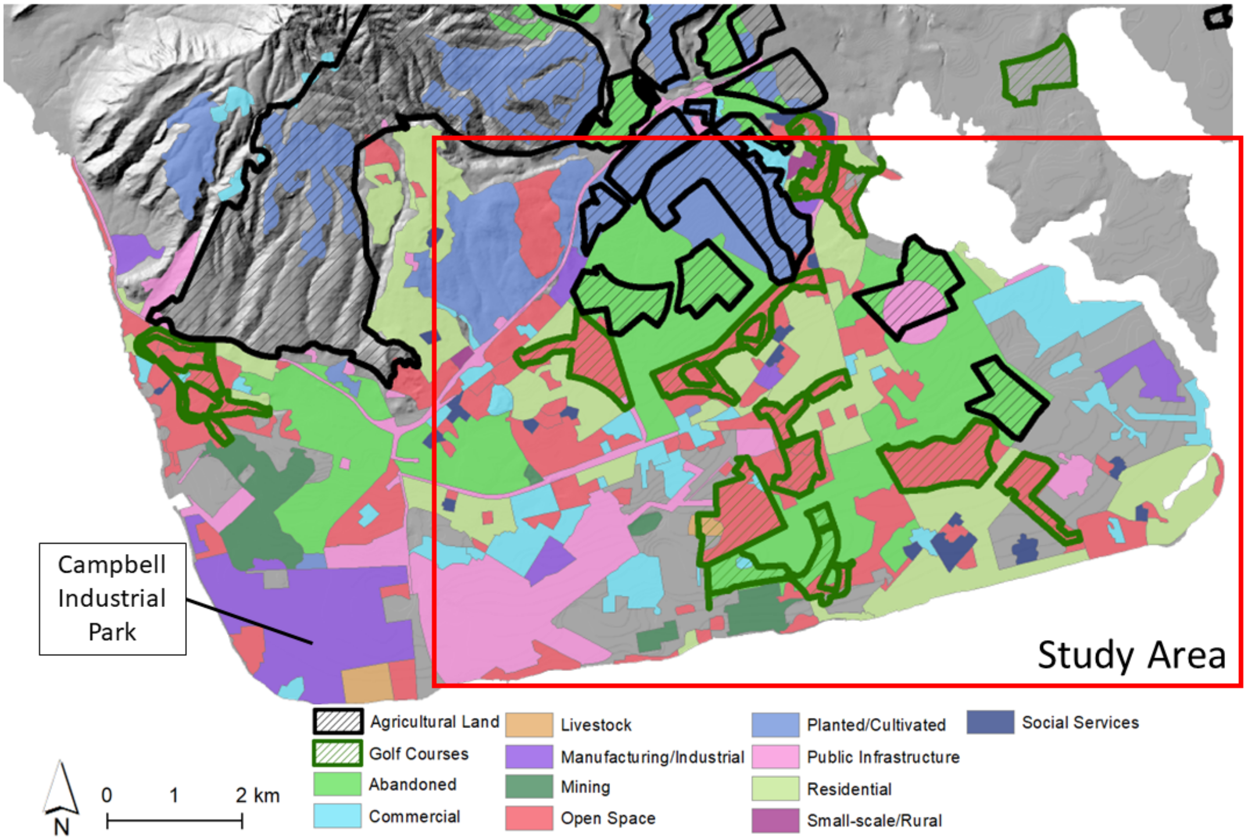

***Figure 8**: Current land use and land cover for the 'Ewa Plain. "Abandoned" (light green) is a general category for any land that is not currently being used for any other category (Hawaii statewide GIS program)*

2.41 Agriculture, Golf Courses Fertilization, and R-1 water irrigation

Agriculture and golf course fertilization are important sources of excess nutrients introduced to groundwater and the nearshore ecosystem of the 'Ewa Plain. The 'Ewa Plain has consistently been used to grow food both for export and local use (Bauer, 1996). Large-scale sugarcane operations originally dominated agriculture, but in the 1980s sugarcane farming declined, and a wider array of crops have taken their place (HSPA, 1994). Currently, much of the agricultural land within the study area is classified by the state of Hawaii as "diversified crops" dominated by crops such as papaya, corn, and onions. Much of the water used to irrigate these crops as well as golf courses comes from wells drilled into the upper limestone (Bauer, 1996).

Nutrient loading from fertilizers is compounded by common golf course irrigation using recycled wastewater (termed R-1 water in Hawaii), which can introduce additional concentrations of nitrogen and phosphorus into groundwater (Sakadevan et al., 2000). As discussed further below, our analyses indicate very high concentrations of nitrate and phosphorus present in collected R-1 water samples. For the purpose of illustration **Table 1** shows R-1 recycled water users and their average R-1 recycled water usage for the year of 2012. As of the time of writing, the modern usage of R-1 water is nearly the same (B. Usagawa, HBWS, personal communications, 2022). Each golf course that uses R-1 water is given an allowance from the Board of Water Supply, which collectively totals approximately 7.4 million gallons per day of treated wastewater being used to water grass and landscaping within the project study area (BWS, 2014). The R-1 water used on the ‘Ewa Plain is treated and pumped from the Honouliuli wastewater treatment plant.

Table 1: R-1 Recycled Water Users (2012 avg)

Honouliuli Wastewater Treatment Plant	2.8 mgd
Barber’s Point Golf Course	0.37 mgd
Coral Creek Golf Course	0.54 mgd
Ewa Beach Golf Course	0.45 mgd
Ewa Villages Golf Course and Community	0.53 mgd
Hawaii Prince Golf Course	0.79 mgd
Hoakalei Golf Course	0.51 mgd
Kapolei Golf Course	0.35 mgd
West Loch Golf Course and Community	0.79 mgd
Fort Weaver Rd – Medial Strip	0.05 mgd
Ewa Makai Middle School	0.02 mgd
Dust control to various users	0.032 mgd
City of Kapolei	0.185 mgd

Data from Usagawa, 2014.

2.42 Municipal Wastewater Disposal and OSDS

There are 14,606 OSDS on O’ahu, with 11,253 (77%) being cesspools. The ‘Ewa Plain has more than 1,300 individual OSDS (Whittier and El-Kadi 2009). Of these 1,259 (91%) are cesspools, the least effective OSDS treatment process in terms of nutrient removal. In addition, a high-density cluster of ~900 OSDS are located on the east half of the ‘Ewa Plain and that contains a density upwards of 200 units/mi^2 (**Figure 9 inset**). When combined, all OSDS on the ‘Ewa Plain release an estimated 0.87 million gallons of untreated wastewater per day (Whittier and El-Kadi, 2009) directly into the ‘Ewa Caprock aquifer and eventually ‘Ewa’s coastal waters. The ‘Ewa Plain does have a municipal sewer system,however, and new developments connected to this system send their waste to the Honouliuli Wastewater Treatment Plant. The HWTP treats incoming wastewater and, once treated, pumps it into the ocean through a 4 km (~2.5 mi) outflow pipe, or disperses it as R-1 and R-O water for users as described above. Thus, despite the ‘Ewa Plain having sewer infrastructure in place in its newer housing and commercial properties, a legacy of OSDS remains, especially in the eastern third of the plain (Figure 9 inset).

Many studies have shown that SGD often contains elevated nutrient levels (e.g., Smith et al., 1999; Kroon et al., 2014; Lyons et al., 2014) and Hawaii is no exception (e.g., Garrison et al., 2003; Presto et al., 2007; Johnson et al., 2008; Knee et al., 2008; Glenn et al., 2012; Bishop et al., 2017; Richardson et al., 2017; Ellison, 2020; Mason, 2020). Due to their relatively high hydraulic conductivity (Zhan et al., 2020), many limestone deposits may effectively transport excess nutrients from the source on land to the ocean on geologically fast time scales. This is especially important in areas of the ‘Ewa Plain that lack adequate sewage treatment facilities and rely heavily on low-quality wastewater treatment systems such as cesspools and septic tanks.

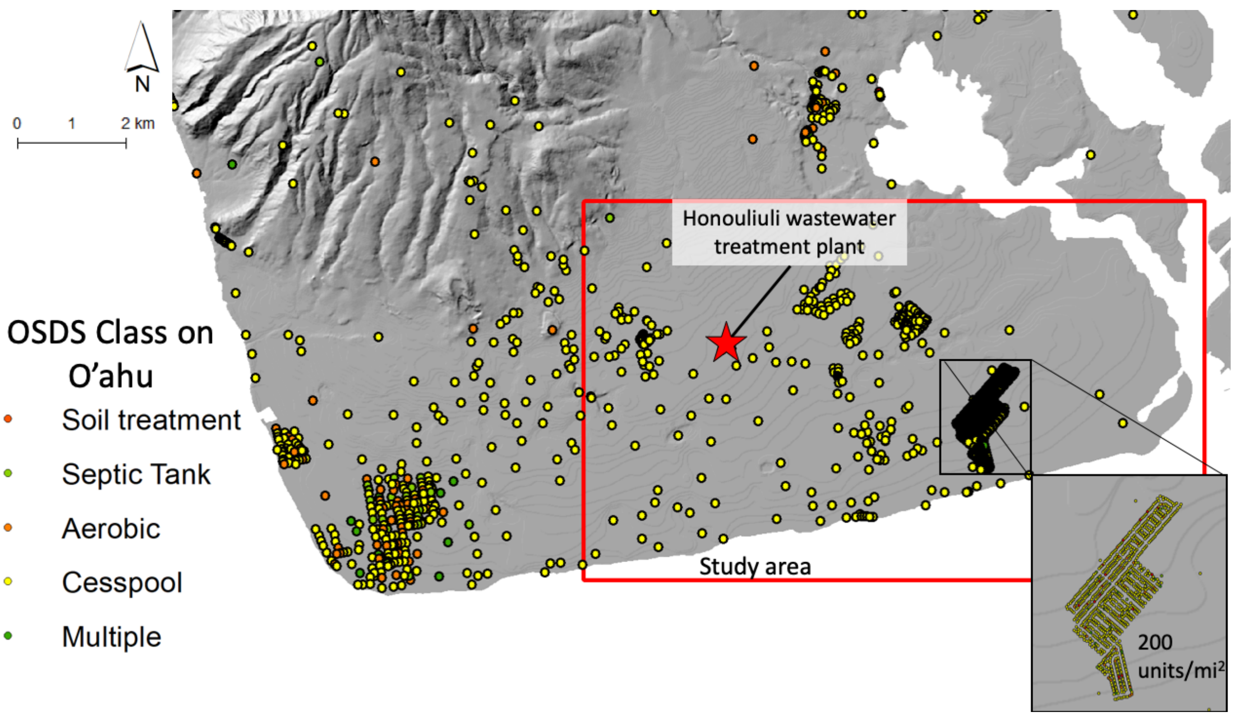

Figure 9: OSDS and OSDS types on the ‘Ewa Plain, with the highest density OSDS zone within the study area, are highlighted in the inset. The Honouliuli wastewater treatment plant location is also shown (Hawaii Statewide GIS Program).

2.5 Beach Parks

Figure 10 shows the location of the three main beach parks used for beachface piezometer water sampling during this study; Pu'uloa ('Ewa Beach), One'ula, and Kalaeloa Beach Parks. These sampling sites covered about 8.5 km of shoreline, some of which are rocky and inaccessible. Pu'uloa Beach Park is directly adjacent to the highest density OSDS zone, One'ula Beach Park is located at an intermediate distance to the highest OSDS density zone, and Kalaeloa Beach Park is the most distal from the high density OSDS zone.

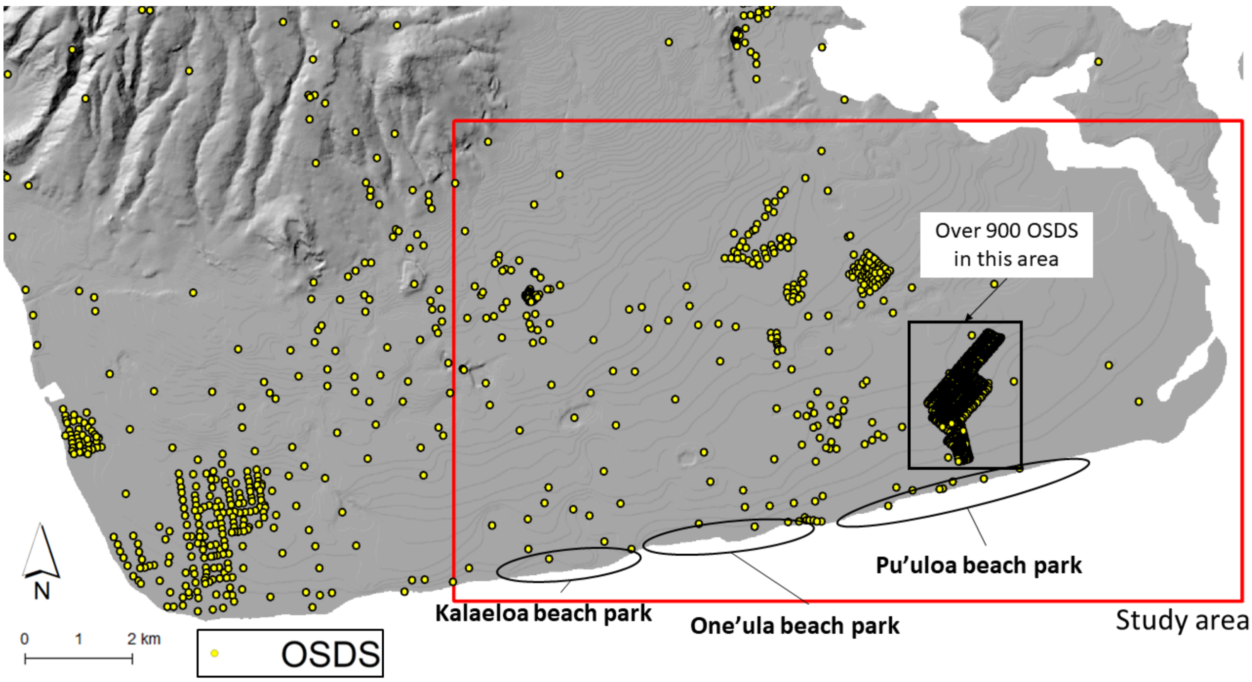

Figure 10*: The three main beach parks used in this study. The OSDS cluster north of Pu'uloa Beach Park has a concentration of 200 units/mi^2 (Whittier and El-Kadi 2009), one of the highest concentrations on the island of O'ahu (OSDS locations provided by Hawaii statewide GIS program)*

3. METHODS

3.1 Electrical Resistance Tomography (ERT)

The regional surficial geology of the 'Ewa Plain has been well described and mapped (Bauer 1996). However, what has remained extremely poorly understood is the extent to which local karstic features such as caves and subsurface conduits are present in and beneath the plain and how these may affect hydraulic conductivity. Therefore, electrical resistivity tomography (ERT) was used as a tool to investigate the near subsurface geology within the study area. Due to how electrical current changes as it passes through differing geologic units, it is possible to interpret collected resistivity data and infer the composition of the subsurface geology (e.g., Workman and Leighton, 1937; Dutta et al., 1970; van Schoor, 2002; Zhou et al., 2002; Beauvais et al., 2003; Dimova et al., 2012). ERT has been used to map and identify subsurface geology and geologic features for decades (Storz et al., 2000), including those indicative of karst environments, such as caves, channels, and fractures (Dutta et al., 1970; Zhu et al., 2011; Meyerhoff et al., 2014; Sawyer et al., 2015). ERT can also provide a clearer picture of subsurface karstic geology including the location and geometry of karst conduits and caves (Tassy et al., 2014; O'Connell et al., 2018).

ERT surveys were conducted across a tidal cycle at Kalaeloa Beach Park and One'ula Beach Park. One'ula Beach Park was targeted specifically due to an identified SGD spring being present at this location. Taking time series measurements across a complete tidal cycle allowed for identification of the expected water table position and its transient movement (e.g., Dailey et al., 1992; Swarzenski et al., 2006, 2007). Utilizing the position of the water table, as interpreted from final ERT cross sections, it is possible to interpret subsurface geology based on the property contrast of water and rock (e.g., Zhu et al., 2011; Dimova et al., 2012; Meyerhoff et al., 2014; Johnson et al., 2015). In our study, we laid a 112 m electrical cable with connecting electrodes parallel to shore and positioned it as high up the beach as possible to minimize washover from waves during high tide intervals. To validate and verify the accuracy of collected images, an inversion methodology was applied to the data collected during this time (e.g., Samouelian et al., 2005; Dimova et al., 2012). Two shore-parallel ERT surveys, consisting of two measurements each, were conducted at study site beach parks to produce high-resolution images of the two locations on the 'Ewa Plain. **Figure 11** shows ERT transects at Kalaeloa Beach Park and One'ula Beach Park. The survey at One'ula Beach Park was located within a few meters of a persistent relatively low salinity SGD spring in the beachface. During the ERT surveys beachface pore water samples were collected and analyzed for a suite of geochemical parameters to further verify the rise and fall of the water table and the presence of SGD. ERT works by injection of direct current into the ground via direct current producing electrodes, the voltage change across the units is then read at different, potential reading electrodes (Daily et al., 1992; Daily et al., 2005). We used an Advanced Geosciences Inc. (AGI) SuperSting R8/IP Unit (Advanced Geosciences Inc., AGI) with an 8-channel receiver connected to the 112 m AGI passive graphite electrode cable. Electrodes were evenly spaced apart at 2 m intervals adding up to 56 total electrodes across the length of the electrical cable. A 2 m interval was chosen to maximize both resolution and lateral distance covered by each ERT survey. 40 cm long stainless-steel spikes were attached to each electrode to ensure constant contact with unconsolidated beach sand substrate. **Figure 12** illustrates the components used in the ERT transects. The cable and electrodes were configured in a dipole-dipole arrangement. Before each measurement, a contact resistance test was conducted to ensure measurements could be done at each electrode location. Measurements are given in Ω-m, providing the resistivity across a set number of meters on the ground. After each measurement, these data were downloaded from the SuperSting to a laptop computer for inversion and interpretation. Using Earth Imager 2D software (AGI), measured resistivity data were inverted to produce an image of the subsurface. The goal of the inversion is to apply a best-fit model to the measured data and create the true results within set parameters determined by the model (Perrone et al., 2014; Sharma and Verma, 2015). Earth Imager 2D comes included with several different inversion types that change the parameters applied to the measured data (Samouelian et al., 2005; Miller et al., 2008; Dimova et al., 2012). For our data, a smooth inversion was applied. A smooth inversion offers a stable result regardless of background noise and applies to most scenarios. The final product is a resistivity pseudosection or a plot of measured and interpreted electrical resistivity data which serves as a visual representation of the subsurface after data correction and inversions are applied. Important to note however, that these results are simplified inversion of the true subsurface geology and, serve as a tool to better understand the subsurface. Using this tool, it is possible, however, to gain an understanding of the general geometry and potential lithology of the subsurface.

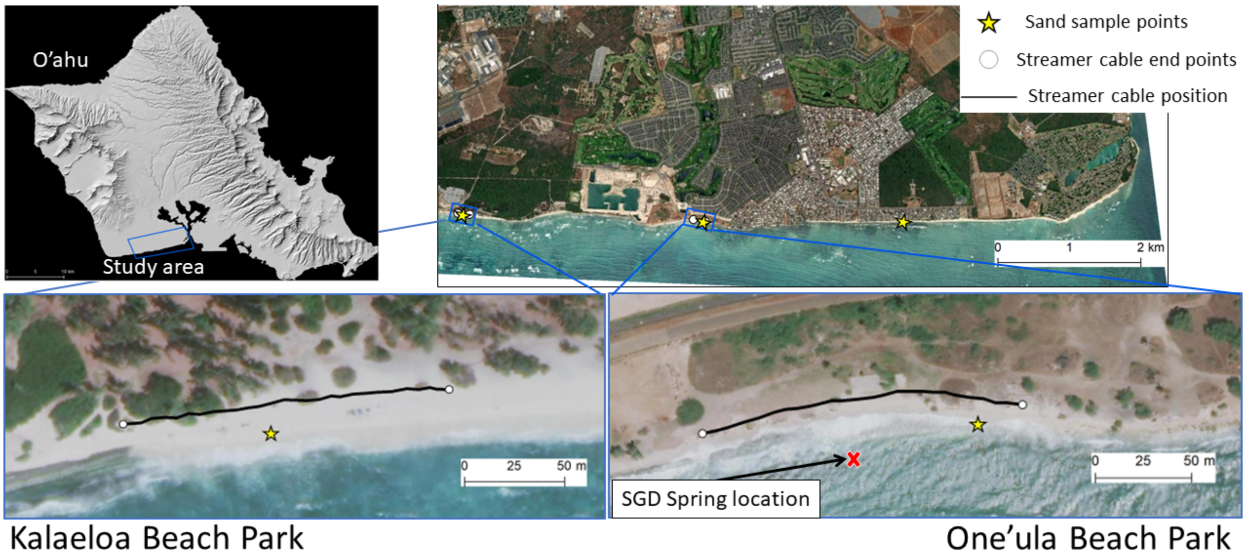

Figure 11*: Map of both ERT transect locations at Kalaeloa Beach Park (right) and One'ula Beach Park (Left) as well as locations of sand samples collected for ex-situ resistivity measurements. The location of the identified SGD spring at One'ula Beach Park is also shown.*

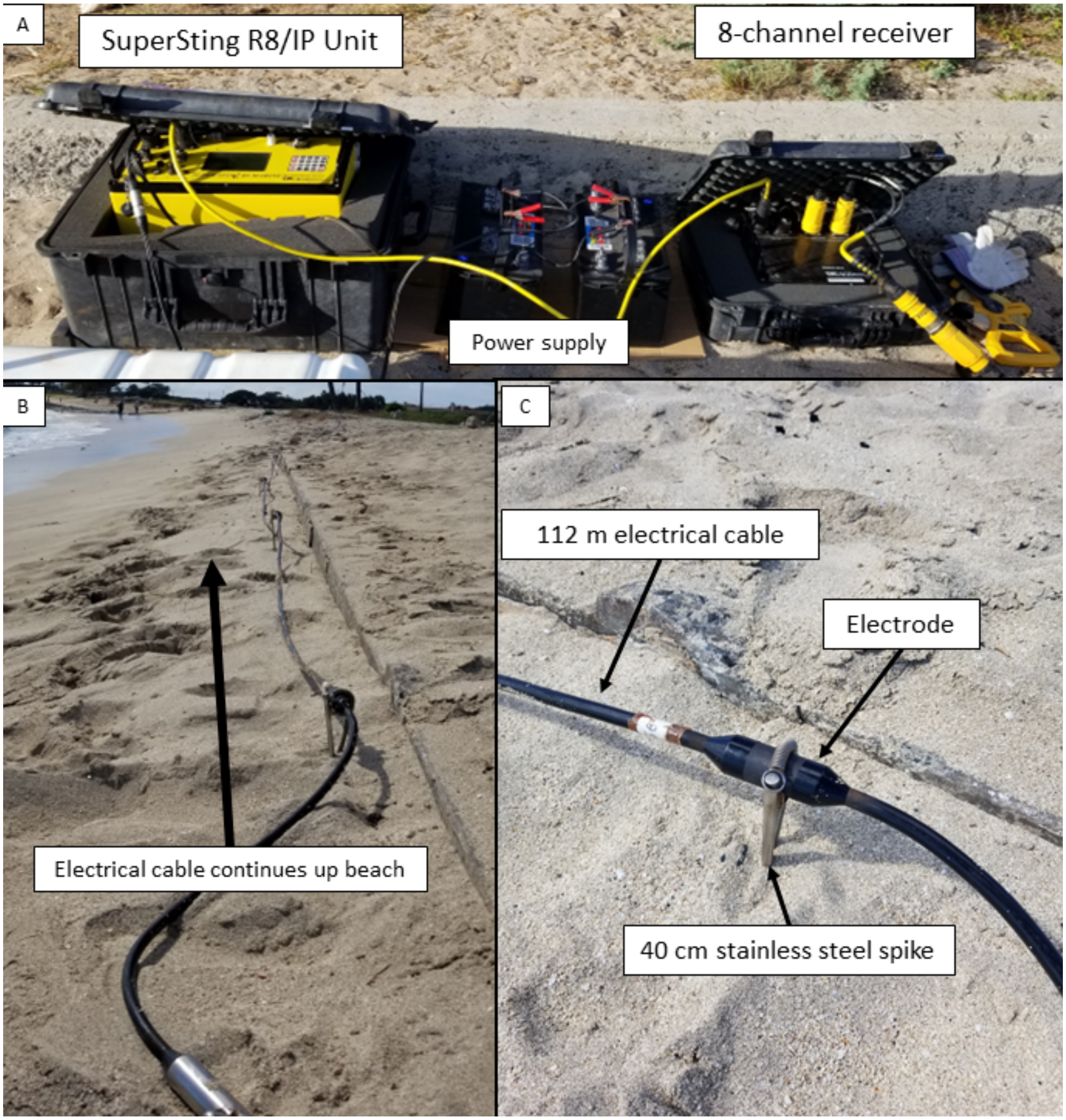

Figure 12: *Photo of setup used for both ERT transects. A: SuperSting R8/IP Unit setup, power supply, and 8-channel receiver. B: 112m electrical cable. C: Close-up of an electrode connected to the ground via 40cm stainless steel spikes.*

3.2 Electrical Resistivity Tests of Collected Sand Samples

Sand samples from three different Beach Parks were analyzed to ascertain the resistivity of unconsolidated sand. **Figure 13** shows the apparatus used. Measurements from the test box are given in Ω-cm (resistivity over the length of the AGI soil test box). Samples were fully dried to ensure moisture would not affect measured values. All samples were measured twice; in one test the sample was fully saturated with fresh tap water, and in the second test the sample was fully saturated with study-site seawater.

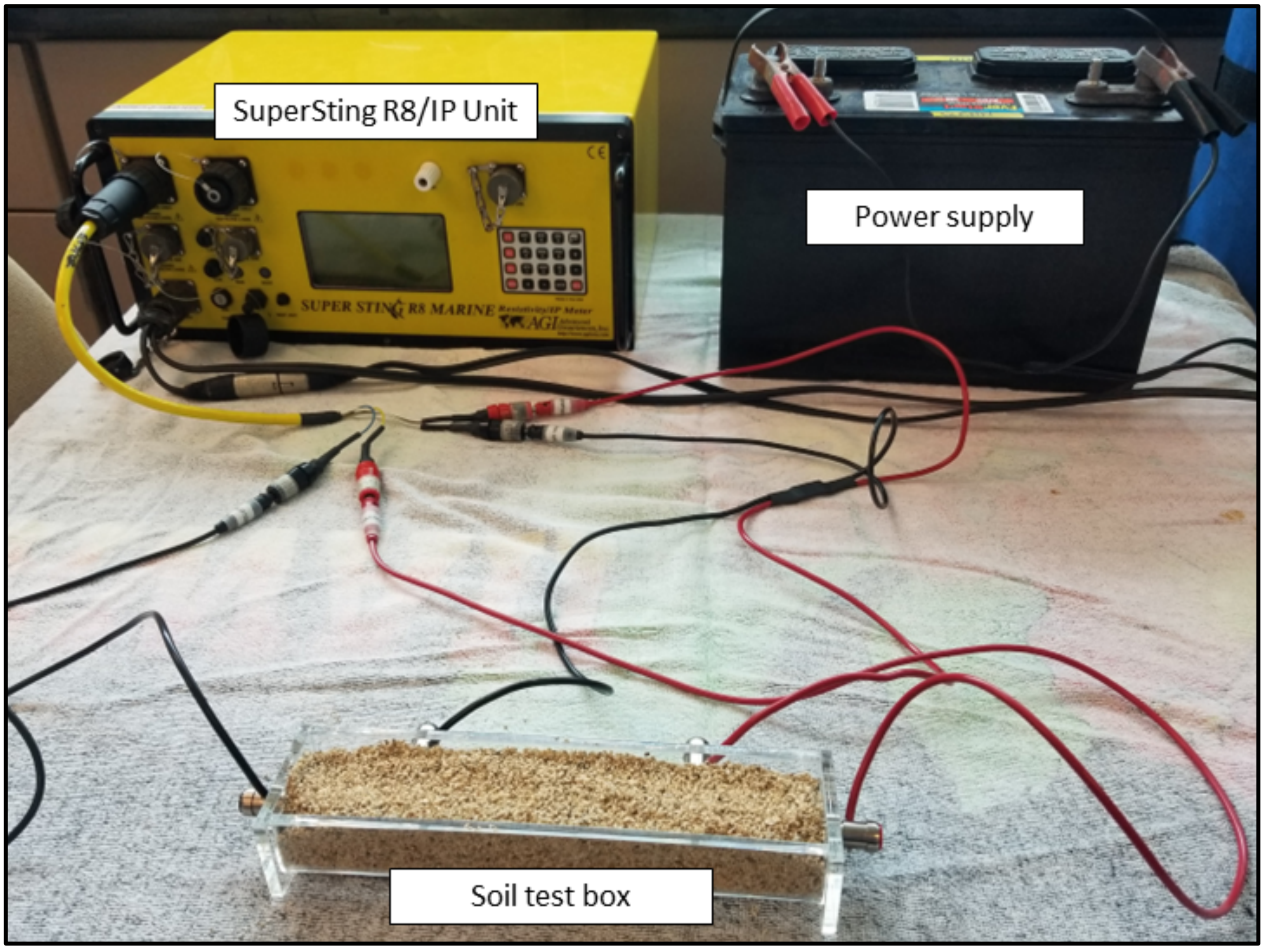

Figure 13*: Setup used to measure the electrical resistivity of variously saturated area beach sand samples using the Advanced Geosciences Inc. soil test box.*

3.3 Groundwater Sampling

Groundwater samples (n=98) were collected between January 2021 and March 2022 on a seasonal basis (wet vs. dry season), with 70 being beachface piezometer samples and 28 being taken directly from groundwater wells. Groundwater well samples came from golf courses and the ‘Ewa Gentry Housing development. Beachface piezometer samples were collected using ¾-inch screened Solinst Ltd. piezometers and pumped via Solinst Ltd. or Global Water Instruments peristaltic pump. Porewater samples were collected from between 0.25 m and 1 m below ground surface. Beachface porewater samples were limited to 1 m in depth as the hard Caprock limestone did not allow piezometers to pass deeper than this. Groundwater well samples were collected using the installed well pumps, and all pumps were purged for at least 10 minutes before the sample was collected. One well without a pump was sampled using Solinst BioBailer groundwater bailers. All samples were filtered through Pall Corp. 0.45μm membrane filters and then bottled in HDPE bottles or glass vials and immediately put on ice to preserve accurate concentrations of nutrients and stable isotopes. HDPE bottles and glass vials were triple rinsed prior to being closed and put on ice. All samples were stored at -12°C until analysis at University of Hawai'i laboratories. In situ parameters including salinity, temperature, and dissolved oxygen were measured from all water collections using a YSI EXO2 multiparameter sonde. All samples were analyzed for dissolved total nitrogen (total N), total phosphorus (total P), phosphate (PO_4), silicate (SiO_2), nitrate (NO_3), nitrite (NO_2), and ammonium (NH_4) at the University of Hawai'i-Manoa SOEST Laboratory for Analytical Biochemistry. Analytically, nitrate + nitrite were analyzed and reported as the sum of NO_3+NO_2, and since nitrate was analyzed separately, nitrate was determined by the difference. In this work we consider NH_4^++NO_3+NO_2 to be dissolved inorganic nitrogen (DIN).

3.4 Coastal Salinity Surveys

To help identify possible locations of groundwater discharge, salinity surveys were completed at Pu'uloa Beach Park and Kalaeloa Beach Park during low tide periods in the second half of April and the first half of May. Measurements were conducted at low tide to maximize presence of fresh or brackish groundwater discharging along the coast. Data collection was done while wading ca. 5-15 m offshore. Measurements were taken using Van Essen Instruments CTD-Diver loggers attached to floatation ensuring measurement within 8 cm of the water surface. Salinity was measured and logged on the diver in 8-second intervals. Salinity is reported in PSU. GPS locations were recorded at 8-second intervals to coincide with salinity data from the diver.

3.5 Numerical Groundwater Model

By applying the groundwater conceptual model described in the following section a numerical model was developed to simulate the hydrogeology of the 'Ewa Caprock and to assess nutrient fate in the subsurface. Specifically, using the Aquaveo Groundwater Modeling System (GMS), the three-dimensional simulation software MODFLOW and MT3DMS codes were used to simulate the impact from different potential sources of groundwater nutrient pollution.

MODFLOW is a finite-difference flow software that is typically used for assessing groundwater levels (or hydraulic head), flow directions and rates, and boundary water fluxes. A calibration process is first conducted to identify values of various parameters, such as hydraulic conductivity, which provides the best match between measured and estimated hydraulic head data. The results of the calibrated MODFLOW are then used as an input to the MT3DMS software, which is a solute transport model able to simulate impact from different dissolved species. Within the context of this study MT3DMS was used as a tool to understand the areas where there is higher relative nitrogen impact from various land use practices.

Because a majority of groundwater wells were only drilled into only the upper limestone portion of the ‘Ewa Caprock Aquifer (Bauer, 1996), we restricted our numerical model to examine this unit. Additionally, as the recharge directly related to OSDS, golf courses, agriculture, and R-1 and R-O water irrigation is recharging into the top of the ‘Ewa Caprock, the impact from these potential nutrient sources is greatest in this unit. Reported and modeled data from Oki et al. (1996) served as the basis for hydraulic conductivity values used in the model calibration process. The upper limestone unit was modeled as being anisotropic. Due to our lack of detailed knowledge of geometry, location, and prevalence of karstic conduits, the upper limestone unit was modeled as an equivalent porous media unit of limestone, avoiding difficulties in adopting a multi-domain approach that includes flow through porous zones and preferential flow through karstic conduits. Because modeling the upper limestone unit as an equivalent porous media devoid of karstic features is not accurate to known data about the ‘Ewa Caprock, the decision to do this limits eventual results but is necessary given the lack of data. Based on borehole logs, the upper limestone unit sits atop and is underlain by a layer of ubiquitous brown mud that is interpreted to be a low permeability unit (Figure 3; Bauer, 1996). This mud layer is thought to be pervasive across the ‘Ewa Plain and in our model separates the upper limestone unit and the deeper limestone and alluvium units of the ‘Ewa Caprock. The boundary of the ‘Ewa Caprock Aquifer used in the model was the previously illustrated CWRM boundary (diagonally lined area in Figure 7).

3.51 Conceptual Model and MODFLOW Set Up

The conceptual model and numerical-model grid are shown in **Figure 14**. Using known boundaries of the ‘Ewa Caprock Aquifer (CWRM, 2018), the model area covers the entire ‘Ewa Plain from Kahe on the west to the West Loch of Pearl Harbor on the east. Although these boundaries extend beyond those of the previously mentioned study, we adopted this regional approach in order to best analyze all data including flow into the study area. The western, southern, and eastern boundaries of the model were set as the coast (at mean sea level) but were assigned a specified head value of 0.01 m to avoid dry cells. Following A specified head of 0.43 m was set for the inland boundary of the numerical grid. The inland boundary head value was estimated using elevation and slope data by Nakanishi, 2002. Horizontal hydraulic conductivity values for the upper limestone unit vary greatly with low-end estimates being ~0.6 m/d and high-end estimates being ~11,000 m/d (Oki et al., 1996). Beneath the upper limestone unit is a layer of low-permeability mud (Bauer 1996; Oki et al., 1996, Figure 3). This mud layer was defined as non-marine by Resig (1969) and is thought to limit groundwater flow between the upper and lower limestone units (Bauer, 1996). Oki et al., (1998) assigned 0.03 m/d for both horizontal and vertical conductivity of the mud layer. The mud lay was assumed to be isotropic. Uncertainties exist regarding the amount of recharge the ‘Ewa Caprock receives from the volcanic aquifer. Current estimates for this value fall between 2.33 m^3/d and 2.94 m^3/d per meter of cross-sectional area (Oki et al., 1996; Oki et al., 1998). An average of these two values was taken and was assigned to the top layer of the inland border of the model to act as recharge from the volcanic aquifer. Vertical recharge data was collected from Engott et al. (2017) who calculated total recharge into the upper limestone aquifer considering rainfall, irrigation, OSDS related leakage, land use/land cover, and evapotranspiration. Data for both pumping wells and observation wells were taken from the CWRM well inventory. For the final model, 54 pumping wells and 30 observation wells were included. Topographic data was downloaded from the Hawaii Statewide GIS program and cell top elevations were assigned to the model grid. Using these parameters, a steady-state MODFLOW groundwater model was created and calibrated. Modeled parameters are listed in **Table 2**.

A three-dimensional grid was constructed for the area. The grid consisted of 100 m x 100 m wide cells and was 10 layers thick. Within all 10 layers of the grid there were 34,130 active cells. The aquifer was modeled as a wedge-shaped polyhedron to match caprock geometry with variable thickness (**Figure 15**). Caprock thickness data was based on Izuka et al. (2018), who estimated caprock thickness across O'ahu and borehole core data from Oki et al. (1996).

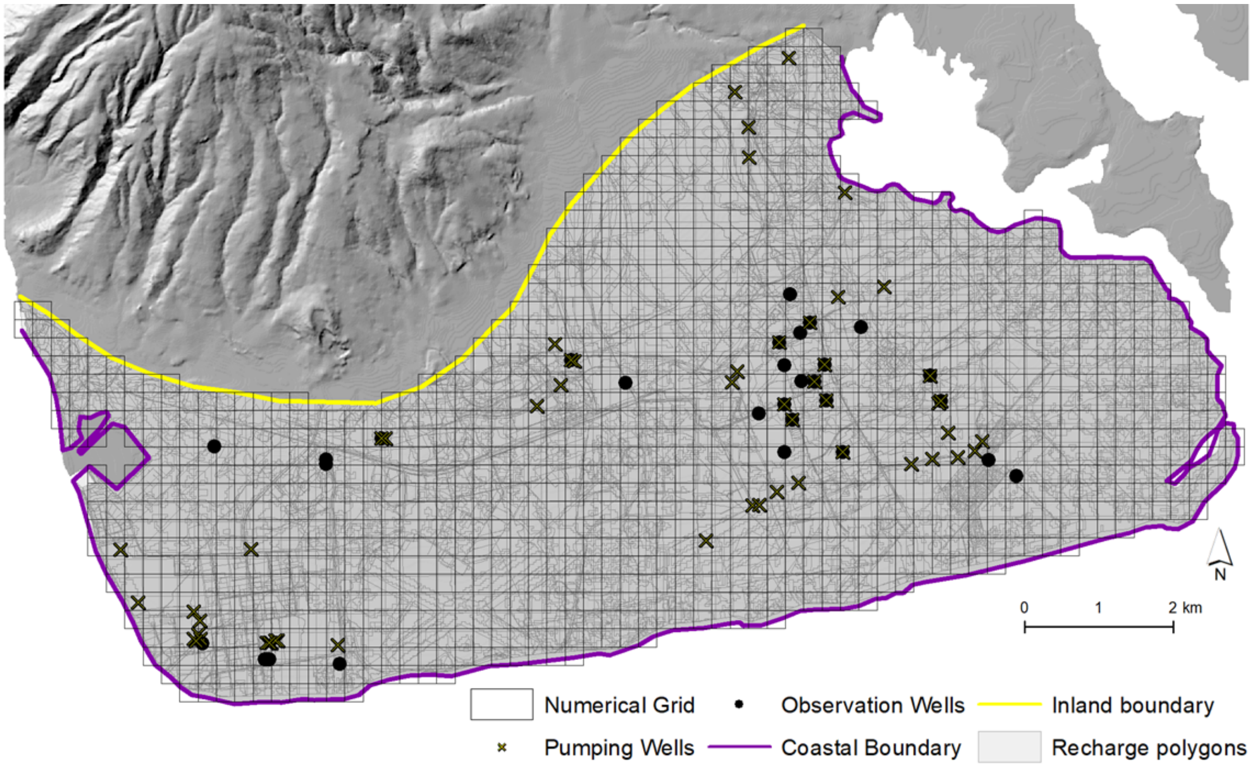

***Figure 14**: Conceptual model inputs and MODFLOW grid created to calibrate numerical groundwater model*

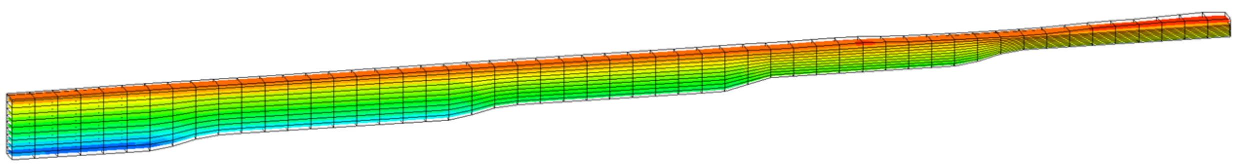

***Figure 15**: Oblique cross-section view of the model showing the wedge-shaped polyhedron form. 5x vertical exaggeration.*

Table 2: Full parameters and other information used in the conceptual model			
Parameters and other data	**Value**	**Units**	**Data source**
Elevation	0 - 14.3	m	Hawaii Statewide GIS Program
Pumping wells pumping rate	81.8 - 16898.1	m^3/d	CWRM well inventory log
Observation well head	0 - 0.914	m	CWRM well inventory log
Specified head level for the coast	0.01	m	Mason, 2020
Specified head level for inland boundary	0.43	m	Nakanishi, 2002
Horizontal Conductivity (h_k)	1100 - 11000	m/d	Conductivity ranges from Oki et al., 1996
Vertical Conductivity (v_k)	110-1100	m/d	Manually calibrated
Vertical anisotropy (h_k/v_k)	10		Oki et al., 1996
Recharge from volcanic aquifer	33615	m^3d	Calculated from Oki et al., 1996
Caprock thickness	16 - 83	m	Izuka et al., 2018
Mud thickness	1.75 - 10.13	m	Bauer 1996; Oki et al., 1996

3.52 MODFLOW Model calibration

Our steady-state MODFLOW model was calibrated via parameter estimation software PEST (Doherty et al., 2011; PEST, 2021) by using the pilot points approach. This approach assigns 2D scatter points, called pilot points, to certain locations within the grid and optimizes the horizontal hydraulic conductivity that produces the lowest overall hydraulic head errors (Doherty et al., 2011). Following Oki et al. (1996), the caprock was assumed to be anisotropic with a ratio of the horizontal hydraulic conductivity to the vertical hydraulic conductivity of 10 for all upper limestone unit layers. Using published data for hydraulic conductivity values from Oki et al. (1996), the limits of horizontal hydraulic conductivity were set from 1100 m/d to 11000 m/d. For our model, 88 pilot points were used and 75 PEST calibration iterations computed the optimized hydraulic conductivity values.

3.53 MT3DMS Setup

MT3DMS was used to simulate total dissolved nitrogen (TDN) and dissolved inorganic nitrogen (DIN) to simulate the areas of the ‘Ewa Plain where impact from different sources of nitrogen would be the highest. TDN is the concentration of total dissolved nitrogen in the system and that includes ammonium, organic and reduced nitrogen, and nitrate-nitrite. DIN is the sum of the readily available forms of N, nitrate, nitrite, and ammonium. TDN and DIN were modeled separately to assess the impact from all N in the system compared to DIN. Simulating relative DIN concentrations allows for a simulation of a conservative nitrogen species while still accounting for all inorganic nitrogen within the system. We designated average nutrient TDN and DIN concentrations we measured in the groundwaters, thereby indirectly accounting for the biogeochemical reactions within and driving chemical speciation between nitrogen pools (1.e. nitrogen fixation, ammonification, nitrification, denitrification, etc.) In this approach, recharge concentration values were assigned to five different sources of nutrient pollution comprising, general background soil processes, OSDS effluent, agricultural fertilization, golf course fertilization, and R-1 water irrigation (**Figure 16**). Using data from our geochemical analyses of water samples recharge concentrations for each source was estimated. These concentrations were then split up into TDN recharge concentration and DIN recharge concentration for their respective source. The model was run for 100 years until steady-state conditions were met.

It is important to note that the MT3DMS model was not calibrated with collected field data. Beachface porewater samples generally had much lower concentrations of TDN than well water samples. This pattern is illustrated in **Figure 17**. While the MT3DMS model was uncalibrated, the results serve as a tool to show areas where different sources of nitrogen are having the largest relative impact on the groundwater. Collected field data was used to calculate the simulated DIN from each source. This allows the MT3DMS simulations to be internally consistent with and illustrate the impact from DIN relative to one another despite being uncalibrated.

Nitrogen inputs for Cambell Industrial Park (CIP) (Figure 16) is limited to background processes and ~180 OSDS units, and are underestimated and thus inaccurate due to a combination of lack of accurate recharge data for this area (J.A. Engott, U.S.G.S California Water Science Center, August 3, 2022, personal communication) as well as lack of knowledge on the specific industrial happening within the CIP. These industrial processes may likely contribute excess nitrogen input into the region but, as discussed below, our results do not reflect this input.

Due to how MT3DMS interprets nitrogen recharge data, point source locations of recharge, such as OSDS or R-1 water to specific golf courses were grouped into polygons. To accomplish this a grid was created and all cells that did not contain any OSDS were removed. Two sewage samples were taken at the Honouliuli Wastewater Treatment Plant and served as the OSDS endmember. TDN and DIN values for the OSDS endmember do not account for complex nitrogen transformations and assume the eventual outcome is most nitrogen within in the system is converted to nitrate. This assumption follows our geochemical analyses data in which the DIN was largely nitrate but did have a non-zero concentrations of both ammonium and nitrite. As specific conditions and fertilizer use are not known for each golf course the model assumed the golf courses that do use R-1 water do not alter their fertilizer regimes to account for increased nitrogen derived from R-1 water irrigation.

R-1 water is treated wastewater that is not potable, however it is and may be used for irrigation of green spaces, such as golf courses and parks. Currently, R-1 water is primarily used by golf courses to irrigate various golf courses on the ‘Ewa Plain. Several other locations use R-1 water but the quantities of R-1 water used are significantly lower than that by the golf courses. In total, golf courses use an average of 7.4 million gallons of R-1 water per day (BWS 2014). All the R-1 water used on the ‘Ewa Plain is treated and pumped from the Honouliuli wastewater treatment plant (location shown in figure 9) to users on the ‘Ewa Plain.

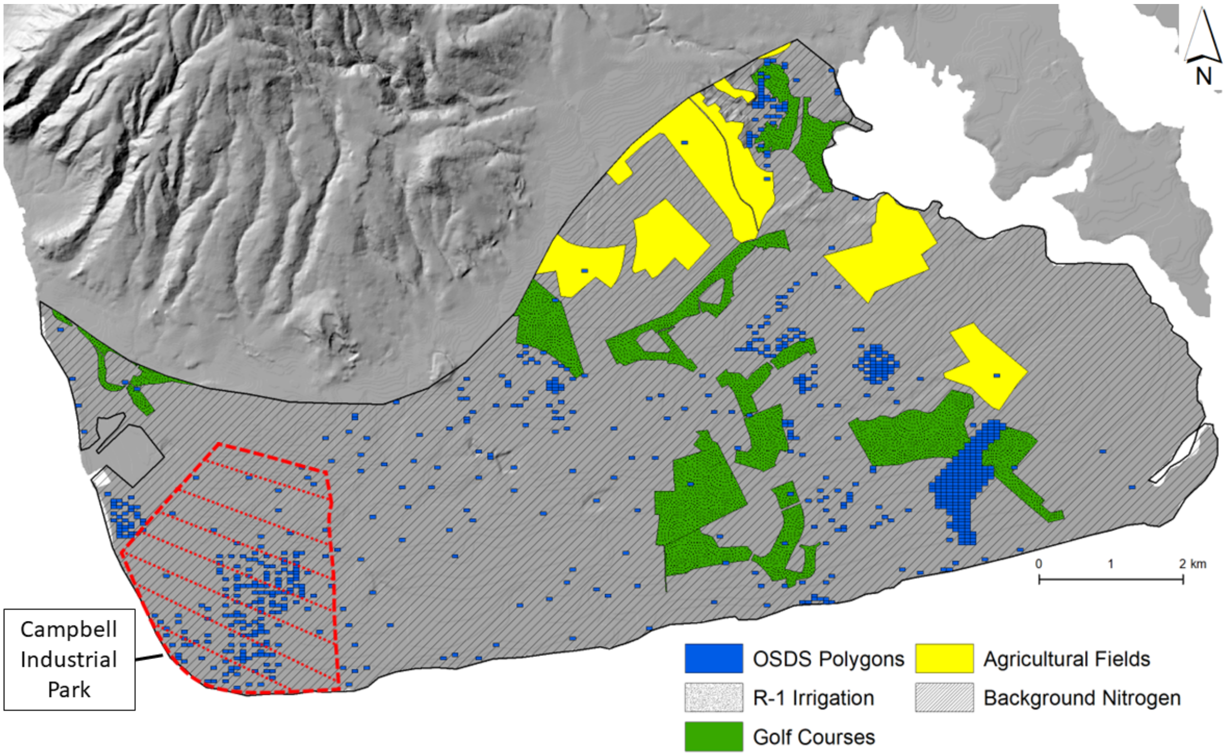

Figure 16: *MT3DMS model set up showing the spatial variation of each land-use source of nitrogen input. Red outline indicates area of under-modeled recharge*

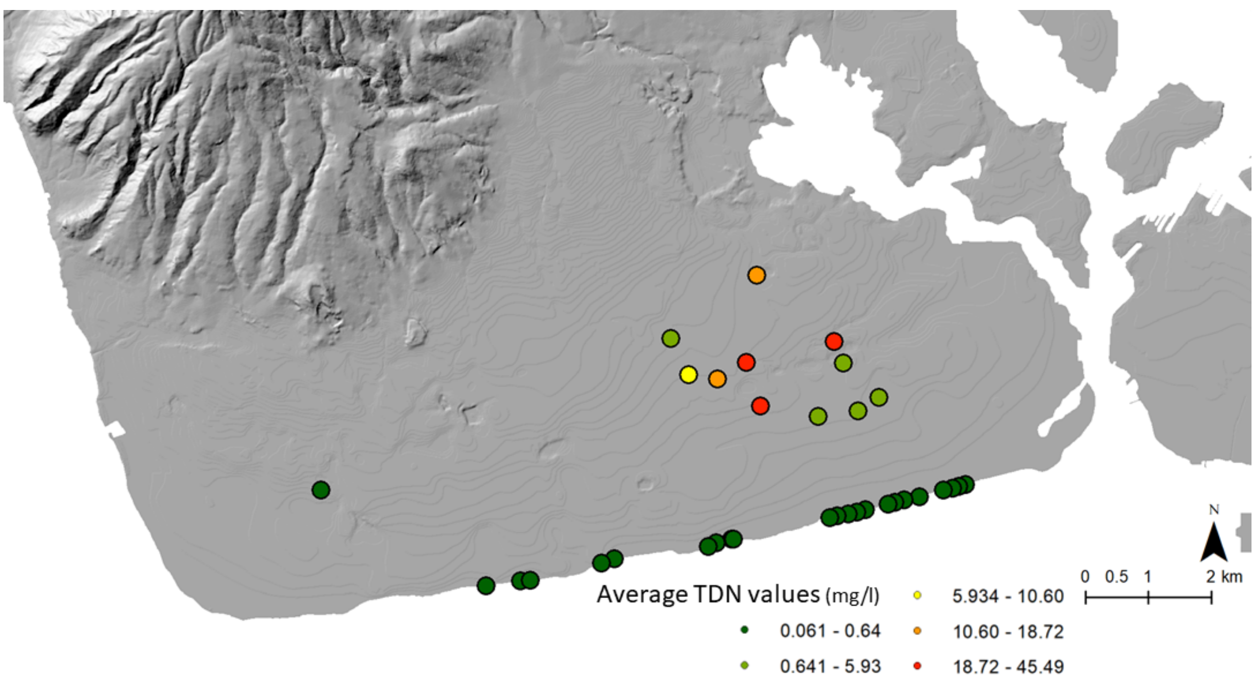

Figure 17: *Map of TDN concentrations from the beachface porewater samples and groundwater well samples. Wells showed higher TDN values than beachface porewater samples*

4 RESULTS AND DISCUSSION

4.1 Electrical Resistivity Tomography Transects

Inverted pseudosections (**Figures 18** and **19**) were created after ERT data was uploaded to Earth Imager 2D to visualize the collected resistivity data. These pseudosections are produced by an application of a non-linear model interpreting measured resistivity data and producing a visual representation of the near subsurface geology. Inverted means that these single resistivity measurement points have been interpolated across the length of the ERT transect, and thus a full cohesive cross-section is created showing resistivity for subsurface units. A by-product of the inversion process is that reported values at the sides and bottom of each section are less accurate than at the top or middle. Figures 18 and 19 specifically show the results from ERT transects conducted during high tide and low tide at One'ula and Kalaeloa Beach Parks, respectively. In both Figures 18 and 19 the cooler colors (blues and greens) indicate areas of low electrical resistivity indicating electrical current passes through those layers easier than in areas shown by warmer colors (reds and yellows). To properly interpret inverted resistivity pseudosections it is important to understand how different geologic units respond to electrical current. Several main factors control the electrical resistivity of a given geologic unit. These factors include water-rock interactions and physical characteristics of the unit such as the porosity and permeability (Hersir and Bjornsson, 1991). **Table 3** provides general electrical resistivity value ranges for relevant geologic materials as well as fresh groundwater and seawater from Saad et al. (2012). These are expected ranges not applicable to all situations but do provide an important reference.

Results from One'ula Beach Park and Kalaeloa Beach Park share similarities across the high and low tide measurements. The dashed black line in Figures 17 and 18 denotes the contact of the saline water table and overlying beach sediments that are not fully saturated by salt water above them. These zones were inferred based on collected data from each ERT transect and resistivity of collected sand samples which helped to constrain the resistivity of sediments saturated with saltwater. The measured resistivity values for the area under the black dashed line are < 1.4 Ω-m for both transects. These resistivity measurement ranges fall within published ranges for both seawater and seawater saturated materials (Zhody and Jackson, 1969; Saad et al., 2012) and are lower than values expected for fresh groundwater and groundwater in sedimentary units (See Table 3). Beachface pore water samples collected during ERT transects had an average salinity of ~34, suggestive of some freshwater, but only in minor amounts. Despite the top layer of the ‘Ewa Caprock being composed of marine-derived limestone, a high-resistivity signal for limestone (e.g. 50 to 4000 Ω-m; Table 3) was not itself detected. Limestone has a much higher resistivity than what was measured at either of our ERT transects (Gelis et al., 2010; Saad et al., 2012; Sun et al., 2017), and the lack of significant limestone resistivity values is most likely due to proximity to the coast and the presence of saltwater dominating all measured resistivity values (Pujari and Soni, 2008) below the black dashed line.

Marked by high relative resistivity, the area above the black dashed line in Figures 17 and 18 is where sediments not fully saturated by water are found. Above the water line, both transects share similar geometry with a generally horizontal shape and high relative resistivity zones spanning the length of the transect. The measured resistivity of the areas above the black dashed line is > 3 Ω-m. This area of high resistivity is a layer of loose beach sediments atop more compacted beach sediments neither of which are fully saturated by water. The values seen at One’ula Beach Park are slightly below the expected values for general alluvium (Table 3). General alluvium is not a perfect proxy for beach sand sediment but the values do still provide resistivity values for unconsolidated sediment resistivity values. As stated previously, the ERT transect at One’ula was selected due to its proximity to an SGD spring. However, if there are specific conduits feeding this SGD spring, they are not evident in either the high tide or low tide pseudosections from One’ula Beach Park.

Due to minor variations in the sampling array, there are several small areas of erroneous data across the four measurements. These areas do not have an impact on the overall quality of each pseudosection but are important to note. Data included in all pseudosections is accurate with a 95% confidence level, meaning data shown is an accurate representation of in-situ conditions along each transect. In addition, the SuperSting R8 platform and Earth Imager 2D software can remove erroneous measurements decreasing total error across each inverted pseudosection produced. The source of errors during ERT transects is largely unclear, but can stem from voltage leakage across electrodes, changing environmental conditions, or faults within the equipment itself (Oldernborger et al., 2005; La Brecque et al., 2007). It is unlikely these errors contributed to misinterpretations of the final inverted pseudosection as all erroneous measurements were removed before the final inversion of measured data. **Figures 20** and **21** are an error crossplot of resistivity data and error histogram from all measurements. In Figure 21 a vertical blue line indicates all data to the right of the line was not included in the final inversion calculations. Figures 20 and 21 also show that most individual measurements fell within the 95%

confidence interval with a few higher resistivity measurements not being included in final pseudosection inversion.

The four ERT measurements conducted across two transects produced high-resolution images of the ‘Ewa subsurface. Importantly, all four inverted resistivity pseudosections of these sections failed to show distinct point source locations of SGD, pointing to a different process that causes SGD along the ‘Ewa Coast. However, due to its proximity to the coast, most of each section is dominated by a seawater signal.

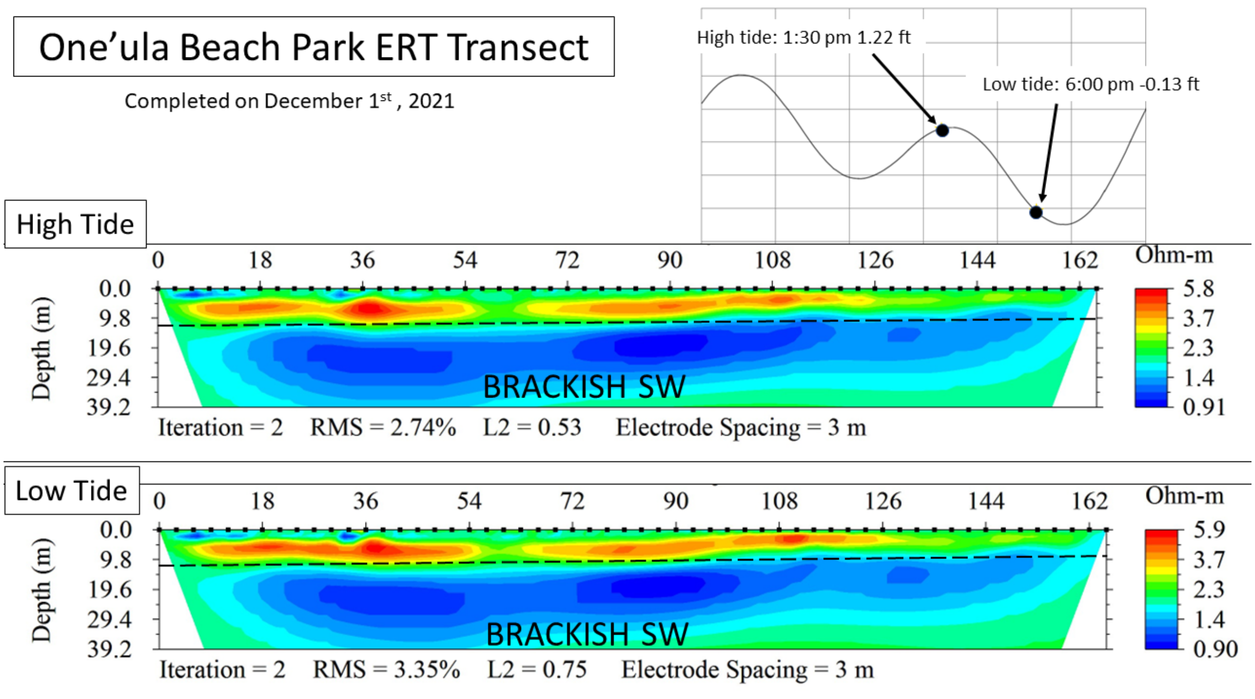

***Figure 18**: Inverted resistivity pseudosection produced from shore-parallel One’ula Beach Park transect. Dots at the surface show distance in meters. The Black dashed line indicates the contact between the unsaturated area and the area that is fully saturated by seawater.*

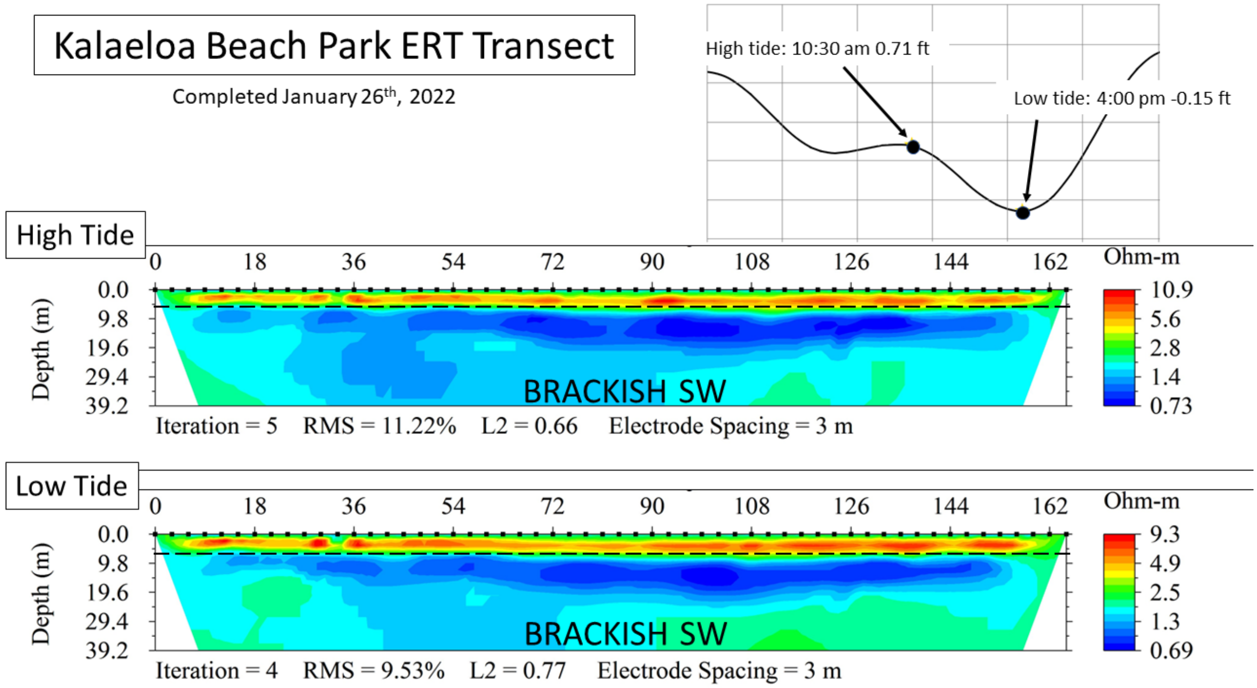

Figure 19: *Inverted resistivity pseudosection produced from shore-parallel Kalaeloa Beach Park transect. Dots at the surface show distance in meters. The Black dashed line indicates the contact between the unsaturated area and the area that is fully saturated by seawater.*

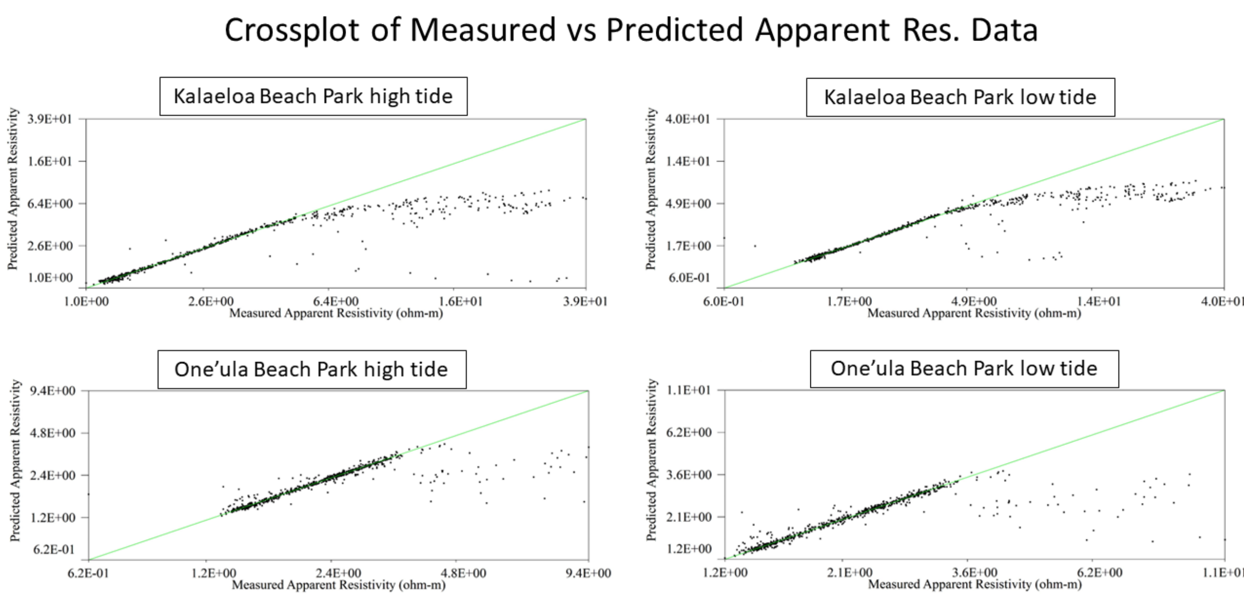

Figure 20: *Error crossplots for the four ERT measurements done along the two Beach Park transects*

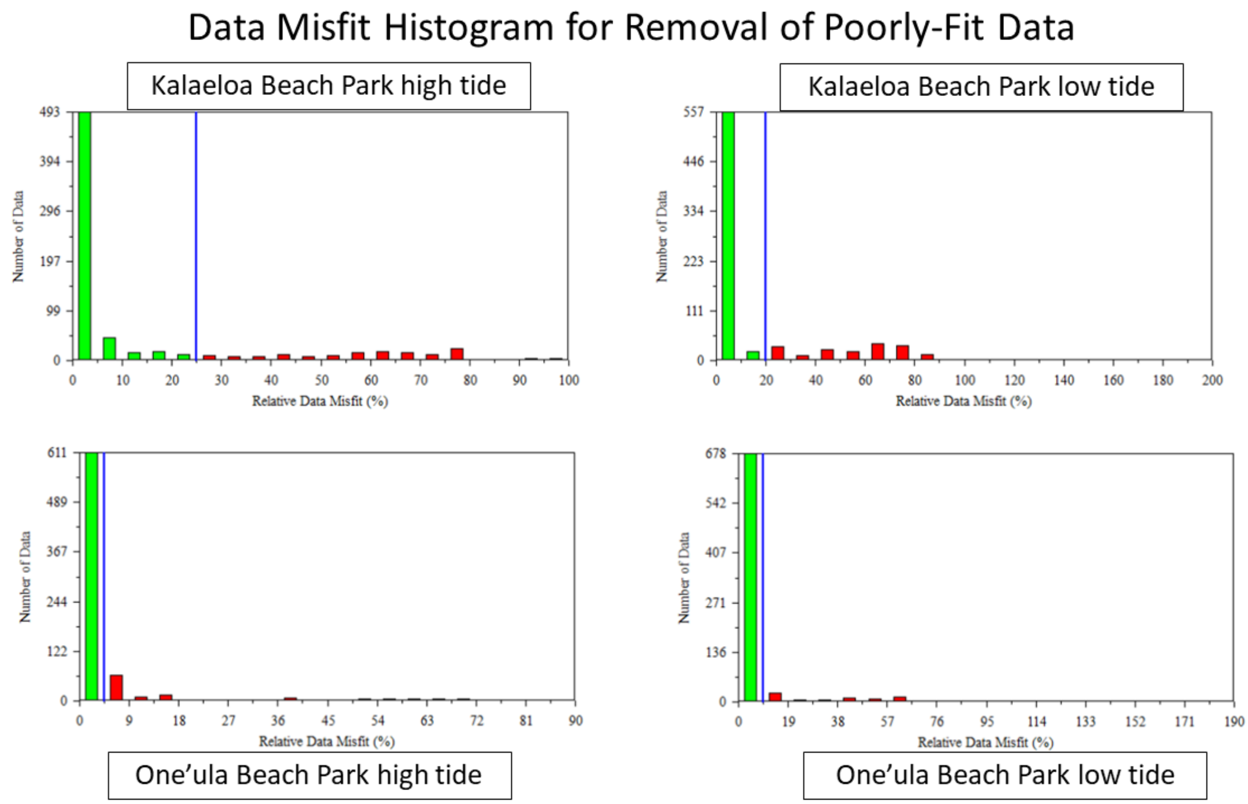

Figure 21: Data misfit histogram from all four ERT measurements from both Beach Park transects. Any histogram bar to the right of the blue line, or colored red, was labeled as erroneous and excluded from the final pseudosection.

Table 3: Table of general resistivity values of various geologic units (Saad et al., 2012)

Material	Resistivity (Ω-m)
Alluvium	10 to 800
Sand	60 to 1000
Clay	1 to 100
Fresh Groundwater	10 to 100
Sandstone	8 to 4000
Limestone	50 to 4000
Seawater	~0.2
Groundwater in sedimentary units	>1

4.2 Electrical Resistivity of Collected Sand Samples

Results from ERT sand sample lab tests are shown in **Table 4** and indicate, as expected, that freshwater saturated sands show considerably higher resistivity than samples saturated with saltwater. This supports the conclusion that the large area below the dashed line in Figures 17 and 18 is the saline water table. Freshwater saturated sand sample results create an interpretation problem, however. Values of the freshwater saturated sand samples all fall within the range of the high resistivity areas (areas above the black dashed line in Figures 18 and 19) from the in situ transects. Therefore, it is likely that pore space in the beach sediments above the saline water table are unsaturated vadose zone sediments that are not saturated by significant discharging groundwater. The lack of point source locations of discharging freshwater is supported by field observations, beachface pore water samples, and salinity surveys conducted over many months that indicate a lack of freshwater SGD occurring at these beaches. This is also illustrated by a lack of SGD discharge along this coast as detected by aerial infrared imaging in previous work (Kelly, 2012). This does not totally preclude the presence of SGD along the ʻEwa Coast, however. Freshwater SGD may be discharging further offshore or is being diluted by infiltrating seawater to a point that it is not seen clearly on the ERT transects, or some combination of both. Notwithstanding, the interpretation of dry unconsolidated and consolidated sediments offers a valid explanation for the high resistivity zones of surface beach sand sediments seen in the in situ transects. It should be noted that a limitation of collecting loose surface sand in measurements may not be 100% indicative of the resistivity of deeper limestone, but due to the depth of the limestone units, surficial beach sand offers the best proxy.

Table 4: Measured resistivity results from collected sand sediment samples

Sample	Ohms-cm
Pu'uloa Beach Park freshwater fully saturated	7.60
One'ula Beach Park freshwater fully saturated	4.89
Kalaeloa Beach Park freshwater fully saturated	3.68
Pu'uloa Beach Park salt water fully saturated	0.920
One'ula Beach Park salt water fully saturated	0.768
Kalaeloa Beach Park salt water fully saturated	0.711

4.3 Groundwater Geochemistry

A table with locations of geochemical samples and their abbreviated names can be found in **Table 6** and the full geochemical analysis results are shown in **Table 7**. On average, samples from groundwater wells have dramatically higher concentrations of all measured nutrients compared to beachface pore waters. Additionally, samples from groundwater wells have a much lower average salinity of 1.73 indicating these wells lie above the zone of saline groundwater below (Figure 5). Beachface pore water samples have a much higher average salinity of 33.43 combined with lower overall concentrations of nutrients. These lower nutrient values indicate the fresh groundwater carrying the nutrients is being diluted by saline seawater. The exception to this is the one beachface SGD spring sampled at One'ula Beach Park. This spring had a salinity of 18.77 and much higher nutrient concentrations the all the other beachface pore water samples. The spring's nutrient concentrations also indicate a significant freshwater component as the nutrient concentrations were much closer to the groundwater well nutrient concentrations than pore water nutrient concentrations. When compared to other studies conducted in Hawaii (**Table 7**), 'Ewa has higher average concentration values in both beachface porewaters and groundwater from wells. While not significantly higher than other studies, concentrations of nutrients in our well samples indicate an equal or greater amount of nutrient pollution occurring on the 'Ewa Plain. This is specifically the case for nitrate, which have average measured nitrate concentrations of 307.2 μmol/l.

4.4 Coastal Salinity Survey

Over 500 individual salinity measurements were collected throughout the salinity surveys at Pu'uloa and Kalaeloa Beach Parks. Of these, only 19 detected a salinity below 31, with the lowest overall salinity being ~15. Open ocean waters around Hawai'i have an average salinity of ~35 (Talley, 2002). The 19 locations with salinities below 31 may indicate mixtures of freshwater SGD. **Figure 22** is the map of these measurements and **Table 9** is the full set of data collected during the two salinity surveys. These data indicate that most groundwater discharging along the coast is saline with some mixtures of diffuse and point-sourced brackish freshwater. The 'Ewa Caprock may also divert groundwater discharge to farther offshore which would limit the amount of low salinity discharge seen directly along the coast.

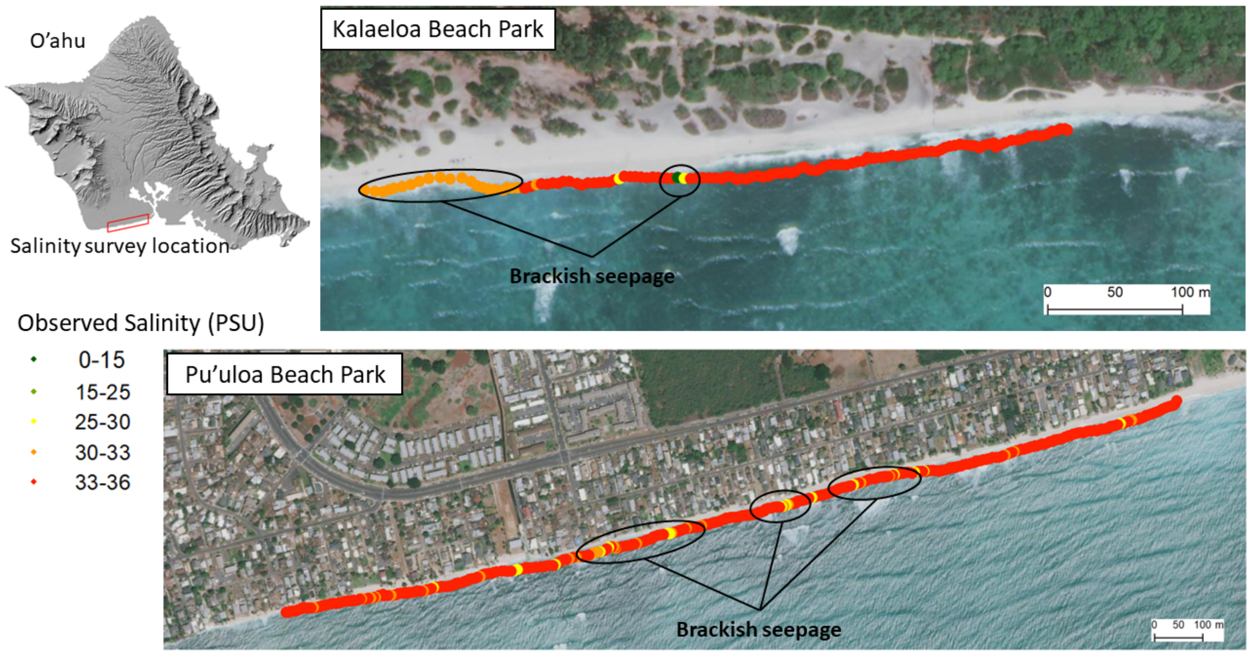

***Figure 22**: Results from the two salinity surveys conducted at One'ula Beach Park and Kalaeloa Beach Park. Circled are zones of lower salinity and thus potential beach leakage of SGD.*

4.5 Numerical Groundwater Model

4.51 Calibrated MODFLOW Hydraulic Head Values

Hydraulic head values computed by MODFLOW are shown in **Figure 23**. Computed head values range from 0.43 m to -0.07 m. The upper and lower limits of horizontal hydraulic conductivity were set at 1100 m/d and 11000 m/d and found to produce the lowest overall error. Horizontal hydraulic conductivity values below 1100 m/d would cause errors with PEST and did not produce reliable or useable results. This result does not mean that hydraulic conductivity for the plain does not fall below 1100 m/d, but instead the ability for PEST to estimate outside of the 1100 m/d to 11000 m/d boundary was limited so the final hydraulic conductivity values were limited within this range. This limits the accuracy of the final modeled head values but allowed for PEST to run normally. The negative computed head values in the plot were in locations of local groundwater pumping operations where drawdown caused a cone of depression causing head values to be lower than sea level. Campbell Industrial Park in the southwest corner of the 'Ewa Plain has significant groundwater pumping operations and is visible as an area of near or below 0 m computed head values (Figure 23).

As the ‘Ewa Plain lacks significant elevation changes, observed hydraulic head values are both generally low and are within 1.0 m. Overall, the model underestimated the head values for most observation points as seen in **Figure 24**. Shown in **Table 5** are the GMS calculated hydraulic head error values. The mean residual error is the mean of all data points, the mean absolute residual is the true mean of the data as negative and positive points do not cancel. The root mean squared residual is calculated by taking the average of the square of all the errors and then taking the square root. The sum of squared weighted residual is the property that PEST works to minimize through its iterations.

A variety of factors may lead to the poor match including localized karstic features greatly altering horizontal hydraulic conductivity, lack of data in certain locations, and well hydraulic head data collected at varying times. Modeling the entirety of the upper limestone unit without karstic features can also cause under-estimated head values. Tidal attenuation may have a significant impact on observed values (Nakanishi, 2002), which may cause certain head values to be either under or over-reported if they were measured during times of tidal extremes. Additionally, inflow from the volcanic aquifer has not been directly measured, and the value used in our model (33615 m^3/d) is an approximation and again, likely adds a significant amount of uncertainty to the computed head values.

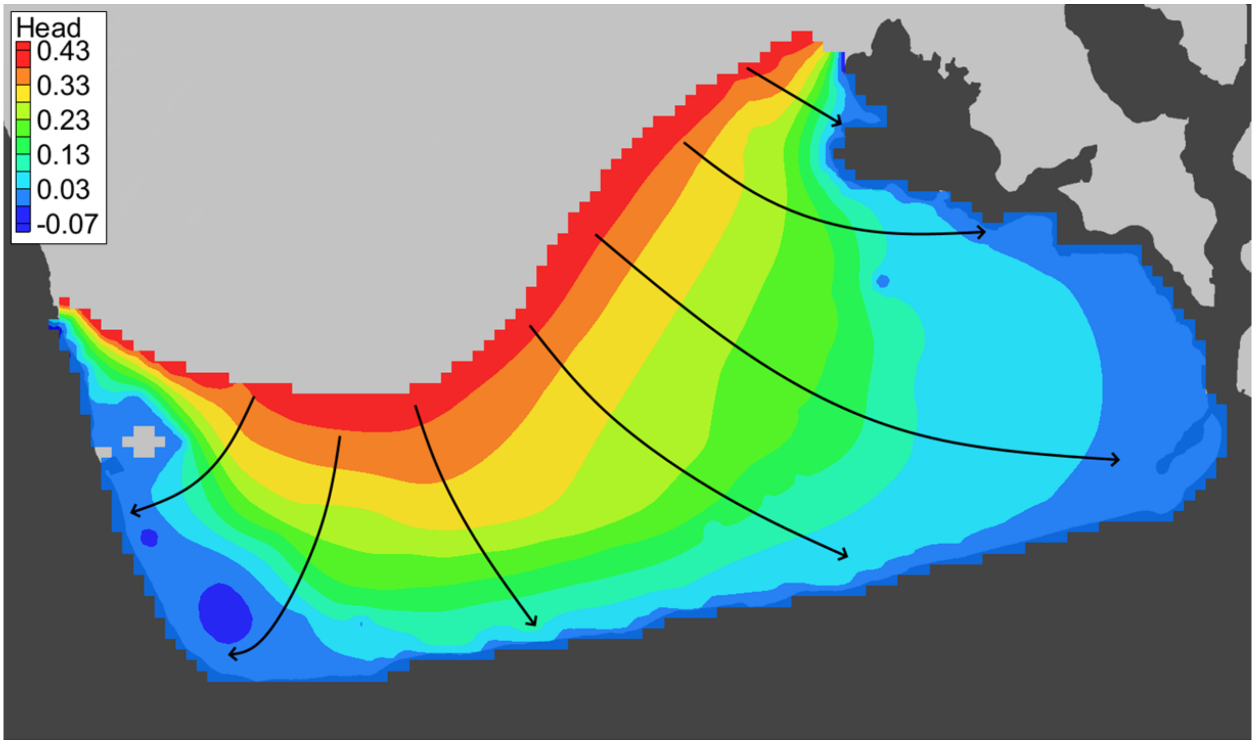

Figure 23: *MODFLOW calculated head values for the upper limestone unit of the 'Ewa Caprock. Interpretive groundwater flow paths are shown as black arrows.*

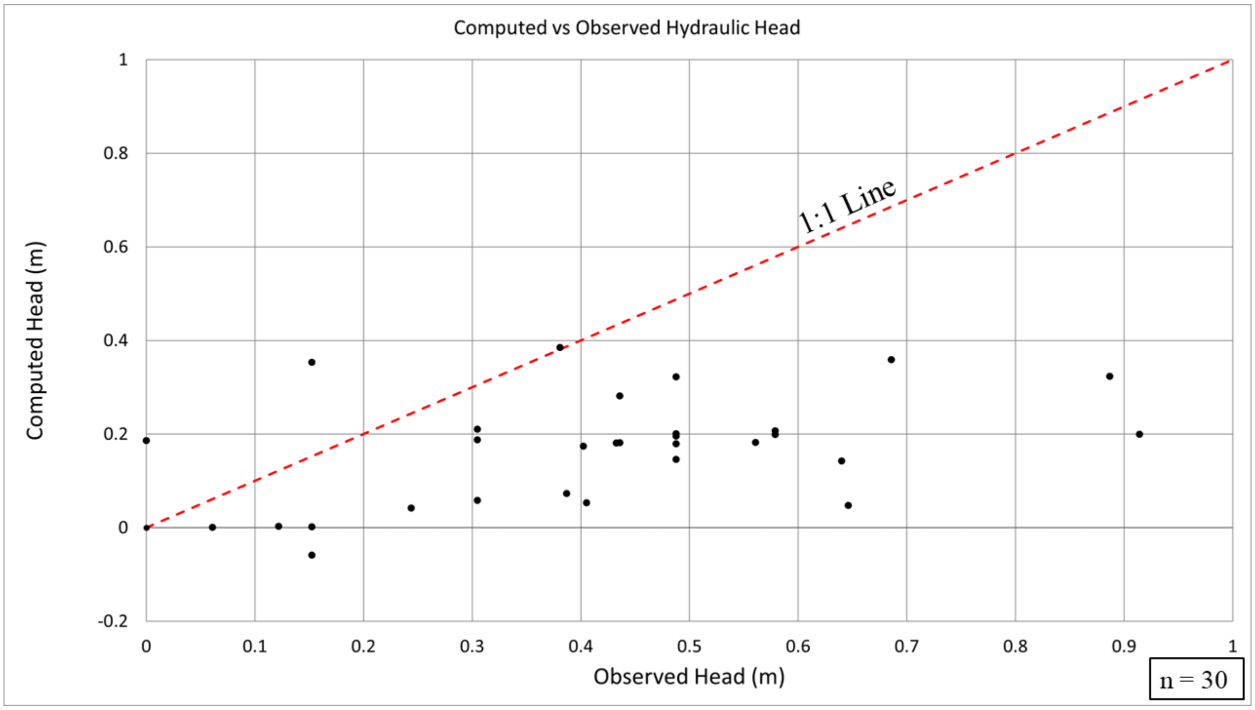

Figure 24: *Computed vs. observed hydraulic head values after 50 PEST parameter calibration iterations, n = 30.*

Table 5: Full error results after MODFLOW calibration	
Property	Value (m)
Mean Residual (Head)	0.25
Mean Absolute Residual (Head)	0.28
Root Mean Squared Residual (Head)	0.32
Mean Weighted Residual (Head + Flow)	0.5
Mean Absolute Weighted Residual (Head + Flow)	0.55
Root Mean Squared Weighted Residual (Head + Flow)	0.63
Sum of Squared Weighted Residual (Head + Flow)	11.86

4.52 MT3DMS Results and limitations

Results for MT3DMS model total dissolved nitrogen (TDN) and dissolved inorganic nitrogen (DIN) simulations are shown in **Figures 24** and **25**, respectively. It is important to note that the color-scaled legends that are different for each nutrient source in Figure 25, constructed such that that the impact of each nutrient source can be visualized. Additionally, it is important to acknowledge the limitations of the MT3DMS results. As the MT3DMS simulations were uncalibrated, the final concentrations as shown in Figures 24 and 25 are not expected to be accurate conditions on the ‘Ewa Plain if compared to a fully calibrated MT3DMS model. What the MT3DMS simulations do illustrate are locations where there are relatively high concentrations of either TDN, DIN, or both, and the sources that are producing the highest relative concentrations of each. Also, the reason TDN and DIN were simulated separately was to model the impacts from two different yet similar sources. TDN was simulated within one layer whereas DIN was separated into the previously mentioned five sources. This was done as DIN species are the nitrogen species which have the highest environmental impact so understanding the locations on the ‘Ewa Plain where these concentrations are expected to be highest is important in future mitigation efforts.

The main goal of the MT3DMS simulations were to create a better understanding of the areas and sources of DIN and TDN that have the highest relative impact on the groundwater quality beneath the ‘Ewa Plain. The outcome of these simulations indicates that OSDS are producing the highest relative concentrations of DIN on the ‘Ewa Plain. The spatial extend of OSDS impact is much smaller than other sources of nitrogen, however, due largely to how many OSDS are clustered in one small area within the city of ‘Ewa Beach. R-1 water irrigation, on the other hand, accounts for a relatively high concentrations of the DIN input into the subsurface which covers a much broader area than OSDS. The R-1 water, and the 7.4 million gallons used per day to irrigate green spaces, may be having a much more profound impact on groundwater quality than previously thought. When R-1 water irrigation is combined with standard golf course fertilization regimes it is possible that golf courses and other green spaces that use both R-1 and fertilizer, are introducing significant concentrations of nitrogen into the subsurface. DIN derived from agriculture has a relatively small impact. Our model does not account for different fertilizers used for the various crops grown, however. The impact from background processes is low and in line with the understanding that anthropogenic sources of nitrogen are generally much higher than what is naturally occurring in the soil and subsurface.

Another important facet of the MT3DMS simulations is the transport of DIN. While the concentrations of DIN are not fully accurate, due to the MT3DMS model being uncalibrated, the transport paths illustrate the areas of the ‘Ewa Plain that may be seeing higher than normal concentrations of DIN, such as the high density OSDS area in ‘Ewa Beach, or the locations of golf courses using R-1 water for irrigation. In the case for both TDN and DIN, OSDS, R-1 water irrigation, and golf course fertilization, the southern coast of the ‘Ewa Plain appears as the zone of highest concentrations. This makes sense given the concentration of both OSDS and golf courses in this area and the direction groundwater is flowing beneath this area. Agricultural DIN appears to not flow towards the southern shore of the ‘Ewa Plain but instead is most highly concentrated towards the west loch of Pearl Harbor. Understanding the directions nitrogen pollution takes is an important step in mitigating the impact and the results from the MT3DMS simulation aids in this task.

In **Figures 25** and **26** the red diagonally marked areas indicate the Campbell Industrial Park (CIP). As discussed above, this area is the location of numerous industrial processes which most likely release nitrogen into the subsurface. The results of both the total nitrogen and DIN MT3DMS simulations failed to calculate significant amounts of nitrogen in this area. As only background processes and OSDS values were assigned to this area these results are expected. This lack of modeled nitrogen of any kind in this area does not mean that no nitrogen input is happening within the boundaries of the CIP. It is probable that industrial processes are releasing nitrogen into the subsurface within the CIP, but, due to a lack of accurate recharge data and lack of knowledge of specific CIP processes, our model undercalculates input within the CIP. Additionally, despite the presence of greater than 180 OSDS units in the CIP there is a near total lack of modeled OSDS-derived nitrogen. This is likely due to the recharge data used for

MT3DMS model simulations. The recharge data used for our model (Engott et al., 2017) included effluent recharge from OSDS units in their calculations of total recharge. It is possible however, that parcels containing OSDS in or near the CIP were not included in the Engott et al., 2017 final recharge calculations. Similar concentrations of OSDS units are found across the ‘Ewa Plain, and are seen in our final model output in Figures 25 and 26, indicating a different reason for the lack of modeled OSDS derived nitrogen within the boundaries of CIP area.

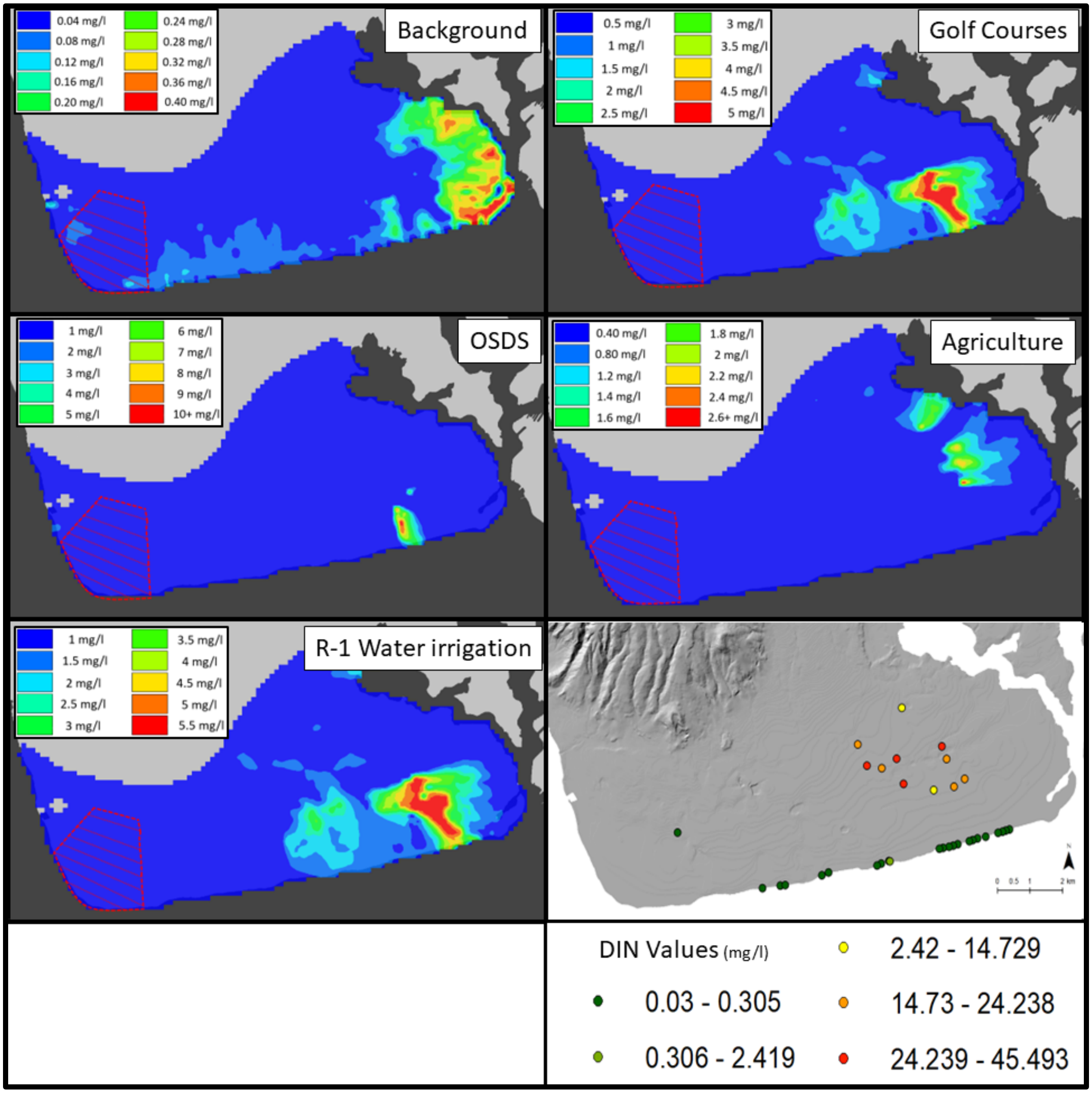

Figure 25: Results from MT3DMS model simulation of dissolved inorganic nitrogen (DIN) pollution for the five major land-use types on the 'Ewa Plain. Note the different scales used for each box. The bottom right box shows measured values of DIN from collected samples from groundwater wells and beachface porewaters.

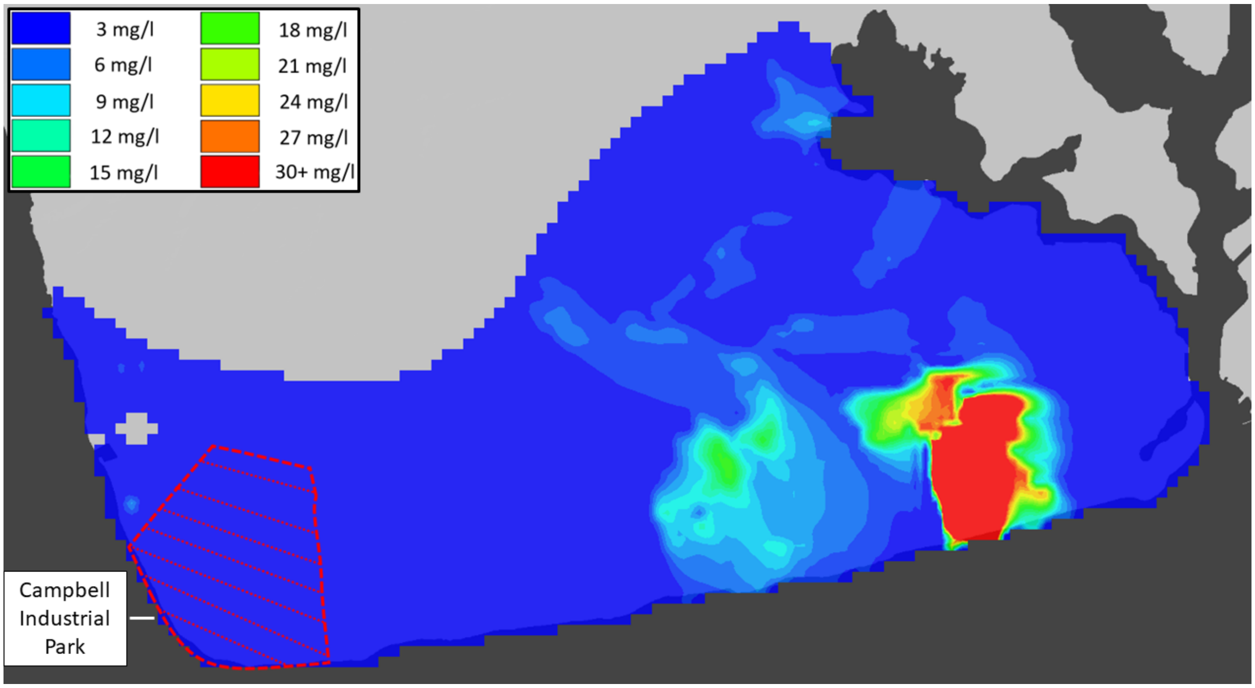

Figure 26: Results from MT3DMS simulation of total nitrogen pollution on the 'Ewa Plain. Areas of higher relative concentration indicate zones where different modeled sources are having the largest impact on nitrogen input.

4.53 R-1 Water Irrigation and Golf Courses

The relative impact from R-1 water irrigation as simulated by our MT3DMS model indicates that R-1 irrigation may be a cause of excess nitrogen into the subsurface. Relative to other simulated sources of nitrogen, the MT3DMS results point towards R-1 water irrigation as having a greater and more widespread impact on excess nitrogen on the ‘Ewa Plain than other sources (Figure 25). Most R-1 irrigation is associated with golf courses but it remains unclear if golf courses have adjusted their fertilization regimes in response to R-1 water usage. The combination of both may be causing much higher-than-normal concentrations of nitrogen to contaminate the upper limestone of the ‘Ewa Caprock.

4.54 Model Assumptions and Limitations

As is the case with any model, there are a few key general assumptions that must be made and limitations with the outcomes because of these assumptions. Several important assumptions were made in the creation of our numerical groundwater model. The primary of these is related to the assumption of steady-state flow conditions. Winter rainstorms and large tidal shifts may cause drastically different conditions than during the summer dry season. However, well hydraulic head values taken over many years show that hydraulic head values have not changed significantly, indicating that steady-state conditions are a valid assumption. Additionally, based on Darcey’s law, the relatively small changes are expected considering the large values of calibrated effective hydraulic conductivity. Simulating a detailed upper limestone aquifer is, however, a more realistic but not practicable as it is not possible to know the location of localized geologic features and the need for an appropriate model that includes these features. Modeling the upper limestone unit as a heterogeneous-anisotropic porous material with a valid Darcy’s law is expected to minimize the impact from karstic conduits that could carry pollution much faster than homogeneous porous media system, even with large conductivity values of 1100 m/d to 11000 m/d.

The model also assumed a constant nitrogen recharge concentration and ignored the fact that golf courses may use differing levels of fertilizer in certain areas of the course. Greens and tee boxes generally receive higher fertilizer use than fairways and rough (May et al., 2009). It is also unknown to the extent golf courses alter fertilization regiments to account for excess nitrogen found in R-1 water. Across the ‘Ewa Plain golf courses use 7.4 million gallons of R-1 water per day so the nitrogen load from this source may be unaccounted for by golf courses and land managers.

Areas of the ‘Ewa Plain which are not developed are largely covered in Kiawe trees. These trees are a known nitrogen fixer (Dudley et al., 2014), and may alter the nitrogen concentration and composition of the upper portion of the ‘Ewa Caprock. As stated above, this was another reason why DIN was selected to simulate and why collected groundwater well samples were used to calculate the DIN recharge concentrations. Simulating the relative impact of DIN allows for assumptions to be made about the nitrogen cycle and the complexities of different nitrogen species changing as they move through the subsurface.

5. SUMMARY AND CONCLUSIONS

Groundwater nutrient pollution leading to adverse human and ecosystem health impacts are well documented and the identification of nutrient loading and its mitigation in the 21st century remains an important task for nearly all countries and territories across the globe. Islands are particularly susceptible to nutrient pollution as on them most of the populace live directly adjacent to the coast. Our study of the ‘Ewa Plain on Oahu is an important example of this problem in an insular setting where a rapidly growing populace struggles with a lack of local fresh water combined with stressors of high-density legacy cesspool OSDS, the needs for fertilizers and adaptation to wastewater reuse to cope with recreation, and a heightened awareness of the need to protect its coastal ecosystem from environmental degradation. To address this problem, our study combined multispecies groundwater tracing, geochemical nutrient analyses of water samples, electrical resistivity transects, and salinity surveys to find the sources and fate of nutrient pollution within this region, which is the most rapidly growing region within the state of Hawaii.

Two electrical resistivity transects were completed and represent some of the first high-resolution interpretations of the ‘Ewa Plain subsurface. Results from these transects showed areas of loose beach sediments on top of saltwater-saturated limestone beneath. The transects showed uniformity in beach sediment geometry across the two transects and the saltwater zone is generally a uniform depth. These transects failed to identify karstic dissolution features and may be due to recrystallization of the dissolved limestone causing a lack of obvious karstic conduits. Laboratory resistivity tests of collected sediment samples helped to further our understanding of the field ERT transects. Of the beach sediments were collected, half were saturated with freshwater and half with seawater. Laboratory results from each verified that the results from the ERT transects were valid and demonstrated dry or undersaturated beach sediments directly atop the saltwater zone below.

Geochemical analyses of groundwater and beachface porewater samples revealed elevated levels of nutrients in nearly all samples. Groundwater well nutrient concentrations were very high and point directly to groundwater pollution occurring beneath the ‘Ewa Plain. Samples of treated reused wastewater used for irrigation (R-1 water) had very high concentrations of total nitrogen indicating this may be a significant source of nitrogen in the subsurface. Currently, there are about 7.4 million gallons of R-1 water being used for irrigation on the ‘Ewa Plain daily which may have large-scale impacts on coastal ecosystem health, and thus warrant further study.

Two coastal salinity surveys were conducted to locate sources of groundwater discharge directly along the coast. Individual point-source locations of groundwater discharge were not found in either salinity survey, which indicate a different regime by which groundwater enters the coastal zone along the ‘Ewa Coast. Specifically, the ‘Ewa Caprock may be transporting groundwater and nutrient pollution further offshore causing adverse ecological effects further offshore than expected.

A numerical groundwater model incorporating our field data was constructed and employed to simulate the different sources and regions of nitrogen input to groundwaters. The results from the MT3DMS solute transport model indicates that dissolved inorganic nitrogen from OSDS and R-1 water irrigation have a higher relative impact than agricultural fields and normal golf course fertilization. These previously mentioned assumptions and limitations are certainly affecting the accuracy of the models’ final predictions. However, when the results of the MT3DMS tests are used as a tool to understand the flow paths and relative impact TDN and DIN, the results become useful in guiding future contamination control and mitigation efforts. Additionally, understanding which sources are having the highest relative impact is important for regulators when planning and implementing multi-phased approaches to stopping nitrogen pollution.

Table 6: Abbreviations used for geochemical sample locations and types	
Geochemical sample name	Sample location
PBP	Pu'uloa Beach Park
OBP	One'ula Beach Park
KBP	Kalaeloa Beach Park
WPB	White Plains Beach
EG	'Ewa Gentry Housing Association
HPGC	Hawaii Prince Golf Club
CCGC	Coral Creek Golf Course
VIP	VIP Sanitation
OBS	Observation Well
KGC	Kapolei Golf Club

Table 7: Geochemical nutrient analysis results

		Total N	Total P	Phosphate	Silicate	N+N	Ammonium	Nitrite	Nitrate	Salinity	Latitude	Longitude
Sample Name	Sample Type	µmol/L	µmol/L	µmol/L	µmol/L	µmol/L	µmol/L	µmol/L	µmol/L			
OBP-001	Beachface	7.54	0.57	0.27	4.97	2.89	0.31	-	2.89	34.80	21.306	-158.026
OBP-002 A	Beachface	22.67	0.59	0.55	4.55	3.52	0.89	-	3.52	34.40	21.306	-158.029
OBP-002 B	Beachface	48.01	0.86	0.64	3.88	3.51	2.18	-	3.51	34.40	21.306	-158.029
OBP-003	Beachface	12.42	0.70	0.46	10.39	7.05	0.41	-	7.05	33.72	21.305	-158.030
PBP-001	Beachface	3.16	0.20	0.18	4.11	1.00	0.05	-	1.00	-	21.314	-157.991
PBP-002 A	Beachface	4.12	0.26	0.25	4.16	1.01	0.09	-	1.01	-	21.314	-157.992
PBP-002 B	Beachface	6.85	0.61	0.54	5.87	1.55	0.20	-	1.55	-	21.314	-157.992
PBP-003	Beachface	4.12	0.32	0.30	3.15	1.17	0.15	-	1.17	-	21.313	-157.993
PBP-004	Beachface	3.95	0.38	0.26	3.17	1.19	0.11	-	1.19	-	21.313	-157.994
PBP-005	Beachface	6.25	0.47	0.34	10.97	1.65	0.33	-	1.65	-	21.313	-157.995
PBP-006	Beachface	5.54	0.65	0.54	7.79	1.29	0.22	-	1.29	34.06	21.312	-157.996
PBP-007	Beachface	6.92	0.42	0.29	7.73	2.97	0.22	-	2.97	34.52	21.312	-157.998
PBP-008	Beachface	5.69	0.45	0.33	9.21	1.26	0.19	-	1.26	34.40	21.311	-158.001
PBP-009	Beachface	5.33	0.30	0.22	7.29	1.71	0.09	-	1.71	34.49	21.311	-158.001
PBP-010	Beachface	4.49	0.20	0.13	2.43	1.72	0.05	-	1.72	34.60	21.310	-158.006
PBP-011	Beachface	4.81	0.26	0.08	6.06	0.62	0.20	-	0.62	34.41	21.310	-158.010
PBP-012	Beachface	5.35	0.21	0.12	9.45	1.07	0.15	-	1.07	33.70	21.309	-158.012
PBP-001	Beachface	8.22	0.47	0.38	8.01	0.93	0.99	0.05	0.88	33.90	21.314	-157.991
PBP-002	Beachface	6.29	0.37	0.31	4.78	1.20	0.19	0.03	1.17	34.53	21.314	-157.992
PBP-003	Beachface	7.03	0.34	0.29	4.69	1.27	0.62	0.03	1.24	34.49	21.313	-157.993
PBP-004	Beachface	5.47	0.32	0.31	3.27	0.96	0.20	0.03	0.93	34.68	21.313	-157.994
PBP-005 A	Beachface	6.28	0.29	0.24	5.55	1.04	0.19	0.03	1.01	34.61	21.312	-157.998
PBP-005 B	Beachface	6.34	0.27	0.24	5.77	1.03	0.20	0.03	1.00	34.66	21.312	-157.998
PBP-006	Beachface	6.40	0.24	0.17	3.93	0.69	0.28	0.02	0.67	34.66	21.312	-158.000
PBP-007	Beachface	6.24	0.34	0.34	6.60	1.61	0.07	0.03	1.58	34.58	21.311	-158.001
PBP-008	Beachface	6.75	0.35	0.18	4.74	0.85	0.20	0.03	0.82	34.60	21.311	-158.003
PBP-009	Beachface	6.01	0.25	0.24	7.37	1.59	0.18	0.03	1.56	34.55	21.310	-158.006
PBP-010	Beachface	6.38	0.21	0.15	4.11	0.76	0.28	0.02	0.74	34.48	21.310	-158.007
PBP-011	Beachface	5.24	0.20	0.12	3.81	0.57	0.14	0.02	0.55	34.71	21.310	-158.009
PBP-012	Beachface	6.42	0.15	0.08	2.59	0.45	0.09	0.03	0.42	34.75	21.309	-158.010
PBP-013	Beachface	5.23	0.20	0.11	3.83	0.85	0.12	0.03	0.82	34.78	21.309	-158.011

OBP-003	Beachface	10.19	0.31	0.22	4.24	3.06	0.42	0.11	2.95	34.73	21.305	-158.031
OBP-002 Seep A	Beachface	81.49	1.53	1.17	313.91	73.06	0.38	0.19	72.87	18.77	21.306	-158.026
OBP-002 Seep B	Beachface	82.38	2.04	1.47	317.02	73.45	0.34	0.16	73.29	18.77	21.306	-158.026
KBP-001 A	Beachface	7.54	0.44	0.29	4.81	1.05	0.41	0.13	0.92	34.86	21.300	-158.064
KBP-001 B	Beachface	6.02	0.32	0.21	3.98	0.80	0.23	0.11	0.69	34.86	21.300	-158.064
KBP-003	Beachface	6.51	0.31	0.24	7.98	2.04	0.21	0.03	2.01	34.75	21.300	-158.062
KBP-004	Beachface	8.27	0.29	0.19	5.04	3.95	0.46	0.02	3.93	34.81	21.301	-158.057
WPB-002 A	Beachface	4.43	0.30	0.25	1.93	0.93	0.02	0.03	0.90	32.88	21.303	-158.046
WPB-002 B	Beachface	5.99	0.40	0.34	2.41	1.37	0.19	0.05	1.32	32.88	21.303	-158.046
OBP-SEEP2 A	Beachface	9.51	0.60	0.55	24.73	4.63	0.16	0.08	4.55	33.22	21.306	-158.026
OBP-SEEP2 B	Beachface	9.48	0.58	0.56	24.68	4.62	0.13	0.08	4.54	33.22	21.306	-158.026
PBP-001	Beachface	6.54	0.32	0.22	5.17	2.62	<0.02	0.07	2.55	34.60	21.330	-158.033
PBP-002	Beachface	5.68	0.30	0.17	4.75	1.98	<0.02	0.04	1.94	34.49	21.314	-157.991
PBP-003	Beachface	4.63	0.35	0.26	5.92	1.42	<0.02	0.03	1.39	34.74	21.314	-157.992
PBP-004	Beachface	3.91	0.36	0.20	5.70	0.57	<0.02	0.04	0.53	34.67	21.313	-157.993
PBP-005 A	Beachface	4.35	0.24	0.16	6.70	1.10	0.09	0.03	1.07	34.52	21.313	-157.994
PBP-005 B	Beachface	5.02	0.27	0.21	7.89	1.34	0.04	0.03	1.31	34.52	21.312	-157.998
PBP-006	Beachface	4.24	0.19	0.17	6.35	1.06	0.03	0.03	1.03	34.64	21.312	-157.998
PBP-007	Beachface	4.57	0.18	0.15	5.70	1.60	0.02	0.02	1.58	34.48	21.312	-158.000
PBP-008	Beachface	4.40	0.21	0.14	4.45	1.21	<0.02	0.03	1.18	34.49	21.311	-158.001
PBP-009 A	Beachface	4.06	0.18	0.13	5.35	1.16	0.03	0.02	1.14	34.57	21.311	-158.003
PBP-009 B	Beachface	4.72	0.17	0.12	6.13	1.37	0.16	0.03	1.34	34.57	21.310	-158.006
PBP-010	Beachface	5.03	0.18	0.11	5.26	1.78	<0.02	0.03	1.75	34.44	21.310	-158.006
PBP-011	Beachface	4.91	0.19	0.10	6.63	1.11	0.08	0.06	1.05	34.33	21.310	-158.007
PBP-012	Beachface	4.31	0.19	0.06	4.09	0.72	0.07	0.03	0.69	34.55	21.310	-158.009
PBP-013 A	Beachface	3.93	0.09	0.04	2.57	0.43	<0.02	0.03	0.40	34.45	21.309	-158.010
PBP-013 B	Beachface	3.96	0.16	0.05	2.40	0.44	0.10	0.03	0.41	34.45	21.309	-158.011
WPB-001	Beachface	6.31	0.22	0.18	5.65	2.48	<0.02	0.05	2.43	34.59	21.304	-158.044
WPB-002	Beachface	9.24	0.70	0.68	7.11	4.09	<0.02	0.05	4.04	34.77	21.303	-158.046
OBP-001	Beachface	8.84	0.62	0.53	8.96	3.76	0.23	0.06	3.70	33.99	21.306	-158.026
OBP-002 A	Beachface	7.46	0.49	0.44	8.06	2.98	<0.02	0.03	2.95	34.35	21.306	-158.029
OBP-002 B	Beachface	7.49	0.50	0.44	8.07	3.04	0.18	0.03	3.01	34.35	21.306	-158.029
OBP-003	Beachface	6.82	0.30	0.25	7.22	2.10	<0.02	0.02	2.08	34.73	21.305	-158.030
KBP-001	Beachface	8.10	0.34	0.19	6.07	2.11	<0.02	0.04	2.07	34.74	21.300	-158.064
KBP-003	Beachface	11.68	0.60	0.50	9.59	7.69	0.18	0.07	7.62	34.83	21.300	-158.059
KBP-004	Beachface	10.06	0.88	0.77	10.77	5.66	<0.02	0.04	5.62	34.74	21.301	-158.057
WPB-1	Beachface	7.94	0.61	0.57	10.73	4.54	0.07	0.06	4.48	33.88	21.304	-158.044
R-1	R-1 Water	1498.33	131.85	112.44	856.59	562.85	581.34	61.61	501.24	0.79	-	-
R-1D	R-1 Water	1544.88	132.74	112.52	896.61	561.30	635.25	61.30	500.00	0.79	-	-
Shower	Well	211.25	8.38	6.69	1467.99	186.21	0.15	0.07	186.14	0.39	-	-
VIP well	Well	30.73	0.74	0.51	519.13	0.47	0.05	0.06	0.41	1.09	-	-
KGC-1	Well	327.42	1.35	1.25	927.18	295.46	<0.02	0.06	295.40	1.19	-	-
HP-1’	Well	166.73	1.39	1.20	849.06	145.78	<0.02	0.06	145.72	1.16	-	-
HP-3’	Well	355.13	0.98	0.98	800.92	328.72	0.18	0.07	328.65	1.33	-	-
HP-5’	Well	448.04	0.88	0.73	633.61	415.04	0.07	2.08	412.96	1.49	-	-
CCGC-001	Well	409.23	1.42	1.20	774.19	379.03	3.55	-	379.03	1.68	-	-
HPGC-001	Well	373.92	1.29	0.77	1003.07	343.29	0.26	-	343.29	1.43	-	-
HPGC-002	Well	488.47	0.72	0.72	662.51	458.54	1.52	-	458.54	0.95	-	-
Canal 1	Well	195.13	1.76	1.53	1476.16	147.29	9.69	8.55	138.74	0.81	21.316	-158.007
Canal 2	Well	59.09	24.76	21.87	674.85	1.36	0.65	0.12	1.24	2.05	21.315	-158.007
Canal 3 A	Well	49.79	23.40	20.58	509.82	0.89	1.17	0.07	0.82	2.88	21.314	-158.006
Canal 3 B	Well	46.98	24.68	22.03	640.26	0.63	1.05	0.06	0.57	2.93	21.314	-158.006
Canal 4	Well	41.20	17.01	15.14	626.62	8.01	2.91	4.17	3.84	3.30	21.313	-158.006
Canal 5	Well	117.27	4.54	4.18	567.18	46.38	11.10	5.22	41.16	3.68	21.312	-158.006
CCGC-1	Well	279.57	3.17	3.07	374.92	250.28	6.98	0.15	250.13	6.79	-	-

EG-12	Well	774.80	0.95	0.91	995.65	733.75	<0.02	0.01	733.74	1.73	-	-
EG-13	Well	322.59	1.15	1.02	884.16	301.71	0.52	0.08	301.63	1.56	-	-
EG-29	Well	261.14	0.95	0.94	1328.39	237.53	0.11	0.06	237.47	1.98	-	-
EG-35(1) A	Well	367.06	0.42	0.39	730.56	341.49	0.38	1.07	340.42	1.32	-	-
EG-35(1) B	Well	359.14	0.42	0.38	717.13	333.07	0.31	1.31	331.76	1.32	-	-
EG-35(2)	Well	753.61	0.60	0.58	867.28	706.54	0.55	0.08	706.46	1.35	-	-
EG-45	Well	690.17	0.59	0.52	807.27	651.12	0.23	0.03	651.09	1.61	-	-
HP-1	Well	183.14	1.13	0.90	1243.67	136.49	0.06	0.03	136.46	1.04	-	-
HP-3 A	Well	378.07	0.84	0.70	1050.69	351.54	0.13	0.02	351.52	1.27	-	-
HP-3 B	Well	377.80	0.84	0.68	1092.98	351.40	0.12	0.02	351.38	1.27	-	-
HP-5	Well	399.17	0.80	0.74	953.54	366.07	2.59	0.06	366.01	1.57	-	-
OBS-1	Well	756.80	8.33	7.54	540.89	724.46	7.23	4.43	720.03	1.20	-	-
Seawater Average	-	5.06	0.26	0.09	1.03	0.05	-	-	-	-	-	-
Well Average	-	408.89	13.27	11.42	849.10	312.22	2.06	5.59	307.20	1.73	-	-
Beachface Average	-	9.37	0.40	0.30	15.54	4.06	0.25	0.05	4.02	33.91		
		Total N	Total P	Phosphate	Silicate	N+N	Ammonium	Nitrite	Nitrate	Salinity	Latitude	Longitude
		µmol/L	µmol/L	µmol/L	µmol/L	µmol/L	µmol/L	µmol/L	µmol/L			

Table 8: Average nutrient concentrations from ‘Ewa Plain and selected other areas from Hawaii

		Total N	Total P	Phosphate	Silicate	N+N	Ammonia	Nitrite	Nitrate	Salinity
		µmol/L	µmol/L	µmol/L	µmol/L	µmol/L	µmol/L	µmol/L	µmol/L	ppt
Station ALOHA (2021) Hawaii Ocean Time-series Data Organization & Graphical System										
Seawater Average	-	5.06	0.26	0.09	1.03	0.05	-	-	-	-
This study average values for ‘Ewa Plain										
This study Well Average	-	408.89	13.27	11.42	849.10	312.22	2.06	5.59	307.20	1.73
This study Beachface Average	-	9.37	0.40	0.30	15.54	4.06	0.25	0.05	4.02	33.91
Ellison (2021) averaged values for Waialua region, north shore Oahu										
Well Average		174.02	4.7	4.17	1019.04	140.35	0.36	-	-	0.23
Beachface Average		28.54	1.12	0.98	238.27	22.74	0.42	-	-	28.54
Mathioudakis (2018) averaged values for Kahaluu region, leeward Oahu										
Well Average		36.34	2.28	-	477.88	6.39	21.39	-	-	-
Beachface Average		37.42	1.57	-	469.28	11.47	17.55	-	-	-
Glenn et al. (2012) averaged values for leeward West Maui										
Production well Average		1330	100	72	19283	969.1	1.4	1.1	968	-
Monitoring Well Average		2342	91	52	16206	1614.2	0	6.2	1608	-

Table 9: Salinity survey results					
Latitude	**Longitude**	**Pressure**	**Temperature C**	**Conductivity**	**Salinity**
PU'ULOA BEACH PARK SALINITY SURVEY 04/29/2022					
21.3133262	-157.99254	1042.25	25.39	53.89	35.31
21.3132701	-157.99257	1039.45	25.31	52.65	34.45
21.3132396	-157.9926	1041.73	25.27	53.57	35.16
21.3132271	-157.99266	1039.63	25.18	53.16	34.92
21.3132208	-157.99269	1040.09	25.23	53.24	34.94
21.3132432	-157.99273	1039.28	25.23	53.23	34.93
21.3132679	-157.99273	1040.73	25.23	53.19	34.90
21.3132718	-157.99273	1040.91	25.23	53.12	34.85
21.3132817	-157.99274	1039.10	25.23	53.14	34.86
21.3132448	-157.99273	1040.15	25.24	53.17	34.88
21.3131941	-157.99276	1039.39	25.23	52.47	34.38
21.313173	-157.99281	1038.46	25.21	53.13	34.88
21.3131544	-157.99285	1038.93	25.21	52.89	34.70
21.3131351	-157.9929	1037.29	25.22	52.07	34.09
21.3131182	-157.99294	1043.24	25.23	53.18	34.89
21.3131064	-157.99298	1038.98	25.24	52.18	34.16
21.3130891	-157.99302	1041.43	25.23	53.11	34.85
21.3130724	-157.99307	1040.62	25.24	53.08	34.82
21.3130602	-157.99311	1043.30	25.23	53.12	34.86
21.3130535	-157.99315	1043.42	25.23	53.11	34.84
21.3130258	-157.9932	1040.56	25.23	53.12	34.85
21.3130037	-157.99325	1040.97	25.25	53.15	34.86
21.3130006	-157.99329	1038.58	25.26	52.64	34.47
21.3129826	-157.99333	1039.10	25.25	52.36	34.28
21.3129771	-157.99337	1039.16	25.28	52.64	34.47
21.3129635	-157.99341	1041.78	25.26	53.20	34.89
21.3129761	-157.99343	1037.41	25.25	52.83	34.62
21.31297	-157.99344	1038.05	25.25	50.64	33.02
21.31297	-157.99349	1038.28	25.24	51.90	33.95
21.31294	-157.99352	1042.08	25.25	53.26	34.94
21.31293	-157.99356	1038.58	25.26	52.83	34.62
21.31291	-157.99359	1040.09	25.26	52.43	34.32
21.3129	-157.99364	1039.22	25.27	53.13	34.83
21.3129	-157.99367	1038.75	25.29	44.84	28.79
21.31288	-157.99373	1039.74	25.27	53.20	34.88
21.31287	-157.99377	1039.45	25.28	53.21	34.88
21.31286	-157.99382	1040.38	25.28	53.30	34.95
21.31285	-157.99387	1040.27	25.29	52.90	34.65
21.31282	-157.99392	1040.79	25.31	53.27	34.90
21.31281	-157.99396	1040.38	25.31	53.22	34.86
21.3128	-157.994	1041.61	25.33	53.23	34.86
21.3128	-157.99405	1038.23	25.31	53.29	34.91
21.31278	-157.9941	1042.08	25.29	53.29	34.93
21.31277	-157.99415	1042.31	25.30	53.30	34.93
21.31278	-157.99419	1041.96	25.31	53.31	34.93
21.31277	-157.99425	1039.92	25.32	53.13	34.79
21.31277	-157.99429	1043.07	25.35	53.29	34.89
21.31276	-157.99433	1040.79	25.33	53.26	34.88
21.31275	-157.99438	1042.95	25.33	53.30	34.91
21.31273	-157.99442	1043.07	25.34	53.29	34.90

21.31274	-157.99447	1040.62	25.35	53.31	34.90
21.31273	-157.99452	1040.91	25.35	53.21	34.83
21.31272	-157.99458	1039.45	25.34	52.41	34.25
21.31271	-157.99462	1040.09	25.34	53.21	34.84
21.3126935	-157.99466	1042.89	25.34	53.06	34.72
21.3126818	-157.99471	1038.93	25.34	52.37	34.22
21.3126629	-157.99475	1042.43	25.32	53.27	34.89
21.3126613	-157.99477	1038.93	25.32	52.80	34.55
21.3126447	-157.9948	1042.25	25.32	52.39	34.25
21.3126251	-157.99485	1040.44	25.33	53.15	34.80
21.3126191	-157.99489	1041.26	25.33	53.16	34.81
21.3126097	-157.99494	1039.63	25.33	53.16	34.81
21.3126029	-157.99499	1039.10	25.34	53.03	34.71
21.3125846	-157.99502	1036.59	25.34	53.19	34.82
21.3125784	-157.99506	1041.73	25.34	53.23	34.85
21.3125681	-157.9951	1041.08	25.34	53.12	34.77
21.3125499	-157.99514	1039.45	25.34	53.26	34.88
21.3125338	-157.99518	1040.91	25.32	53.24	34.88
21.3125297	-157.99524	1040.27	25.35	53.03	34.70
21.3125194	-157.99528	1036.07	25.36	52.68	34.44
21.312495	-157.99533	1042.78	25.31	53.20	34.85
21.3124976	-157.99539	1042.43	25.31	53.26	34.90
21.3124822	-157.99542	1040.09	25.31	53.23	34.88
21.3124739	-157.99547	1044.29	25.30	53.18	34.84
21.3124654	-157.99551	1039.74	25.29	53.24	34.90
21.3124464	-157.99556	1039.63	25.28	53.15	34.84
21.3124354	-157.99561	1040.44	25.28	53.07	34.78
21.3124334	-157.99567	1039.98	25.28	52.91	34.66
21.3124129	-157.99571	1038.23	25.28	52.98	34.71
21.3124043	-157.99577	1037.93	25.28	52.79	34.57
21.3123878	-157.9958	1037.23	25.29	49.78	32.36
21.3123782	-157.99585	1041.96	25.31	53.10	34.78
21.312364	-157.99589	1037.23	25.33	52.80	34.54
21.3123389	-157.99594	1040.97	25.33	52.35	34.21
21.3123298	-157.99599	1035.95	25.30	50.70	33.03
21.3123139	-157.99604	1042.78	25.32	52.76	34.52
21.3122997	-157.99607	1038.46	25.32	53.08	34.75
21.3122859	-157.99612	1041.96	25.30	53.27	34.91
21.3122865	-157.99618	1041.73	25.34	53.34	34.93
21.3122817	-157.99624	1042.08	25.37	53.31	34.89
21.3122681	-157.99628	1043.13	25.33	53.34	34.94
21.3122541	-157.99633	1040.97	25.29	53.29	34.94
21.3122507	-157.99636	1041.61	25.29	53.17	34.85
21.3122391	-157.99642	1042.43	25.29	53.31	34.95
21.3122298	-157.99647	1041.61	25.29	53.28	34.92
21.3122209	-157.99652	1042.60	25.29	53.30	34.93
21.312217	-157.99656	1040.09	25.34	53.15	34.79
21.3122013	-157.99658	1040.62	25.32	53.14	34.80
21.312191	-157.99662	1041.26	25.27	53.20	34.88
21.3121742	-157.99667	1043.30	25.30	53.30	34.94
21.3121623	-157.99671	1040.38	25.31	53.26	34.89
21.31216	-157.99676	1044.47	25.33	53.32	34.93
21.312148	-157.99682	1043.24	25.32	53.32	34.93
21.3121278	-157.99687	1041.78	25.30	53.34	34.96
21.3121178	-157.99692	1040.97	25.29	53.18	34.85

21.3121057	-157.99696	1042.08	25.31	53.31	34.93
21.3121044	-157.997	1041.96	25.32	52.84	34.58
21.3121016	-157.99704	1041.08	25.32	53.35	34.95
21.3120939	-157.99709	1042.95	25.33	53.36	34.95
21.3120752	-157.99713	1039.74	25.38	53.25	34.84
21.3120655	-157.99717	1041.43	25.36	53.38	34.95
21.3120499	-157.99722	1042.13	25.34	53.24	34.86
21.3120459	-157.99726	1041.73	25.28	53.28	34.93
21.3120304	-157.99731	1042.95	25.25	53.22	34.91
21.3120405	-157.99736	1040.09	25.22	53.21	34.92
21.3120515	-157.99743	1042.43	25.17	53.12	34.90
21.3120428	-157.99748	1043.42	25.16	53.15	34.92
21.3120432	-157.99753	1037.41	25.14	52.67	34.59
21.3120325	-157.99757	1041.26	25.15	53.09	34.89
21.3120337	-157.99761	1039.92	25.14	47.35	30.69
21.3120274	-157.99764	1038.75	25.15	53.12	34.91
21.3120329	-157.99768	1043.07	25.14	53.14	34.93
21.3120327	-157.99773	1043.48	25.13	53.14	34.94
21.3120226	-157.99777	1040.27	25.19	52.78	34.63
21.3120128	-157.9978	1036.88	25.23	32.71	20.33
21.3119972	-157.99785	1040.27	25.21	53.12	34.87
21.3120107	-157.9979	1041.96	25.20	53.15	34.89
21.3120146	-157.99794	1042.60	25.20	53.14	34.89
21.3120092	-157.998	1044.64	25.22	53.17	34.90
21.3119981	-157.99803	1042.89	25.23	53.16	34.88
21.3119926	-157.99808	1040.38	25.25	53.06	34.79
21.3119806	-157.99813	1040.79	25.24	52.98	34.74
21.3119736	-157.99818	1043.30	25.26	53.19	34.89
21.3119711	-157.99821	1036.24	25.26	44.56	28.61
21.3119626	-157.99824	1042.95	25.30	53.24	34.89
21.3119459	-157.9983	1037.58	25.30	49.54	32.18
21.3119417	-157.99833	1038.75	25.26	52.99	34.74
21.3119416	-157.99838	1038.75	25.24	53.10	34.84
21.3119373	-157.99841	1037.76	25.23	52.87	34.67
21.3119328	-157.99846	1041.73	25.23	53.14	34.87
21.3119232	-157.99851	1042.31	25.24	53.14	34.86
21.3119136	-157.99855	1040.09	25.25	53.14	34.85
21.3118989	-157.99859	1042.78	25.26	53.16	34.86
21.3118927	-157.99869	1043.30	25.34	53.30	34.91
21.3118794	-157.99872	1042.25	25.35	53.34	34.92
21.311863	-157.99877	1041.14	25.36	53.26	34.86
21.3118378	-157.99883	1042.43	25.37	53.32	34.90
21.3118236	-157.99888	1040.62	25.37	51.63	33.66
21.3118194	-157.99893	1040.62	25.37	53.29	34.87
21.3118026	-157.99899	1039.80	25.39	53.32	34.88
21.311789	-157.99903	1041.78	25.40	44.38	28.40
21.3117673	-157.99908	1039.92	25.40	53.01	34.65
21.3117599	-157.99912	1042.13	25.39	53.38	34.93
21.3117466	-157.99917	1040.27	25.41	53.42	34.93
21.3117392	-157.99923	1039.92	25.43	53.44	34.94
21.311723	-157.99928	1039.39	25.41	53.43	34.94
21.3117086	-157.99933	1039.45	25.37	53.35	34.92
21.3116807	-157.99939	1041.78	25.41	53.32	34.86
21.3116659	-157.99944	1041.26	25.43	53.35	34.87
21.3116498	-157.99948	1038.11	25.47	53.24	34.76

21.3116413	-157.99952	1040.44	25.47	52.81	34.45
21.3116187	-157.99956	1041.43	25.46	53.41	34.90
21.3116052	-157.99962	1041.43	25.51	53.52	34.94
21.3115985	-157.99967	1038.40	25.50	52.95	34.53
21.3115911	-157.99971	1037.58	25.50	52.68	34.33
21.3115827	-157.99975	1041.61	25.60	53.37	34.76
21.3115642	-157.99981	1040.09	25.52	53.21	34.70
21.3115561	-157.99986	1037.12	25.53	46.15	29.59
21.3115403	-157.99992	1041.26	25.53	53.49	34.90
21.3115176	-157.99997	1040.27	25.60	52.75	34.31
21.3115051	-158.00003	1040.09	25.55	52.70	34.30
21.3114996	-158.00008	1038.75	25.54	53.11	34.62
21.3114875	-158.00014	1040.27	25.56	53.31	34.75
21.3114555	-158.00018	1041.96	25.56	53.56	34.93
21.3114455	-158.00023	1040.73	25.61	53.50	34.84
21.3114361	-158.00028	1040.09	25.63	52.83	34.34
21.3114258	-158.00034	1041.61	25.64	51.97	33.71
21.3114219	-158.00038	1038.46	25.65	34.74	21.53
21.3113993	-158.00042	1036.42	25.64	52.29	33.95
21.3113896	-158.00047	1042.78	25.61	45.17	28.83
21.3113777	-158.00051	1039.28	25.61	53.26	34.68
21.3113823	-158.00057	1042.60	25.59	53.32	34.73
21.3113772	-158.00062	1040.56	25.56	53.51	34.89
21.3113652	-158.00068	1041.61	25.53	53.54	34.93
21.3113569	-158.00074	1040.62	25.59	53.30	34.72
21.3113398	-158.00079	1036.59	25.60	52.36	34.03
21.3113058	-158.00082	1039.74	25.60	53.47	34.84
21.3112912	-158.00087	1041.73	25.59	53.50	34.87
21.31128	-158.00094	1037.41	25.58	52.76	34.33
21.3112448	-158.00099	1043.59	25.55	53.28	34.73
21.31124	-158.00104	1041.08	25.52	53.44	34.87
21.3112345	-158.0011	1043.30	25.49	53.40	34.87
21.3112344	-158.00115	1043.77	25.49	53.41	34.87
21.3112264	-158.0012	1044.12	25.53	53.45	34.88
21.3112212	-158.00126	1044.29	25.57	53.46	34.85
21.3112078	-158.00131	1043.24	25.56	53.40	34.82
21.311195	-158.00135	1044.47	25.52	53.26	34.74
21.3111907	-158.00139	1037.41	25.49	53.20	34.72
21.3111921	-158.00144	1040.27	25.49	53.30	34.79
21.3111954	-158.00149	1040.97	25.49	53.26	34.76
21.3111824	-158.00152	1042.95	25.50	53.32	34.79
21.3111743	-158.00158	1042.60	25.50	53.32	34.80
21.3111567	-158.00163	1042.89	25.47	53.06	34.63
21.3111381	-158.00169	1043.24	25.46	53.26	34.78
21.3111209	-158.00172	1042.60	25.47	52.48	34.21
21.3111055	-158.00177	1037.58	25.43	52.42	34.19
21.3111008	-158.00182	1039.57	25.39	53.20	34.79
21.311083	-158.00187	1043.30	25.39	53.24	34.82
21.3110627	-158.00193	1038.58	25.38	52.94	34.61
21.3110624	-158.00198	1042.25	25.37	53.22	34.82
21.311053	-158.00202	1042.66	25.36	53.22	34.83
21.3110436	-158.00208	1041.32	25.36	50.78	33.04
21.3110228	-158.00212	1044.12	25.33	53.11	34.77
21.3110171	-158.00217	1038.23	25.28	52.57	34.41
21.3110128	-158.00222	1040.09	25.26	52.63	34.47

21.3110029	-158.00228	1042.43	25.26	53.20	34.89
21.3109906	-158.00233	1040.44	25.26	53.03	34.76
21.3110011	-158.00238	1041.43	25.30	50.07	32.57
21.3109777	-158.00242	1046.98	25.25	53.02	34.76
21.3109589	-158.00247	1039.16	25.16	52.84	34.70
21.3109517	-158.00253	1042.25	25.14	53.12	34.91
21.3109302	-158.00258	1039.74	25.13	53.12	34.92
21.310923	-158.00263	1038.75	25.18	52.84	34.69
21.3109084	-158.00268	1040.27	25.24	49.41	32.12
21.3108927	-158.00271	1035.08	25.23	38.47	24.32
21.3108967	-158.00275	1038.46	25.24	47.52	30.76
21.3108769	-158.00284	1041.26	25.20	53.08	34.85
21.3108724	-158.0029	1042.60	25.20	53.16	34.90
21.3108638	-158.00295	1041.90	25.23	52.53	34.42
21.3108534	-158.00299	1042.78	25.26	53.20	34.89
21.3108358	-158.00304	1038.93	25.32	53.04	34.73
21.3108005	-158.00308	1041.96	25.30	52.35	34.24
21.3107851	-158.00314	1040.97	25.24	53.18	34.89
21.3107755	-158.00317	1044.23	25.26	53.24	34.92
21.3107671	-158.0032	1042.95	25.28	53.27	34.93
21.3107517	-158.00324	1043.77	25.23	53.23	34.93
21.3107384	-158.00329	1037.88	25.31	53.10	34.78
21.3107234	-158.00334	1041.43	25.22	53.18	34.90
21.3107115	-158.00338	1039.92	25.15	51.72	33.88
21.3107017	-158.00343	1040.44	25.20	53.21	34.94
21.3106918	-158.00348	1042.43	25.32	53.26	34.88
21.3106815	-158.00353	1042.60	25.32	53.21	34.85
21.3106726	-158.00358	1042.08	25.29	53.20	34.86
21.3106585	-158.00367	1040.44	25.21	53.18	34.91
21.3106437	-158.00372	1041.26	25.29	53.22	34.88
21.3106256	-158.00376	1043.77	25.42	53.38	34.90
21.3106261	-158.0038	1037.76	25.39	51.81	33.77
21.3106493	-158.00381	1042.13	25.36	53.33	34.91
21.3106562	-158.00383	1037.76	25.32	51.63	33.69
21.3106514	-158.00389	1042.95	25.33	53.22	34.85
21.3106435	-158.00394	1037.06	25.38	37.45	23.52
21.3106137	-158.00397	1042.83	25.36	53.32	34.91
21.3105865	-158.00402	1042.43	25.36	53.26	34.86
21.3105639	-158.00411	1038.28	25.41	42.86	27.31
21.3105563	-158.00416	1037.58	25.43	51.22	33.32
21.310548	-158.00421	1037.23	25.44	51.76	33.71
21.3105374	-158.00425	1035.95	25.50	51.76	33.66
21.3105178	-158.00429	1039.74	25.50	52.07	33.89
21.3105039	-158.00433	1043.24	25.43	53.17	34.74
21.3104857	-158.00438	1042.08	25.41	53.16	34.75
21.3104781	-158.00442	1043.24	25.44	53.09	34.68
21.31047	-158.00448	1039.45	25.42	53.21	34.78
21.3104784	-158.00454	1044.41	25.44	53.05	34.65
21.3104683	-158.00459	1041.08	25.54	52.19	33.95
21.3104572	-158.00465	1041.67	25.54	53.15	34.65
21.3104479	-158.0047	1041.26	25.41	53.14	34.73
21.3104407	-158.00473	1036.88	25.41	51.34	33.42
21.3104268	-158.00479	1043.42	25.34	53.24	34.86
21.3104137	-158.00485	1043.30	25.39	53.25	34.83
21.3103912	-158.0049	1043.42	25.34	53.24	34.86

21.3103619	-158.00496	1043.59	25.34	53.24	34.86
21.310332	-158.00501	1037.23	25.31	43.81	28.05
21.310312	-158.00505	1039.63	25.28	52.46	34.33
21.3103079	-158.00512	1042.13	25.30	53.25	34.90
21.3102992	-158.00519	1043.77	25.29	53.24	34.90
21.3102906	-158.00525	1044.12	25.41	53.11	34.72
21.3102847	-158.00529	1046.28	25.47	52.94	34.54
21.3102779	-158.0054	1042.95	25.45	53.09	34.67
21.3102745	-158.00545	1038.75	25.44	52.49	34.23
21.3102639	-158.00552	1040.09	25.41	53.02	34.65
21.3102606	-158.00556	1039.74	25.40	53.19	34.78
21.3102727	-158.00559	1041.78	25.42	53.23	34.79
21.3102614	-158.00563	1039.63	25.44	53.12	34.69
21.3102479	-158.00567	1041.78	25.51	52.98	34.55
21.3102488	-158.00572	1043.59	25.52	53.26	34.74
21.3102407	-158.00577	1037.23	25.54	33.19	20.52
21.3102181	-158.00583	1039.10	25.58	45.93	29.39
21.3102093	-158.0059	1041.73	25.61	53.38	34.76
21.3102023	-158.00597	1043.13	25.59	53.45	34.83
21.310212	-158.00602	1043.94	25.55	53.31	34.75
21.3102133	-158.00608	1041.61	25.54	53.39	34.82
21.3101976	-158.00619	1038.93	25.56	53.45	34.85
21.3101839	-158.00625	1041.08	25.56	53.34	34.76
21.3101728	-158.00629	1039.74	25.56	53.38	34.80
21.3101686	-158.00634	1040.38	25.59	53.53	34.89
21.3101631	-158.00638	1043.83	25.57	53.53	34.90
21.3101553	-158.00643	1038.75	25.57	53.02	34.53
21.3101388	-158.00648	1041.61	25.57	53.50	34.88
21.3101162	-158.00652	1037.23	25.56	49.41	31.91
21.3100976	-158.00658	1040.79	25.58	53.53	34.89
21.3100756	-158.00663	1044.29	25.62	53.60	34.92
21.3100693	-158.00669	1041.08	25.59	53.62	34.95
21.310062	-158.00673	1040.27	25.57	53.54	34.91
21.3100433	-158.00676	1039.10	25.57	53.50	34.88
21.3100262	-158.00682	1042.25	25.56	53.50	34.89
21.3100117	-158.00686	1038.93	25.56	53.51	34.89
21.3100003	-158.00689	1042.78	25.58	53.58	34.94
21.3099903	-158.00693	1042.43	25.58	53.60	34.94
21.3099925	-158.00697	1040.62	25.50	53.46	34.90
21.3099861	-158.007	1041.96	25.49	53.47	34.91
21.3099664	-158.00703	1039.80	25.48	53.50	34.94
21.3099504	-158.00706	1040.09	25.47	53.42	34.89
21.3099402	-158.00711	1042.25	25.46	53.43	34.91
21.3099303	-158.00716	1040.44	25.45	53.48	34.95
21.3099252	-158.00722	1039.63	25.42	53.24	34.79
21.3099269	-158.00727	1042.43	25.41	53.04	34.66
21.3099272	-158.0073	1041.78	25.40	53.40	34.93
21.309914	-158.00734	1039.28	25.38	52.98	34.63
21.3099117	-158.00738	1039.92	25.37	53.40	34.95
21.3099178	-158.00742	1042.78	25.37	53.32	34.90
21.3099154	-158.00746	1035.89	25.36	46.51	29.95
21.3098903	-158.00749	1043.77	25.37	53.36	34.92
21.3098779	-158.00754	1037.12	25.36	52.58	34.36
21.3098706	-158.00758	1039.45	25.36	52.73	34.47
21.3098514	-158.00762	1043.42	25.37	53.33	34.90

21.3098488	-158.00766	1039.22	25.37	52.00	33.93
21.3098452	-158.0077	1044.29	25.33	52.69	34.46
21.3098412	-158.00774	1042.25	25.32	53.14	34.80
21.3098488	-158.00778	1041.73	25.34	53.29	34.89
21.3098346	-158.00783	1042.78	25.34	53.26	34.87
21.3098256	-158.00788	1041.14	25.33	53.33	34.93
21.3098216	-158.00793	1039.63	25.34	53.34	34.93
21.3098078	-158.00797	1043.24	25.35	53.37	34.94
21.3098055	-158.00802	1039.63	25.36	53.28	34.87
21.3098204	-158.00801	1042.25	25.37	53.36	34.92
21.30981	-158.00807	1040.91	25.37	53.41	34.96
21.3098107	-158.00811	1043.30	25.40	53.34	34.89
21.3098043	-158.00816	1042.60	25.40	53.44	34.96
21.3097801	-158.0082	1041.43	25.39	53.41	34.95
21.3097749	-158.00826	1040.62	25.39	53.45	34.97
21.3097729	-158.0083	1040.44	25.36	51.09	33.27
21.3097686	-158.00837	1040.09	25.34	53.28	34.89
21.3097652	-158.00843	1041.61	25.33	53.40	34.99
21.309768	-158.00846	1039.92	25.31	52.98	34.69
21.3097892	-158.00847	1040.73	25.32	53.17	34.82
21.3097771	-158.0085	1040.62	25.33	53.38	34.97
21.3097663	-158.00855	1039.10	25.32	53.34	34.94
21.3097536	-158.00858	1041.32	25.30	53.32	34.94
21.3097382	-158.00862	1035.60	25.29	50.37	32.79
21.3097324	-158.00866	1042.13	25.27	53.30	34.95
21.309726	-158.00871	1038.23	25.26	48.79	31.66
21.3097185	-158.00876	1043.24	25.28	52.24	34.17
21.3097024	-158.0088	1041.32	25.30	53.42	35.02
21.3097048	-158.00885	1041.78	25.36	53.45	35.00
21.3097088	-158.00889	1040.27	25.34	48.62	31.49
21.3097023	-158.00893	1043.48	25.33	53.40	34.99
21.30969	-158.00896	1040.44	25.32	53.36	34.96
21.3096719	-158.00901	1043.07	25.32	53.43	35.01
21.3096804	-158.00906	1044.00	25.33	53.45	35.02
21.3096699	-158.0091	1041.96	25.36	53.42	34.98
21.3096684	-158.00915	1041.26	25.37	53.38	34.94
21.3096699	-158.00919	1042.25	25.32	53.40	34.99
21.3096602	-158.00923	1039.45	25.34	52.46	34.28
21.3096436	-158.00932	1041.08	25.34	53.22	34.85
21.3096344	-158.00936	1043.42	25.36	53.46	35.01
21.3096186	-158.00941	1040.91	25.37	53.50	35.02
21.3096245	-158.00945	1041.73	25.35	53.08	34.73
21.309618	-158.00949	1047.97	25.34	53.27	34.88
21.3096101	-158.00954	1037.93	25.36	53.38	34.94
21.3095956	-158.0096	1041.08	25.35	53.44	35.00
21.3095932	-158.00963	1042.25	25.33	52.90	34.62
21.3095853	-158.00967	1042.83	25.33	53.32	34.93
21.3095729	-158.00972	1041.61	25.35	53.40	34.97
21.3095593	-158.00977	1040.27	25.35	53.45	35.00
21.3095475	-158.00982	1038.46	25.36	53.46	35.01
21.3095538	-158.00986	1039.10	25.37	50.63	32.93
21.3095441	-158.00991	1043.94	25.36	53.54	35.06
21.309541	-158.00995	1040.09	25.26	53.47	35.08
21.3095415	-158.00999	1039.74	25.23	53.46	35.11
21.3095403	-158.01004	1041.14	25.22	52.93	34.72

21.3095397	-158.01009	1043.30	25.22	53.46	35.11
21.3095244	-158.01013	1042.48	25.22	53.34	35.02
21.3095041	-158.01017	1041.96	25.24	53.48	35.11
21.3094854	-158.01021	1042.78	25.21	53.44	35.10
21.3094886	-158.01024	1039.80	25.24	52.55	34.42
21.3094844	-158.01028	1043.48	25.36	53.62	35.12
21.3094783	-158.01033	1041.43	25.41	53.70	35.15
21.3094652	-158.01036	1042.78	25.38	53.14	34.75
21.3094672	-158.01041	1042.60	25.42	53.67	35.11
KALAELOA BEACH PARK SALINITY SURVEY 05/03/2022					
Latitude	**Longitude**	**Pressure**	**Temperature C**	**Conductivity**	**Salinity**
21.300448	-158.05803	1045.98	24.45	49.70	32.89
21.3004399	-158.05796	1046.98	24.62	49.84	32.88
21.3004389	-158.0579	1046.80	24.66	49.92	32.90
21.3004504	-158.05785	1045.34	24.68	48.36	31.74
21.3004609	-158.05782	1043.59	24.68	48.78	32.05
21.3004727	-158.05776	1043.48	24.68	48.87	32.12
21.3004832	-158.0577	1046.10	24.70	48.88	32.11
21.3005058	-158.05764	1043.30	24.72	48.84	32.07
21.3005228	-158.05757	1043.59	24.72	49.12	32.27
21.3005308	-158.05749	1043.48	24.72	49.09	32.25
21.30052	-158.05742	1042.83	24.72	49.22	32.35
21.3005267	-158.05733	1042.31	24.72	49.68	32.69
21.3005029	-158.05727	1045.46	24.72	49.76	32.74
21.3004741	-158.05722	1042.66	24.74	49.80	32.76
21.3004639	-158.05719	1041.43	24.75	49.67	32.66
21.3004526	-158.05714	1055.67	24.73	49.69	32.68
21.3004502	-158.05709	1044.12	24.74	49.68	32.67
21.3004442	-158.05704	1041.26	24.74	49.38	32.45
21.3004595	-158.05701	1039.74	24.74	49.66	32.66
21.3004571	-158.05697	1063.02	24.74	49.85	32.80
21.3004585	-158.05694	1060.16	24.74	49.84	32.79
21.3004558	-158.05688	1046.16	24.73	50.70	33.43
21.3004674	-158.05684	1052.98	24.74	50.66	33.40
21.300479	-158.0568	1038.40	24.73	50.11	33.00
21.3004855	-158.05676	1057.13	24.72	50.93	33.61
21.3004827	-158.05672	1048.96	24.71	51.13	33.76
21.3004887	-158.05668	1058.00	24.70	51.24	33.86
21.300486	-158.05664	1044.82	24.69	51.11	33.77
21.3004998	-158.05661	1049.66	24.70	51.38	33.95
21.3004994	-158.05656	1057.65	24.68	51.41	34.00
21.3004864	-158.05651	1069.03	24.67	51.49	34.06
21.3004752	-158.05647	1051.29	24.68	51.50	34.06
21.3004886	-158.05643	1051.82	24.69	51.52	34.08
21.3004879	-158.05638	1057.83	24.69	51.57	34.11
21.3004888	-158.05634	1044.64	24.68	51.49	34.06
21.3004927	-158.05631	1057.36	24.68	52.09	34.50
21.3004918	-158.05628	1055.03	24.69	52.11	34.50
21.3005081	-158.05624	1044.64	24.68	52.07	34.48
21.3005145	-158.0562	1039.45	24.68	44.19	28.70
21.3005311	-158.05617	1049.95	24.67	52.21	34.60
21.300528	-158.05613	1044.64	24.69	52.20	34.58
21.3005271	-158.05609	1041.96	24.70	52.23	34.59
21.3005268	-158.05605	1044.12	24.72	52.21	34.56
21.3005202	-158.05601	1042.89	24.73	52.05	34.43

21.300525	-158.05596	1043.13	24.76	52.08	34.44
21.3005225	-158.05592	1051.82	24.76	52.14	34.47
21.3005185	-158.05588	1051.00	24.77	52.15	34.47
21.3005165	-158.05586	1046.74	24.79	51.94	34.31
21.3005159	-158.05583	1055.61	24.82	51.90	34.26
21.3005212	-158.05579	1040.62	24.83	26.07	15.97
21.3005154	-158.05574	1040.91	24.84	43.80	28.31
21.3005132	-158.05569	1049.60	24.84	51.85	34.20
21.3005211	-158.05564	1047.97	24.85	52.04	34.34
21.3005177	-158.0556	1045.98	24.86	51.99	34.29
21.3005187	-158.05556	1052.46	24.85	52.52	34.70
21.3005171	-158.05551	1052.17	24.84	52.98	35.04
21.3005112	-158.05547	1053.86	24.83	53.26	35.26
21.3005234	-158.05544	1050.59	24.82	53.27	35.27
21.3005246	-158.0554	1044.82	24.81	53.27	35.29
21.3005045	-158.05536	1051.76	24.84	53.02	35.07
21.3005115	-158.05533	1050.18	24.83	53.32	35.30
21.3005069	-158.05529	1043.83	24.86	53.16	35.16
21.3005243	-158.05525	1060.51	24.86	53.21	35.20
21.3005281	-158.05521	1045.46	24.82	51.91	34.26
21.3005197	-158.05517	1040.73	24.82	52.77	34.90
21.3005266	-158.05514	1038.46	24.82	52.98	35.06
21.3005383	-158.05511	1050.83	24.80	52.96	35.06
21.3005441	-158.05507	1052.52	24.82	53.30	35.29
21.3005438	-158.05503	1054.15	24.82	53.30	35.30
21.3005536	-158.055	1043.77	24.80	53.28	35.29
21.3005455	-158.05497	1056.31	24.80	53.27	35.29
21.3005574	-158.05494	1059.34	24.80	53.29	35.30
21.3005803	-158.0549	1043.42	24.82	53.26	35.27
21.3005859	-158.05487	1055.78	24.84	53.29	35.27
21.3005655	-158.05484	1056.83	24.85	53.29	35.26
21.3005598	-158.05479	1057.48	24.84	53.27	35.26
21.3005709	-158.05476	1056.37	24.84	53.27	35.26
21.3005898	-158.05473	1048.49	24.83	53.26	35.26
21.3006026	-158.05468	1049.31	24.81	53.22	35.24
21.3006005	-158.05465	1047.79	24.81	53.16	35.20
21.3006031	-158.05461	1047.97	24.81	53.23	35.26
21.3006002	-158.05457	1044.93	24.80	53.22	35.25
21.300611	-158.05453	1054.68	24.81	53.24	35.26
21.3006201	-158.0545	1055.78	24.82	53.27	35.27
21.3006231	-158.05446	1051.82	24.82	53.28	35.28
21.3006487	-158.05442	1041.96	24.83	53.30	35.29
21.3006417	-158.0544	1065.00	24.82	53.28	35.28
21.3006442	-158.05437	1047.15	24.81	53.26	35.27
21.3006446	-158.05432	1052.98	24.81	53.26	35.28
21.3006514	-158.05428	1050.83	24.80	53.25	35.27
21.3006602	-158.05425	1054.03	24.80	53.26	35.28
21.3006565	-158.0542	1060.33	24.83	53.27	35.26
21.3006604	-158.05416	1042.43	24.85	53.09	35.12
21.3006685	-158.05413	1046.28	24.84	53.25	35.24
21.3006724	-158.05408	1045.75	24.84	53.26	35.25
21.3006813	-158.05403	1054.97	24.84	53.26	35.25
21.3006838	-158.054	1045.75	24.84	53.24	35.23
21.3006875	-158.05396	1047.27	24.85	53.23	35.22
21.3006824	-158.05393	1047.27	24.83	53.23	35.24

21.3006959	-158.0539	1045.81	24.83	53.22	35.22
21.3007108	-158.05387	1050.01	24.84	53.24	35.24
21.3007205	-158.05383	1041.78	24.83	53.23	35.24
21.3007264	-158.0538	1040.62	24.83	51.16	33.71
21.3007339	-158.05376	1053.16	24.83	53.14	35.17
21.3007261	-158.05372	1054.68	24.86	53.12	35.13
21.3007254	-158.05368	1048.67	24.89	53.22	35.19
21.3007213	-158.05365	1048.14	24.89	53.22	35.19
21.3007095	-158.05362	1057.48	24.90	53.22	35.17
21.3007241	-158.05359	1052.81	24.92	53.26	35.20
21.3007351	-158.05355	1055.49	24.94	53.29	35.20
21.3007405	-158.05352	1057.36	24.95	53.27	35.18
21.3007139	-158.0535	1059.98	24.97	53.30	35.18
21.3007256	-158.05347	1050.77	24.97	53.30	35.18
21.3007417	-158.05344	1040.91	24.97	50.96	33.45
21.300758	-158.05339	1042.13	24.97	53.17	35.09
21.3007571	-158.05334	1049.25	24.96	53.27	35.17
21.3007685	-158.0533	1062.20	24.94	53.26	35.17
21.3007831	-158.05326	1048.96	24.95	53.29	35.19
21.3007894	-158.05322	1053.45	24.96	53.31	35.20
21.3007847	-158.05317	1046.28	25.00	53.33	35.19
21.3007996	-158.05313	1067.86	25.01	53.36	35.20
21.3008163	-158.0531	1066.52	25.00	53.36	35.20
21.3008219	-158.05306	1052.63	24.97	53.22	35.13
21.3008336	-158.05304	1071.24	24.98	53.32	35.19
21.3008335	-158.05301	1045.98	25.01	52.54	34.59
21.3008239	-158.05299	1049.60	25.02	53.30	35.14
Latitude	**Longitude**	**Pressure**	**Temperature C**	**Conductivity**	**Salinity**

6. REFERENCES

Babcock, R.W., Lamichhane, K.M., Cummings M.J., and Cheong, G.H., 2014, Condition assessment survey of onsite sewage disposal systems (OSDSs) in Hawaii: Water Science & Technology, vol. 70 no. 6, p. 1083-1089, https://doi.org/10.2166/wst.2014.336.

Bauer, G.R., 1996, Reevaluation of the Ground-Water Resources and Sustainable Yield of the Ewa Caprock Aquifer: State of Hawaii, Department of Land and Natural Resources, Commission on Water Resource Management.

Beauvais, A., Ritz, M., Parisot, J-C., Bantsimba, C., and Dukhan, M., 2004, Combined ERT and GPR methods for investigating two-stepped lateritic weathering systems: Geoderma, v. 119, no. 1-2, p. 121-132, https://doi.org/10.1016/j.geoderma.2003.06.001.

Bishop, J.M., Glenn, C.R., Amato, D.W., and Dulai, H. 2017, Effect of land use and groundwater flow path on submarine groundwater discharge nutrient flux. Journal of Hydrology: Regional Studies: v. 11, p. 194-218, http://dx.doi.org/10.1016/j.ejrh.2015.10.008

Burnett, W.C., Aggarwal, P.K., Aureli, A., Bokuniewicz, H., Cable, J.E., Charette, MA., and Turner, J. V. 2006, Quantifying submarine groundwater discharge in the coastal zone via multiple methods: Science of the Total Environment, vol. 367, no. 2-3, p. 498-543, https://doi.org/10.1016/j.scitotenv.2006.05.009.

Burnett, W.C., Bokuniewicz, H., Huettel, M., Moore, W.S., and Taniguchi, M., 2003, Groundwater and pore water inputs to the coastal zone: Biogeochemistry, vol. 66, no. 1, p. 3-33. https://doi.org/10.1023/B:BIOG.0000006066.21240.53.

Burnett, W.C., and Dulaiova, H, 2003, Estimating the dynamics of groundwater input into the coastal zone via continuous radon-222 measurements: Journal of Environmental Radioactivity, vol. 69, no. 1-2, p. 21-35, https://doi.org/10.1016/S0265-931X(03)00084-5.

Clague, D.A., and Dalrymple, G.B., 1989, The Hawaiian-Emperor Volcanic Chain Part I Geologic Evolution: U.S. Geologic Survey Professional Paper 1350, p. 5-100, https://doi.org/10.1130/DNAG-GNA-N.187.

CWRM (State of Hawaii Commission on Water Resource Management), 2013, 2013 Update of the Hawaii Water Reuse Survey and Report, July 2013. Prepared by The Limtiaco Consulting Group. 188pp. https://files.hawaii.gov/dlnr/cwrm/planning/hwrsr2013.pdf.

CWRM (State of Hawaii Commission on Water Resource Management), 2018, Hydrologic Units of the island of Oahu. Honolulu. https://dlnr.hawaii.gov/cwrm/groundwater/hydrounits/

Daily, W., Ramirez, A., Binley, A., and LaBrecque, D., 2004, Electrical Resistivity tomography: The Leading Edge, vol 23, no. 5, 438-442, https://doi.org/10.1190/1.1729225.

Daily, W., Ramirez, A., LaBrecque, D., & Nitao, J., 1992, Electrical resistivity tomography of vadose water movement: Water Resources Research, vol. 28, no. 5, p. 1429-1442, https://doi.org/10.1029/91WR03087.

State of Hawai'i Department of Health. Report to the Twenty-Ninth Legislature, State of Hawai'i, Relating to Cesspools and Prioritization for Replacement, Hawai'i State Department of Health, 2017, pp. 1–39.

Dimova, N.T., Swarzenski, P.W., Dulaiova, H., and Glenn, C.R., 2012, Utilizing multichannel electrical resistivity methods to examine the dynamics of the fresh water–seawater interface in two Hawaiian groundwater systems: Journal of Geophysical Research: Oceans, vol. 117, no. C2, p. 1-12, https://doi.org/10.1029/2011JC007509.

Doherty, J.E., Fienen, M.N., Hunt, R.J., 2011, Approaches to Highly Parameterized Inversion: Pilot-Point Theory, Guidelines, and Research Directions: U.S. Geological Survey Scientific Investigations Report 2010-5168, 36p., https://doi.org/10.3133/sir20105168.

Dudley, B.D., MacKenzie, R.A., Sakihara, T.S., Dulaiova, H., Waters, C.A., Hughes, R.F., Ostertag, R., 2014, Influences of N-Fixing and Non-N-Fixing Vegetation and Invasive Fish on Water Chemistry of Hawaiian Anchialine Ponds: Pacific Science, vol. 68, no. 4, p 509-523, https://doi.org/10.2984/68.4.5.

Dutta, N.P., Bose, R.N., and Saikia, B.C., 1970, Detection of solution channels in limestone by electrical resistivity method: Geophysical Prospecting, vol. 18, no. 3, p. 405-414, https://doi.org/10.1111/j.1365-2478.1970.tb02121.x.

Ellison, L, 2021, Geochemical and stable isotope source tracking of terrestrial nutrient pollution to the coastal waters of Waialua Bay, North Shore, Oahu. Master of Science Thesis, University of Hawai'i at Manoa.

Engott, J.A., Johnson, A.G., Bassiouni, M., Izuka, S.K., and Rotzoll, K., 2017, Spatially distributed groundwater recharge for 2010 land cover estimated using a water-budget model for the Island of O'ahu, Hawai'i (ver. 2.0, December 2017): U.S. Geological Survey Scientific Investigations Report 2015–5010, 49 p., Revised: December 2017 (ver 2.0) online. https://doi.org/10.3133/sir20155010.

Eppley, R.W., Renger, E.H., and Harrison, W.G., 1979, Nitrate and phytoplankton production in southern California coastal waters: American Society of Limnology and Oceanography, vol. 24, no. 3, p. 483-494, https://doi.org/10.4319/lo.1979.24.3.0483.

Ford, D., Williams, P., 2007, Karst Hydrogeology and Geomorphology. John Wiley & Sons, Ltd, Sussex England, pp. 1-578.

Furumoto, A.S., Campbell, J.F., and Hussong, D.M., 1970, Seismic Studies of Subsurface Structure in the Ewa Coastal Plain, Oahu, Hawaii: Pacific Science, vol. 24, no. 4, p. 529-542.

Garrison, G.H., Glenn, C.R., and McMurtry, G.M., 2003, Measurement of submarine groundwater discharge in Kahana Bay, O'ahu, Hawai'i: Limnology and Oceanography, vol. 48, p. 920-928. https://doi.org/10.4319/lo.2003.48.2.0920.

Gelis, C., Revil, A., Cushing, M.E., Jougnot, D., Lemeille, F., Cabrera, J., De Hoyos, A., and Rocher, M., 2010, Potential of Electrical Resistivity Tomography to Detect Fault Zones in Limestone and Argillaceous Formations in the Experimental Platform of Tournemire, France: Pure and Applied Geophysics, vol. 167, p. 1405-1418. https://doi.org/10.1007/s00024-010-0097-x.

Ghasemizadeh, R., Hellweger, F., Butscher, C., Padilla, I., Vesper, D., Field, M., and Alshawabkeh, A. 2012, Groundwater flow and transport modeling of karst aquifers, with particular reference to the North Coast Limestone aquifer system of Puerto Rico: Hydrogeology Journal, vol. 20, no. 8, p. 1441-1461, https://doi.org/10.1007/s10040-012-0897-4.

Giambelluca, T.W., Chen, Q., Frazier, A.G., Prince, J.P., Chen, Y-L., Chu, P.S., Eischeid, J.K., and Delparte D.M., 2013, Online Rainfall Atlas of Hawaiʻi: Bull. Amer. Meteor. Soc, vol. 94, p. 313-316, https://doi.org/10.1175/BAMS-D-11-00228.1.

Glenn, C.R., Whittier, R.B., Dailer, M.L., Dulaiova, H., El-Kadi, A.I., Fackrell, J., Kelly, J.L., and Waters, C.A., 2012, Lahaina Groundwater Tracer Study – Lahaina, Maui, Hawaii, Final Interim Report, prepared for the State of Hawaii Department of Health, the U.S. Environmental Protection Agency, and the U.S. Army Engineer Research and Development Center. https://archive.epa.gov/epa/sites/production/files/2015-11/documents/lahaina-final-interim-report.pdf.

Halliday, W. R., 1998, History and status of the Moiliili Karst, Hawaii: Journal of Cave and Karst Studies, vol. 60, no. 3, p. 141-145.

Hartley, T. M., Chen, Y. L., 2010, Characteristics of summer trade wind rainfall over Oahu: Weather and forecasting, vol. 25, no. 6, p. 1797-1815, https://doi.org/10.1175/2010WAF2222328.1.

Hawaii Statewide GIS Program, 2022, State of Hawaii Office of Planning and Sustainable Development. Online. https://planning.hawaii.gov/gis/download-gis-data-expanded/.

Hawaiian Sugar Planters' Association: Plantation Archives, 1994, Register of the EWA PLANTATION COMPANY. Online. http://www2.hawaii.edu/~speccoll/p_ewa.html.

Hersir, P,G., and Bjornsson, A., 1991, Geophysical Exploration for Geothermal Resources Principles and application. UNU Geothermal Training Programme.

Honolulu Board of Water Supply (BWS), 2014, 2nd Annual Joint Government Water Conference August 12, 2014: https://health.hawaii.gov/sdwb/files/2014/09/SessionA-02RecycledWaterUseOahu.pdf (accessed July 2022).

Hunt, C.D., 1996, Geohydrology of the Island of Oahu, Hawaii Regional Aquifer-system analysis-Oahu, Hawaii. U.S: Geological Survey Professional Paper 1412-B, https://doi.org/10.3133/pp1412B.

Iturbe, R., Flores, R. M., Flores, C. R., and Torres, L. G., 2004, TPH-contaminated Mexican refinery soil: Health risk assessment and the first year of changes: Environmental Monitoring and Assessment, vol. 91, no. 1, p. 237-255, https://doi.org/10.1023/B:EMAS.0000009239.55534.08.

Izuka, S,K., Engott, J,A., Rotzoll, K., Bassiouni, M., Johnson, A,G., Miller, L,D., and Mair, A., 2018, Volcanic Aquifers of Hawai'i-Hydrogeology, Water Budgets and Conceptual Models: U.S. Geological Survey Scientific Investigations Report 2015-5614 Version 2.0.

Johnson, A.G., Glenn, C.R., Burnett, W.C., Peterson, R.N., and Lucy, P.G. 2008, Aerial infrared imaging reveals large nutrient-rich groundwater inputs to the ocean. Geophysical Research Letters, vol. 35: doi:10.1029/2008GL034574.

Johnson C.D., Swarzenski, P.W., Richardson, C.M., Smith, C.G., Kroeger, K.D., and Gangulai, P.M., 2015 Ground-truthing electrical resistivity methods in support of submarine groundwater discharge studies: Examples from Hawaii, Washington, and California. Journal of Environmental and Engineering Geophysics, vol. 20 (1): p. 81-87. http://dx.doi.org/10.2113/JEEG20.1.81-87. https://doi.org/10.2113/JEEG20.1.81.

Kelly, J., 2012. Identification and quantification of submarine groundwater discharge in the Hawaiian Islands. Doctoral Dissertation, University of Hawaii-Manoa.

Knee, K.L., Layton, B.A., Street., J.H., Boehm, A.B., and Paytan, A., 2008, Sources of Nutrients and Fecal Indicator Bacteria to Nearshore Waters on the North Shore of Kaua'i (Hawai'i, USA): Estuaries and Coasts, vol. 31, p. 607-622, https://doi.org/10.1007/s12237-008-9055-6.

Kroon, F.J., Schaffelke, B., and Bartley, R., 2014, Informing policy to protect coastal coral reefs: Insight from a global review of reducing agricultural pollution to coastal ecosystems: Marine pollution bulletin, vol. 85, no. 1, p. 33-41, https://doi.org/10.1016/j.marpolbul.2014.06.003.

La Brecque, D., Daily, W., and Adkins, P., 2007, Systematic Errors in Resistivity Measurement Systems: Society of Exploration Geophysicists, p. 1153-1160, https://doi.org/10.4133/1.2924620.

Lin, C.W., Liu, S.H., Wu, C.F., and Chang, S.H., 2021, Critical factors for enhancing the bioremediation of a toxic pollutant at high concentrations in groundwater: Toxicity evaluation, degrader tolerance, and microbial community: Journal of Environmental Management, vol. 277, no. 111487, p. 1-7, https://doi.org/10.1016/j.jenvman.2020.111487.

Lyons, D.A., Arvanitidis, C., Blight, A.J., Chatzinikolaou, E., Guy-Haim, T., Kotta, J., and Crowe, T. P., 2014, Macroalgal blooms alter community structure and primary productivity in marine ecosystems: Global Change Biology, vol. 20, no. 9, p. 2712-2724, https://doi.org/10.1111/gcb.12644.

Mason, J., 2020. Tracing Groundwater Connections and Nutrient Flow Between Land and Sea Using UAV Infrared Mapping, Radon, and Numerical Groundwater Modeling: Waialua Region, North Shore, O'ahu. Master of Science Thesis, University of Hawai'i at Manoa.

May, J.H., Hall, J.R., Chalmers, D.R., and Carry, P.R., 2009, Nutrient Management for Golf Courses: Virginia Cooperative Extension Publication, 430-399.

Mathioudakis, M., 2018, Hydrology of Contaminant Flow Regimes to Groundwater, Streams, and the Ocean Waters of Kane'ohe Bay, O'ahu. Master of Science Thesis, University of Hawai'i at Manoa.

Menard, H.W., Allison, E.C., and Durham, J.W., 1962, A Drowned Miocene Terrace in the Hawaiian Islands. Science, vol. 138, no. 3543, 896-897, https://doi.org/10.1126/science.138.3543.896.

Meyerhoff, S.B., Maxwell, R.M., Revil, A., Martin, J.B., Karaoulis, M., and Graham, W.D., 2014, Characterization of groundwater and surface water mixing in a semiconfined karst aquifer using time-lapse electrical resistivity tomography: Water Resources Research, vol. 50, no. 3, p. 2566-2585. https://doi.org/10.1002/2013WR013991.

Miller, C.R., Routh, P.S, Brosten, T.R., McNamara, J.P., 2008. Application of time-lapse ERT imaging to watershed characterization: Geophysics, vol. 73, no. 3, G7-G17. https://doi.org/10.1190/1.2907156.

Montiel, D., Dimova, N., Andreo, B., Prieto, J., García-Orellana, J., and Rodellas, V. 2018, Assessing submarine groundwater discharge (SGD) and nitrate fluxes in highly heterogeneous coastal karst aquifers: Challenges and solutions: Journal of Hydrology, vol. 557, p. 222-242. https://doi.org/10.1016/j.jhydrol.2017.12.036.

Moore, W.S., 2010, The effect of submarine groundwater discharge on the ocean: Annual Review of Marine Science, vol. 2, p. 59-88, https://doi.org/10.1146/annurev-marine-120308-081019.

Nakanishi, P., 2002, 'Ewa Caprock Modeling Study and Wastewater Recharge Response. Master of Science Thesis, University of Hawai'i at Manoa.

O'Connell, Y., Daly, E., Henry, T., and Brown, C., 2018, Terrestrial and marine electrical resistivity to identify groundwater pathways in coastal karst aquifers. Near Surface Geophysics, vol. 16, no. 2, p. 164-175, https://doi.org/10.3997/1873-0604.2017062.

Oki, D., Souza, W., Balke, E., and Bauer, G. 1996, Numerical analysis of ground-water flow and salinity in the Ewa area, Oahu, Hawaii: US Geological Survey Open-File Rep, (96-442).

Oki, D., Souza, W.R., Bolke, E.L., and Bauer, G.R., 1998, Numerical analysis of the hydrogeologic controls in a layered coastal aquifer system, Oahu, Hawaii, USA: Hydrogeology Journal, 6, 243-263. doi: 10.1007/s100400050149.

Okuhata, B., El-Kadi, A.I., Dulai, H., Lee, J., Wada, C.A., Bremer, L.L., Burnett, K.M., Delevaux, J.M.S., and Shuler, C.K., 2021, A density-dependent multi-species model to assess flow and nutrient transport in the coastal Keauhou aquifer, Hawai'i. USA: Hydrogeology Journal 30, 231-250. https://doi.org/10.1007/s10040-021-02407-y.

Oldenborger, G.A., Routh, P.S., and Knoll, M.D., 2005, Sensitivity of electrical resistivity tomography data to electrode position errors: Geophysical Journal International vol. 163, p. 1-9, https://doi.org/10.1111/j.1365-246X.2005.02714.x.

Paerl, H.W., Willey, J. D., Go, M., Peierls, B.L., Pinckney, J.L., and Fogel, M.L., 1999, Rainfall stimulation of primary production in western Atlantic Ocean waters: roles of different nitrogen sources and co-limiting nutrients: Marine Ecology Progress Series, vol. 176, p. 205-214, https://doi.org/10.3354/meps176205.

Palmer, A.N., 1991, Origin and morphology of limestone caves: Geological Society of America Bulletin, vol. 103, no. 1, p. 1-21. https://doi.org/10.1130/0016-7606(1991)103<0001:OAMOLC>2.3.CO;2.

Perrone, A., Lapenna, V., and Piscitelli, S., 2014, Electrical resistivity tomography technique for landside investigation: A review: Earth-Science Reviews, vol. 135, p. 65-82. https://doi.org/10.1016/j.earscirev.2014.04.002.

PEST: Model-Independent Parameter Estimation and Uncertainty Analysis, 2022. https://pesthomepage.org/.

Pujari, P.R., and Soni, A.K., 2009, Sea water intrusion studies near Kovaya limestone mine, Saurashtra coast, India: Environ Monit Assess, vol. 154, p. 93-109. https://doi.org/10.1007/s10661-008-0380-9.

Richardson, C., Dulaiova, H., and R. Whittier, 2017, Sources and spatial variability of groundwater-delivered nutrients in Maunalua Bay, Oahu, Hawaiʻi: Journal of Hydrology: Regional Studies. https://doi.org/10.1016/j.ejrh.2015.11.006.

Resig, J., 1969, Paleontological investigations of deep borings on the Ewa plain, Oahu, Hawaii. Hawaii Institute of Geophysics Report, HIG-69-2, 1-99.

Saad, R., Nawawi, M.N.M., and Tonnizam Mohamad, E., 2012. Groundwater Detection in Alluvium Using 2-D Electrical Resistivity Tomography (ERT): Electronic Journal of Geotechnical Engineering vol. 17, p. 369-376.

Sakadevan, K., Maheshwari, B.L., and Bavor, H.J., 2000, Availability of nitrogen and phosphorus under recycled water irrigation: Australian Journal of Soil Research vol. 38, p. 653-664, https://doi.org/10.1071/SR99040.

Samouëlian, A., Cousin, I., Tabbagh, A., Bruand, A., and Richard, G., 2005, Electrical resistivity survey in soil science: a review: Soil and Tillage Research, vol. 83, no. 1, p. 173-193, https://doi.org/10.1016/j.still.2004.10.004.

Sawyer, A. H., Zhu, J., Currens, J. C., Atcher, C., and Binley, A., 2015, Time-lapse electrical resistivity imaging of solute transport in a karst conduit. Hydrological Processes, vol. 29, no. 23, p. 4968-4976. https://doi.org/10.1002/hyp.10622.

Sharma, S., and Verma, G.K., 2015, Inversion of Electrical Resistivity Data: A Review: International Journal of Computer and Systems Engineering, vol. 9, no. 4, p. 400-406.

Sherman, C.E., Glenn C.R., Jones, A.T., Burnett, W.C., and Schwarcz, H.P., 1993, New Evidence for two highstands of the sea during the last interglacial, oxygen isotope substage 5e: Geology vol. 21, p. 1079-1082. https://doi.org/10.1130/0091-7613(1993)021<1079:NEFTHO>2.3.CO;2.

Shuler, C. K., El-Kadi, A. I., Dulai, H., Glenn, C. R., and Fackrell, J., 2017, Source portioning of anthropogenic groundwater nitrogen in a mixed-use landscape, Tutuila, American Samoa: Hydrogeology Journal vol. 25, p. 2419-2434. https://doi.org/10.1007/s10040-017-1617-x.

Smith, V. H., Tilman, G. D., and Nekola, J. C., 1999, Eutrophication: impacts of excess nutrient inputs on freshwater, marine, and terrestrial ecosystems: Environmental Pollution, vol. 100, no. 1-3, p.179-196, https://doi.org/10.1016/S0269-7491(99)00091-3.

Stearns, H. T., and Chamberlain, T. K., 1967, Deep cores of Oahu, Hawaii and their bearing on the geologic history of the central Pacific basin: Pacific Science, vol. 21, p. 153-165.

Stoner, N.K., 2013, Final Aquatic Life Ambient Water Quality Criteria For Ammonia-Freshwater 2013: Federal Register, vol. 78, no. 163, p. 52192-52194.

Storz, Hm, W. Storz, and F. Jacobs., 2000, Electrical resistivity tomography to investigate geological structures of the earth's upper crust: Geophysical Prospecting, vol. 48, no. 3, p. 455-472. https://doi.org/10.1046/j.1365-2478.2000.00196.x.

Stringfield, V. T., and LeGrand, H. E., 1969, Hydrology of carbonate rock terranes—A review: With special reference to the United States: Journal of Hydrology, vol. 8, no. 3, p. 349-376. https://doi.org/ 10.1016/0022-1694(69)90009-2.

Suter II, G., Cormier, S., Schofield, K., Bowersox, M., Latimer, H., 2022, Sources, Stressors and Responses – Ammonia: United States Environmental Protection Agency CADDIS Volume 2.

Sun, H., Cheng, M., Su, C., Li, H., Z, G., Su, M., Li, S., Zhang, L., and Li, K., 2017, Characterization of shallow karst using electrical resistivity imaging in a limestone mining area: Environ Earth Sci, vol. 76, no. 767, p. 1-9. https://doi.org/10.1007/s12665-017-7112-9.

Swarzenski, P.W., Burnett, W.C., Greenwood, W.J., Herut, B., Peterson, R., Dimova N., Shalem, Y., Yechieli, Y., and Weinstein, Y., 2006, Combined time-series resistivity and geochemical tracer techniques to examine submarine groundwater discharge at Dor Beach, Israel, Geophys. Res. Lett., vol. 33, no. L24405, https://doi.org/10.1029/2006GL028282.

Swarzenski, P. W., Simonds, F.W., Paulson A.J., Kruse, S., and Reich, C., 2007, A geochemical and geophysical examination of submarine groundwater discharge and associated nutrient loading estimates into Lynch Cove, Hood Canal, WA, Environ. Sci. Technol., vol. 41, p. 7022–7029, https://doi.org/10.1021/es070881a.

Tassy, A., Maxwell, M., Borgomano, J., Arfib, B., Fournier, F., Gilli, E., and Guglielmi, Y., 2014, Electrical resistivity tomography (ERT) of a coastal carbonate aquifer (Port-Miou, SE France): Environmental Earth Sciences, vol. 71, no. 2, p. 601-608. https://doi.org/10.1007/s12665-013-2802-4.

Tuholske, C., Halpern, B.S., Blasco, G., Villasenor, J.C., Frazier, M., and Caylor, K, 2021. Mapping global inputs and impacts from of human sewage in coastal ecosystems: PLoS ONE, vol. 16, no. 11, p. 1-16. https://doi.org/10.1371/journal.pone.0258898.

U.S. Census Bureau, 2022, Annual Estimates of the Resident Population for Counties in Hawaii: April 1, 2020 to July 1 2021. https://files.hawaii.gov/dbedt/census/popestimate/2021-county-pop/co-est2021-pop-15.pdf.

United States Environmental Protection Agency, 2022, Chemical Contaminant Rules. Online. https://www.epa.gov/dwreginfo/chemical-contaminant-rules.

van Schoor, M., 2002, Detection of sinkholes using 2D electrical resistivity imaging: Journal of Applied Geophysics, vol. 50, p. 393-399. https://doi.org/10.1016/S0926-9851(02)00166-0.

Whittier, R. B., and El-Kadi, A.I., 2009, Human and environmental risk ranking of onsite sewage disposal systems for Oahu.

Wilson, A.M., and Gardner, L.R., 2006, Tidally driven groundwater flow and solute exchange in a marsh: numerical simulations. Water Resources Research, vol. 42, no. 1, p. 1-9. https://doi.org/10.1029/2005WR004302.

Workman, L. E., and Leighton, M. M., 1937. Search for ground-waters by the electrical resistivity-method. Eos, Transactions American Geophysical Union, vol. 18, no. 2, p. 403-409, https://doi.org/10.1029/TR018i002p00403.

World Health Organization, 2003, Ammonia in Drinking-water: Background document for development of WHO Guidelines for Drinking-water Quality. Guidelines for drinking-water quality, vol 2.

Yates, M. V., 1986. Septic Tank Density and Ground-Water Contamination. Ground Water, vol. 23, p. 5, p. 586-591, https://doi.org/10.1111/j.1745-6584.1985.tb01506.x.

Zhan, J., He, Y., Zhao, G., Li, Z., Yuan, Q., and Liu, L., 2020, Quantitative Evaluation of the Spatial Variation of Surface Soil Properties in a Typical Alluvial Plain of the Lower Yellow River Using Classic Statistics, Geostatistics and Single Fractal and Multifractal Methods: Applied Sciences, vol. 10, p. 1-15. https://doi.org/10.3390/app10175796.

Zhody, A. A.R., and Jackson, Dallas, B., 1969, Application of Deep Electrical Soundings for Groundwater Exploration in Hawaii. Geophysics, vol. 34, no. 4, p. 584-600. https://doi.org/10.1190/1.1440033.

Zhou, W., Beck, B.F., Adams, A.L., 2002, Effective electrode array in mapping karst hazards in electrical resistivity tomography: Environmental Geology vol. 42, p. 922-928. https://doi.org/10.1007/s00254-002-0594-z.

Zhu, J., Currens, J. C., and Dinger, J. S., 2011, Challenges of using electrical resistivity method to locate karst conduits—a field case in the Inner Bluegrass Region, Kentucky: Journal of Applied Geophysics, vol. 75, no. 3, p. 523-530, https://doi.org/10.1016/j.jappgeo.2011.08.009.